



TUD | Technische Petrologie | Schnittpahnstraße 9 | 64287 Darmstadt



TECHNISCHE  
UNIVERSITÄT  
DARMSTADT

Institut für Angewandte Geowissenschaften

Institute for Applied Geosciences

Working report

## **Mineral transformation and sorption at elevated temperatures in fractured crystalline rocks and barrier materials (MUSE)**

Summary Report on Mineralogy of crystalline rocks

Lan Nguyen-Thanh, Rafael Ferreiro Mählmann, Dirk Scheuven, Jörn Kasbohm,  
Daniel Uteau, Alfons Van den Kerkhof

May, 2023

---

# Mineral transformation and sorption at elevated temperatures in fractured crystalline rocks and barrier materials (MUSE)

## Summary Report on Mineralogy of crystalline rocks

### Abstract

Different altered crystalline rocks of two locations from URL Kurt, South Korea (O3 core granite and granitic dyke rocks) and URF Bukov, Czech Republic (O1 hydrothermal altered cataclasite - S8, O1 fracture filling – S8, O1 fracture filling – ZK2, O1 fault breccia filled fractures – BZXII-J) were characterized in order to study on the possibility to use as host rocks of natural barrier for HLW-repository. The characterization works were organized by GRS-gGmbH with the main part of the work concerning characterization of petrology and mineralogy that were performed at the Technical University of Darmstadt, University of Göttingen, and University of Kassel. This report was compiled with the aim to summarize the results, and to compare the results gained in different analyzed methods. The lack of geological settings has limited the interpretation on history of alteration concerning the geological activities in the past. Otherwise, the primary rocks were strongly altered by impact of hydrothermal activities at high range of temperature and low pressure in complicated composition of fluids.

The association of secondary and transformation processes of primary minerals in granite and granitic dykes rocks of URL Kurt (saussuritization, sericitization, albitization, calcitization, scapolitization) have suggested that the metasomatic process was started with a highest temperatures of hydrothermal could be reached to > 400 °C and cooling down to lower temperatures at about 200 °C. Otherwise, the rocks in URF Bukov showed not much high hydrothermal temperature as URL Kurt but also high with temperature range from boiling geothermal of ca. 300 - 400 °C to ca. 200 °C.

The fractures and veins of URL Kurt are filled by scapolite but not carbonate as previous identification. Otherwise, veinlets and micro-cracks inside the rocks are filled by secondary calcite with very fine grain sizes which are observed under microscopy and confirmed by low amounts of this phase from XRD- and FTIR-measurement. The fracture filling S8 of

metamorphosed cataclasite from URF Bukov are composed of granular calcite with coarse grain sizes. They are formed at high temperatures of hydrothermal boiling fluids (300 – 400 °C). In addition, the veinlets and voids in the rocks are filled by microcrystals of calcite which are formed at lower temperature together with transformation processes during hydrothermal events (ca. 200 °C). Another type of carbonate (calcite) is detected as alteration of feldspar and mica as microcrystals of calcite grow on the surface of primary minerals as observed under microscopy.

The secondary minerals indicated a variable range of temperature which additionally controls the behavior of trace element and REEs in the rocks together with host bearing REEs of original impurities. The inhomogeneity of rocks leads to a difficulty in selecting materials for further elevated experiments as well as causing a non-representative of analyzed materials for whole rocks. In addition, the widespread distribution of fractures, veins, and voids systems in the rocks probably could lead to the instability of rocks by increase of porosity and decrease of density during thermal treatment experiments.

Eight sub-cores in granite, breccia and metamorphosed cataclasite were drilled for further experiment. The uncompleted form of the sub-cores has limited the porosity of whole sub-cores. The  $\mu$ CT shows abundant of fissures inside the rocks and therefore it is expected that the stability of rocks will be strongly changed after experiment runs.

**Keywords:** granitic rocks, metamorphosed cataclasite, altered breccia, characterization, mineralogy, fracture filling, hydrothermal alteration, calcite, carbonate

## Content

Abstract	1
Contents	3
Introduction	4
Chapter 1. Petrology, Mineralogy and Rock Characterization	5
1.1 Studied localities and sampling of sub-samples	5
1.2 Petrological and Mineralogical Characterization	7
1.2.1 X-ray diffraction (XRD)	7
1.2.2 Fourier Transformed Infrared Spectroscopy (FTIR)	11
1.2.3 Polarized Microscopy	14
<i>Granite from URL Kurt</i>	15
<i>Granitic dykes from URL Kurt</i>	17
<i>Metamorphosed S8 and S8 carbonate fracture filling from URF Burkov</i>	20
<i>Fracture filling ZK2 from URL Burkov</i>	21
1.2.4 Optical Cathodoluminescence Imaging	25
<i>Bulk material of fault breccia (BZ-XII-J)</i>	25
<i>Carbonate fracture filling S8</i>	25
<i>Fracture filling ZK2</i>	25
1.2.5 Scanning Electron Microscopy (SEM-EDX)	29
Chapter 2. Mineralogy and alteration of host rocks in hydrothermal systems	34
2.1 Granite and granitic dyke rocks in URL Kurt	34
2.2 Rocks in URF Bukov	39
Chapter 3. Relation between mineralogical transformation processes and trace elements	43
Chapter 4. Sub-cores of elevated temperature experiments	46
4.1 Sub-core drillings	46
4.2 Porosity and density of sub-core materials	47
4.3 Structural investigation of sub-cores by $\mu$ CT	48
Chapter 5. Summary and Conclusions	52
Chapter 6. References	54
Appendix	61

## Introduction

This report summarizes results from a joint research project on characterizing the primary lithological types by description of petrographically and mineralogically from rocks in URF Bukov (Czech Republic) and URL Kurt (South Korea). The project is funded by BMWi and initiated by the Gesellschaft für Anlagen- und Reaktorsicherheit (GRS) mbH, and TU-Darmstadt carried out the work.

Different methods were applied in this research, the sample preparation and petrological, mineralogical investigation were made at the Institute of Applied Geosciences – TU-Darmstadt.  $\mu$ CT studies of sub-core materials were performed at Faculty of Organic Agricultural Sciences, University of Kassel and Cathodoluminescence microscope (CL) of infiltrated carbonates were analysed at Institute of Applied Geology, University of Göttingen.

This study aims to present material characteristics of different crystalline rocks in URF Bukov – Czech Republic and URL Kurt – South Korea. Material characterization was conducted in respect to stability and their possible use as host rock in nuclear waste repository.

All analyzed methods, techniques, and results and their evaluation are based on petrological, mineralogical research approaches. The studied rocks come from different genetic origins – granitic and granitic dyke rocks, metamorphic rocks and their hydrothermal fractures fillings, together with tectonic fault breccia filled with carbonates but geological settings are missing in this work. Two main works of this study were carried out: (1) Petrological and mineralogical analysis of bulk materials basing polarized microscopy, FTIR and XRD-measurement to interpret the hydrothermal alteration of 5 rock specimens in Kurt and 4 rock specimens in Bukov. The thin sections were analyzed at the microscopy lab, TU-Darmstadt. Petrological and structure of filling carbonate by SEM-EDX, CL are additionally implemented at TU-Darmstadt and University of Göttingen. (2) Preparation of sub-core samples for elevated temperature experiments as well as analysis of untreated sub-core including density, porosity, and  $\mu$ CT are implemented at TU-Darmstadt and University of Kassel.

The objective of this report are to present summary of the studies done for untreated materials for elevated temperature experiment and compare the petrology and mineralogy of untreated rocks from different methods with the aims (1) to understand the geological history of the primary rocks and (2) transformation of the rock under hydrothermal conditions as well as (3) their relation to behavior of trace and REEs element are other additional purposes of the research.

# Chapter 1. Petrology, Mineralogy and Rock Characterization

## 1.1. Studied localities and sampling of sub-samples

Crystalline rocks were obtained and supported from two locations of Bukov, Czech Republic (Fig 1.1) and Kurt, South Korea (Fig 1.2).

The light colored granitic and granitic dyke rocks are collected from different depths in URL Kurt (Fig. 1.2). Their granular textures of medium to large grain size and mostly in semi-shaped are typical for granite rocks. It is very often seen in rocks the presence of large crystals of feldspars and quartz. The rocks are strongly hydrothermally altered and cut by numerous small fractures, veins, and veinlets systems (mm to 0.1-0.5 cm). They are filled by light color mineral phases which which were previously descriptive as carbonate. Unfortunately the hand-picked fracture materials show no reaction with HCl 1M; therefore it is assumed that the filling materials of granite and granitic dykes are composed of different phases instead of carbonates. The sub-samples of rocks were selected for further investigation and shown in Tab 1.1.

Rocks core in URF Bukov (S8) (Fig 1.1A) is characterized by medium to fine grains of dark color (dark grey to light red) which was identified as metamorphosed gneiss to cataclasite and lately identified as metamorphosed cataclasite under microscopy investigation. A large fracture (~ 0.5-1.5 cm thick) of carbonate cut through the core and a number of veins and veinlets developed in the rocks. The large fulfill fractures of this core were separated to investigate in detail (Fig. 1.1B) and namely D8 fracture filling.

The hand specimen ZK2 (Fig. 1.1D) is another fracture filling which is flattened in form, showing a strong reaction with HCl 1M of carbonate minerals. The rock is composed of light with bands of red carbonate. Their grains are largely associated with the fine grains of dark mineral phases. Surface of the rocks is covered by a layer of dark green fine grains of sheet silicate minerals which is probably chlorite.

The veins and cracks systems are widely occurred as hydrothermal breccia with thick fillings (up to 1 cm). The fracture fillings materials are white and some bands of light minerals. They show a weak reaction with HCl 1M, thus, are expected of Ca-, Mg- and/or Fe-contained carbonates. Macroscopic description presented large euhedral carbonate crystals. They grew either continuously from the host rock towards the middle of veins or fractures. The accessory minerals (chlorite) appear locally in the large voids of the rock or along the vein-host rock contact. They are dark green in color and covered coarse grains. The carbonate shows blocky to elongated blocky anhedral crystals (Fig. 1.1E)

In general, the macro observations show that the rocks in URF Bukov are strongly hydrothermally altered with a lot of fractures, cracks, and veins which are varied from mm to several centimeters and filled by secondary minerals. With the aim to investigate the petrological and mineralogical characteristics of the rocks, different sub-samples were picked and analysed by different methods applied as indicated in Tab. 1.1.

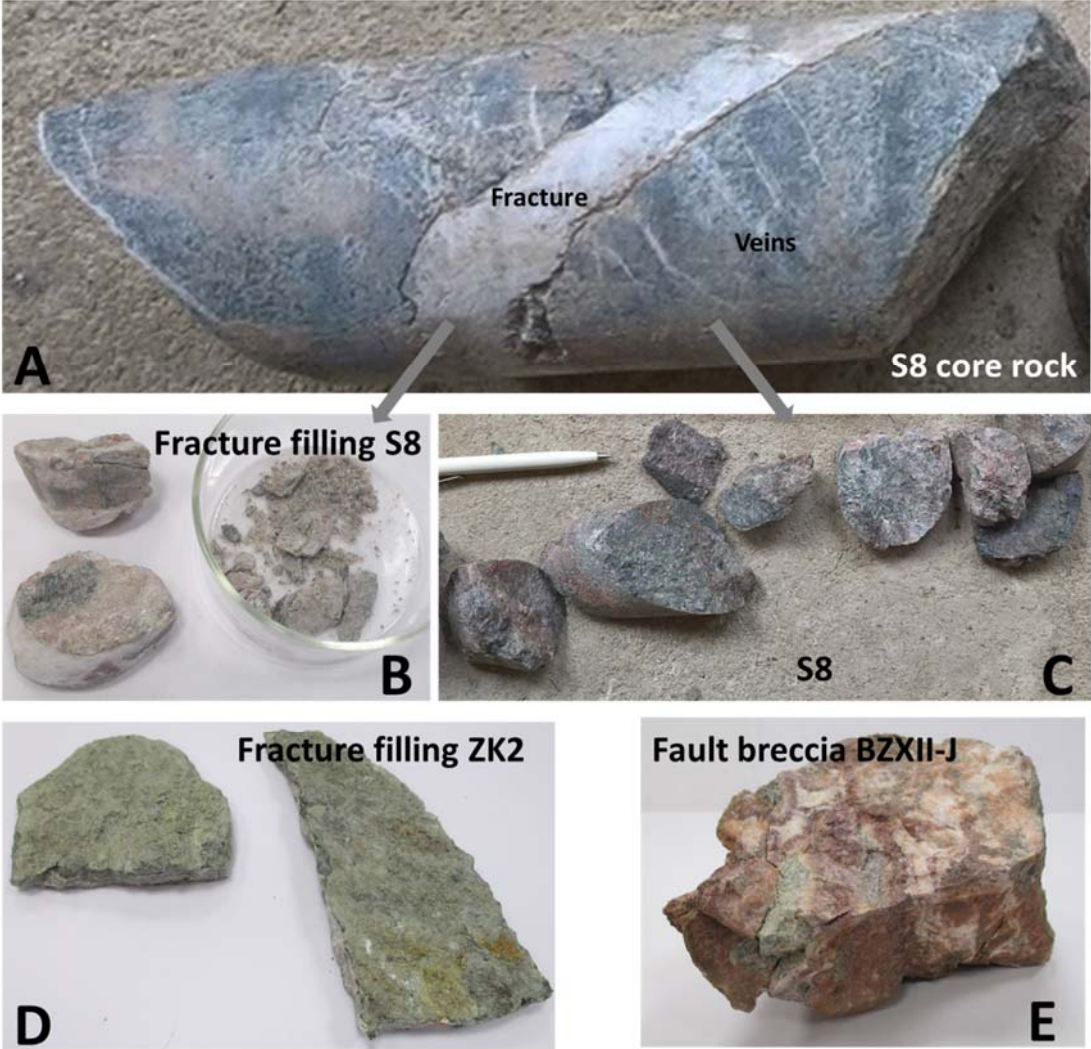


Fig 1.1 Original hand specimens from URF Bukov, full core rock with main fracture and veins of S8 (A)- fracture filling S8 from A; (B) - hydrothermally altered S8 from A, (C) fracture filling ZK2, (D) fault breccia, carbonate - filled fractures BZXII-J.

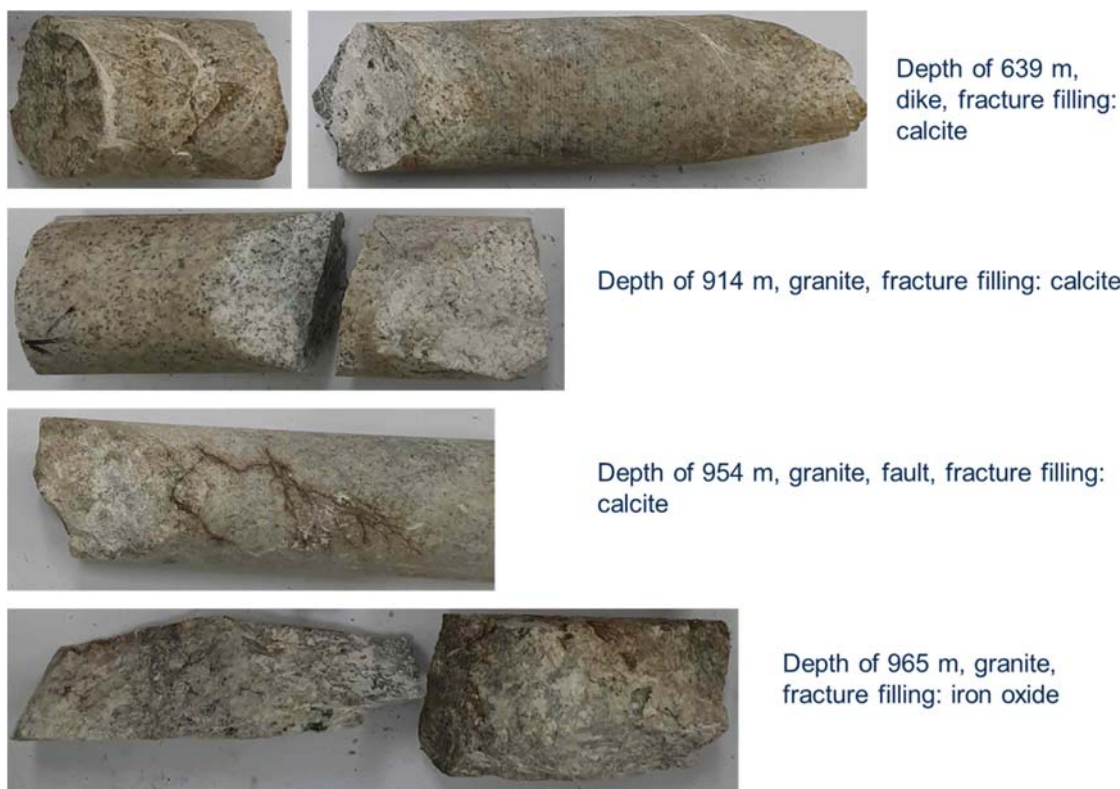


Fig 1.2 Original core samples of granitic rocks from URL Kurt

Tab. 1.1 Samples, sub-samples and applied measurement

Samples	Sub-samples	Sub-cores*	Location	Measurement	Sub sample description	
Granite	Granite 458m		URL Kurt	XRD, PL, SEM	bulk rock	
	Granite 914 m			XRD, PL	Granite in different depth	bulk rock
	Granite 954 m	•		XRD, PL, SEM		bulk rock
dykes of granite	D4		URL Kurt	XRD, PL, SEM	Depth of 639 m, dike, fracture filling	detrital of feldspar in vein
	D5			XRD, PL		bulk rock with vein of feldspar
	Dyke 639-02	•		XRD, PL, SEM, $\mu$ CT	Dyke of granite	bulk rock
hydrothermal cataclasite	S8	•••	URL Bukov	XRD, FTIR, SEM (2)	Gneiss S8, hydrothermal vein (calcite) + cataclasite	bulk rock
	S8-6.2			XRD, FTIR		bulk rock with small vein of calcite
	S8-6			XRD		bulk rock
	S8.7			XRD, FTIR		Bulk rock with calcite
	S8-7.3			XRD, FTIR		Bulk rock with calcite
	S8.9			XRD, FTIR, CL, SEM		Calcite
Fracture infill	S8.11		URL Bukov	XRD, FTIR	ZK2 fracture infill	Small vein of calcite and chlorite
	ZK2-03-03			XRD, FTIR, CL, SEM		chlorite covered calcite
	ZK2-03-04			XRD, FTIR, $\mu$ CT		bulk rock
Breccia	BZ XII-J06	•••		XRD, FTIR, CL, SEM (2)	Breccia BZ-XII_J fault breccia, dolomite-filled fractures	bulk rock

Note: \* sub-cores with porosity, density and  $\mu$ CT-measurements

## 1.2. Petrological and mineralogical characterization

### 1.2.1 X-ray diffraction (XRD)

The powder XRD is a non-destructive analytical technique used to identify the crystalline composition of solid materials through diffraction of X-rays by the lattice planes of atoms within materials. Incident X-ray are hit on the samples and reflected from the parallel planes

of atoms of minerals. They are realized by distinguishing orientation through Miller indices. The diffraction patterns indicated bulk properties of structure. The Bragg law equation was applied to observe the relationship between the wavelength of the incident beam ( $\lambda$ ), the angle of incident beam entry and parallel planes of atoms causing the diffraction ( $\theta$ ), as well as the distance between these planes ( $d$ ). The delivered XRD-pattern represents scans of randomly oriented powders of bulk samples to determine their general mineral composition. XRD-diffractograms of powder materials from studied rocks were recorded over the range  $4 - 70^\circ 2\theta$ , using Panalytical X'Pert Pro Diffractometer (Cu-  $K\alpha_{1,2}$  radiation; 40 kV; 30 mA; 0.5/25 soller collimator, automatic divergence slit, step size  $0.008^\circ 2\theta$ ; time per step 50 s; X'Celerator Scientific line focus detector; 240 mm goniometer PW3050/60 radius) at Institute of Geosciences, Goethe University in Frankfurt am Main. The processing of XRD powder patterns included Rietveld refinement for semi-quantitative determination of essential mineral components by using the software PROFEX (Döbelin and Kleeberg, 2015) as a graphical interface, which has embedded the BGMN software package (Bergmann et al., 1998; Ufer et al., 2008). XRF results are used for an additional cross-checking with XRD results. The  $d(060)$ -value was used to determine the main contribution of individual clay components in the samples (Moore and Reynolds, 1997).

X-ray powder diffraction diagrams of bulk samples from URL Kurt and URF Bukov are presented in Fig 2.1 - 2.4 and mineralogical identification in each sample are summarized in Tab 2.1, in which the semi- quantitative compositions are shown. The additional data of Rietveld refinement from Profex-BGMN are presented in Appedix 1.

The granite rocks at depth of 639 m in Kurt are composed of granitic rock forming minerals with main composition of quartz, mica (illite 2M1-polytype), feldspar (K-feldspars and plagioclase) with trace of fluorite and fluorapatite, no trace of amphibole is found in both samples. The same observation is found in thin sections. The other minerals are identified as secondary phases from hydrothermal alteration of primary rocks. The high amount of zeolite mineral group from laumontite and heulandite occurred in both D4 and D5 samples, especially content of laumontite in D5 reached 40 wt%, but a trace of clinoptilolite is found in D5. Additionally, calcite is detected in the D5 samples but occurs as trace, this phase is not appeared in D4. A large amount of secondary epidote (57 wt%) is probably related to epidote fulfillments in veins of rock as observed in thin section. The availability of chlorite and illite in both samples is comparative with microscopy observation of thin section which indicated that they are products of hydrothermal alteration from biotite and feldspar, respectively.

At different depth, the main phases in mineralogical compositions of granite rocks are limited, and are similar to granitic dykes materials but instead of zeolite, scapolite marialites found as impurities at  $3.86 \text{ \AA}$ ,  $3.46 \text{ \AA}$  and  $3.04 \text{ \AA}$  as impurities (Tab 2.1). In general, the granitic rocks in URL Kurt are strongly hydrothermal altered but the main phases are still recognized. The secondary minerals are detected largely in the rocks and developed mainly

in fractures, veins and voids system as well as growth on primary phases. It was assumed that carbonates are main phases in fractures of rocks but the XRD-diffractograms show differently with trace amount of these phases in rocks.

Three rock specimens in Bukov are employed in this research including ZK2-fracture fill material, hydrothermal altered gneiss S8, and breccia BZ-XII-J. They are all inhomogeneous due to the large fracture systems which are filled by different phases as observed from hand pieces; therefore, the mineralogical compositions of them are variable from area to area. The bulk material of fracture infill ZK2 is composed mainly by calcite, K-feldspar, quartz and chlorite. Titanite is found in traces. Otherwise, the hand-picked powder from this rock contains high amount of chlorite, calcite, quartz, and plagioclase with traces of illite and titanite. The bulk material of breccia rock (BZ XII-J06) contains carbonates of ankerite, dolomite, quartz and barite (Tab 2.1). The mineralogical composition of metamorphosed S8 is quite similar between bulk rocks and bulk rocks with veinlets of calcite which contain main components of quartz, plagioclase, chlorite, illite and calcite. Otherwise, 94 wt% calcite with small amount of quartz (4 wt%) are found in large fractures (fracture filling S8).

Tab. 2.1. Mineral matter of bulk samples – semi-quantitative results by PROFEX/BGMN-processing

Phases/ Samples (wt.%)	D4	D5	Granite 458m	Granite 914 m	Granite 954 m	Dyke 639- 02	S8	S8-6.2	S8-6	S8.7	S8-7.3	S8.9	S8.11	ZK2-03- 03	ZK2-03- 04	BZ XII- J06
Calcite		3	2	1	1	1	8	9	9	17	17	96	4	11	70	7
Ankerite		1														30
Dolomite																23
Illite_2M1	6	2			4	3	23	8	8	9	8		16	2		
Illite_1M			7	10	6	8	0						31			
Chlorite	3	7	3	6	9	4	22	19	19	24	26		11	59	4	
Quartz	15	13	33	27	22	26	0	30	30	29	29	4	19	17	11	22
K-feldspar	20	6	16	17	13	19	29								11	
Plagioclase	6	4	31	37	42	37	15	34	34	20	20		17	7		
Scapolite			3	1	2	2	3									
Laumontite	41	5											2			
Heulandite	7															
linoptilolite		1														
Titanite	1													4	5	
Epidote		56	5	0	2	1										
Fluorite		1														
Fluorapatite		1														
Barite																19

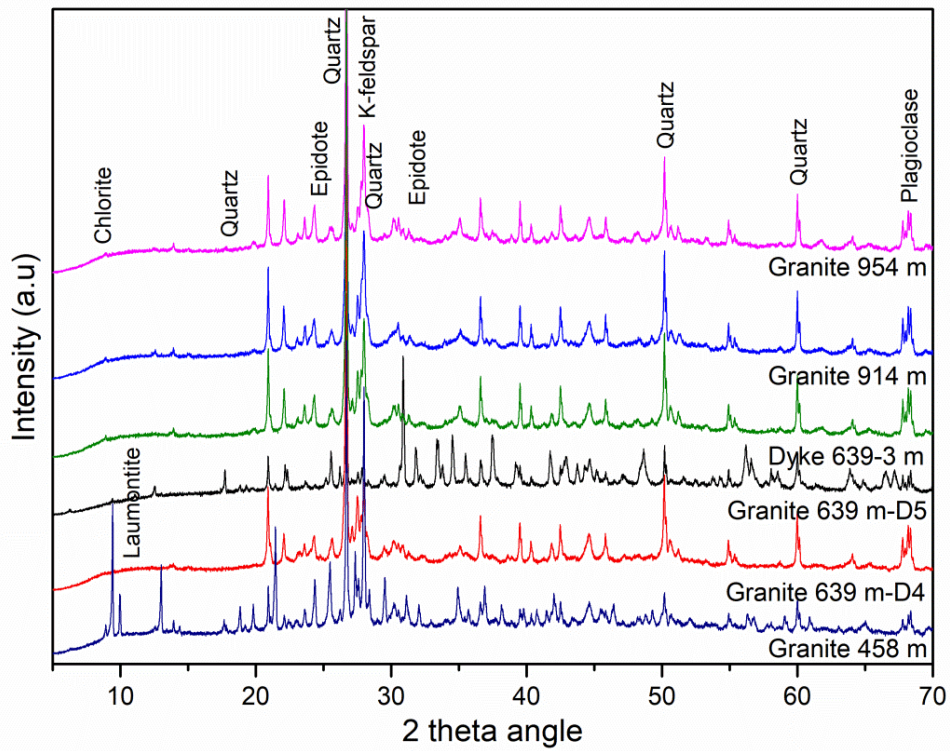


Fig 2.1. X-ray diffractograms of altered granite at different depth and dyke in Kurt, South Korea

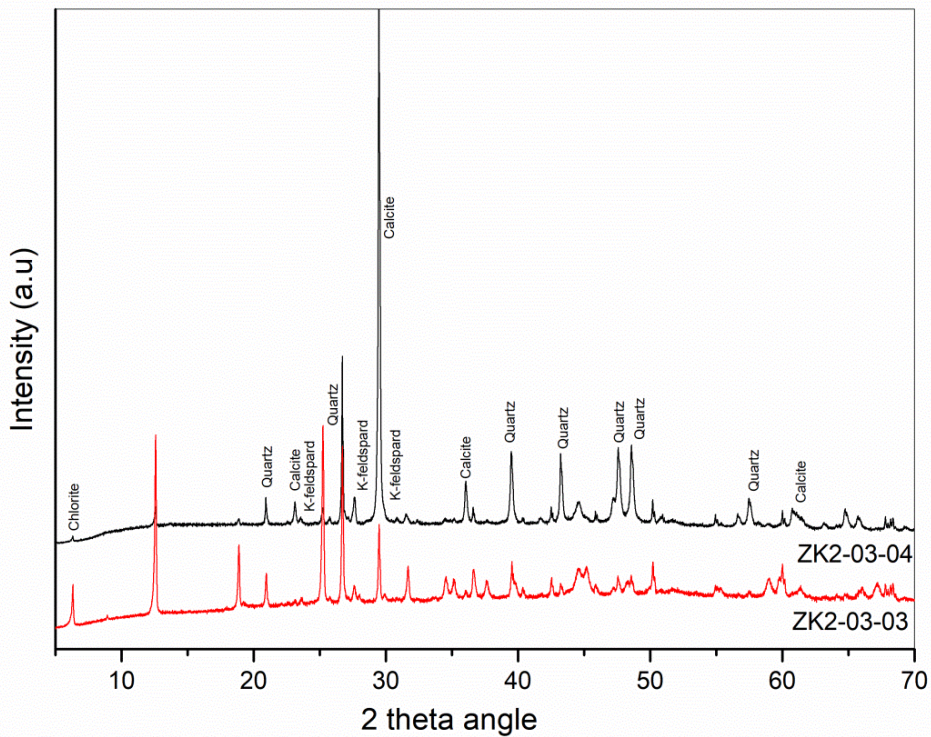


Fig 2.2. X-ray diffractograms of fracture fill (ZK2) in Bukov, Czech

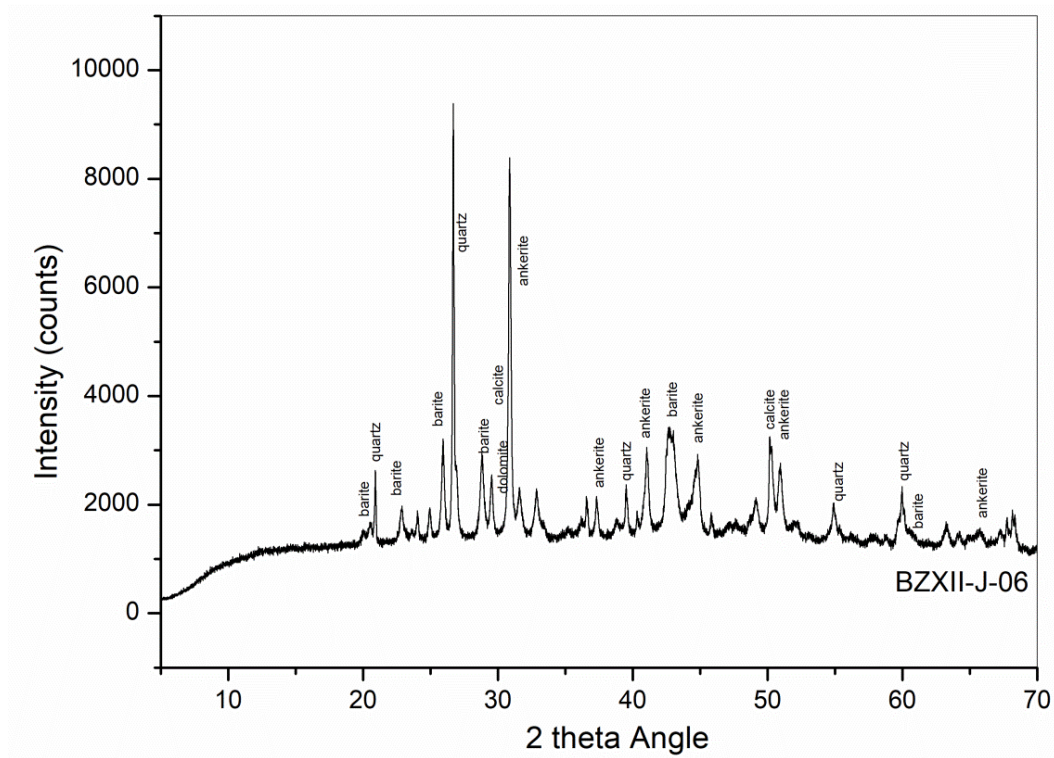


Fig 2.3. X-ray diffractograms of breccia (BZXII-J) in Bukov, Czech

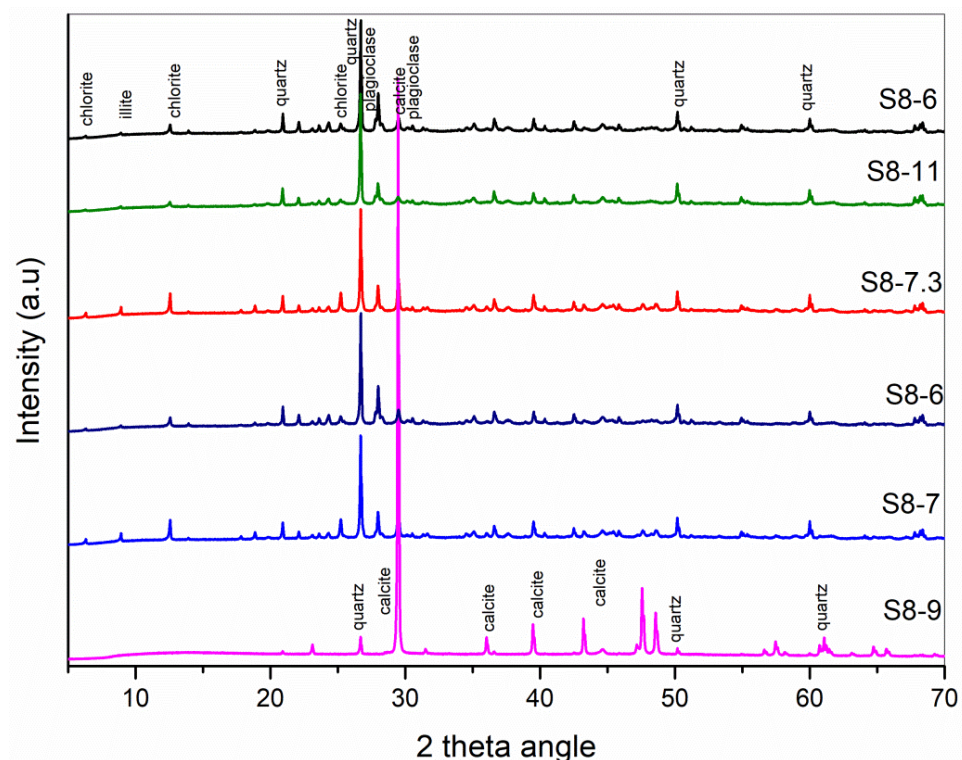


Fig 2.4. X-ray diffractograms of gneiss S8 in Bukov, Czech

### 1.2.2 Fourier Transformed Infrared Spectroscopy (FTIR)

Powder materials of approximately 1-2 mg were mixed homogenously in 120 mg of KBr, which was dried before at 80 °C for at least 6 h, and then placed into a dye under pressure to

form a pellet of 13 mm in diameter. The Varian 670-IR series FTIR spectrometer at TU-Darmstadt was used for recording the spectra of molecular vibrational frequencies in the infrared region of the electromagnetic spectrum in the mid-infrared range, which extends from 400 – 4000  $\text{cm}^{-1}$  with the aim to identify functional group (i.e OH or free water). Vibrations and rotations cause a net change in the dipole moment result in bonds stretching or bending, characterized by frequency, intensity, and band shape unique to each molecular (Balan et al., 2017, Larkin et al., 2018). A Gaussian distribution function was applied to smooth the spectra and to provide the exact value of peak position. The observed wavenumbers of the bands are assigned and analyzed using available literatures of Adler and Kerr (1963), Farmer and Russell (1964). In this work, the FTIR-scans were implemented for rocks in URF Bubov with the aims to identify the carbonate phases in the rocks.

The sub-samples of gneiss S8 are characterized by quartz, plagioclase, calcite, chlorite and illite, but the position wavenumber of them in OH-stretching and OH bending regions are variable due to varying strength of hydrogen bonding between OH and  $\text{H}_2\text{O}$  molecules and some  $\text{O}_2$  in the structure. Otherwise, a handpicked infiltration in fracture of small vein (S8.9) composed purely calcite and trace of quartz.

Carbonate phases in this series of samples are identified as calcite from XRD-measurement. In the mid infrared region (1400 – 1500  $\text{cm}^{-1}$ ) of the spectra, the vibrational modes of the carbonate ions are recognized apparently. The assemblages of the bands in the range 1421-1423  $\text{cm}^{-1}$  and bands at 710, 882, 1803, and 2522, 2868, and 2984  $\text{cm}^{-1}$  are assigned for calcite minerals.

Illite and chlorite are two typical clay minerals in the rocks which appeared widely under thin section and X-ray diffraction. The bands of illite are appeared in bulk rocks (S8-6.2; S8-6; S8-7.3) and small vein (S8.11), the sharp bands of Si-O bending vibration modes in the region of 550 – 900  $\text{cm}^{-1}$  involve the interaction between the hydroxyl group and the octahedral cations as well as those of Si-O framework which are typical for all dioctahedral micas. Furthermore, it is know that the OH-stretching vibration band is near 3620  $\text{cm}^{-1}$  and Si-O stretching vibration at 1019-1022  $\text{cm}^{-1}$  are for illite. Otherwise, the other bands in OH-stretching regions (3400 – 3700  $\text{cm}^{-1}$ ), Si-O bending at 789-791  $\text{cm}^{-1}$  are assigned for chlorite and they are shared with illite and quartz, respectively.

Quartz: the Si-O bonds of quartz are the strongest bonds in the silicate structure and can be realized in the infrared spectra by very strong bands in the region 900 – 1100  $\text{cm}^{-1}$  but they appear less strong in OH-bending region of 400 – 800  $\text{cm}^{-1}$ . In addition, the appearance of bands in the range of 465 – 471 and 510-519  $\text{cm}^{-1}$ , 693-711  $\text{cm}^{-1}$  due to Si-O asymmetrical bending vibrations, and 778-780 and 791 – 795  $\text{cm}^{-1}$  due to Si-O symmetrical stretching vibrations is all attributed to quartz.

Feldspar: the observation of bands in the range 579 – 589  $\text{cm}^{-1}$  due to O-Si(Al)-O bending vibrations and broad band of absorption by structural O-H bond vibration ( $\sim 3,700$  to  $\sim 3,100$   $\text{cm}^{-1}$ ) are typical for plagioclase feldspar.

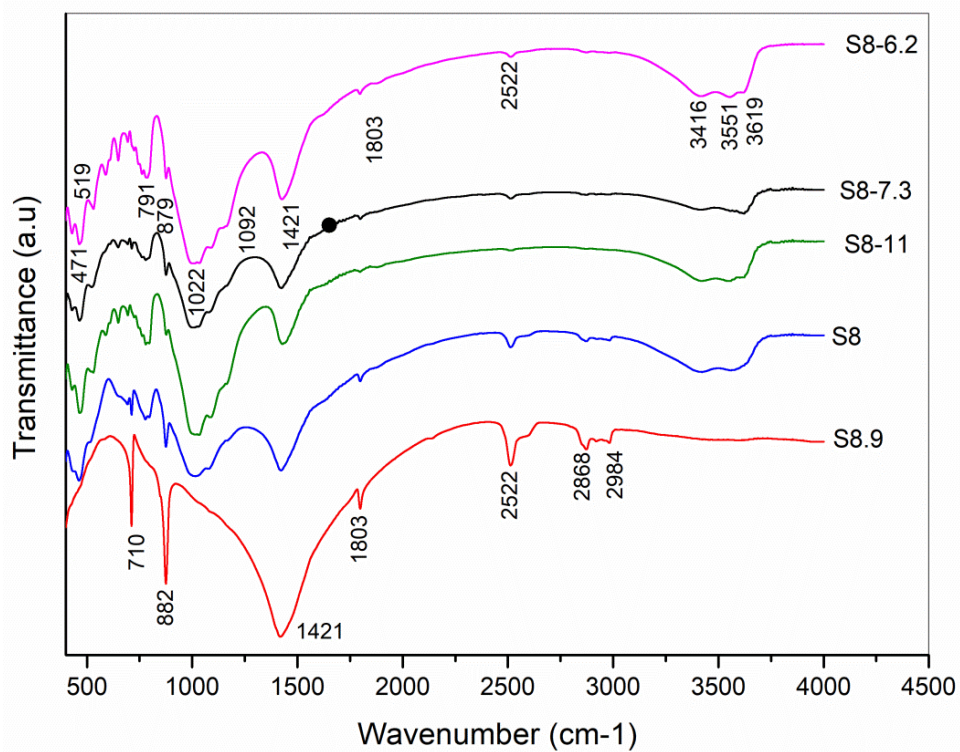


Fig 3.1. FTIR spectra of sub-samples from gneiss S8 rock

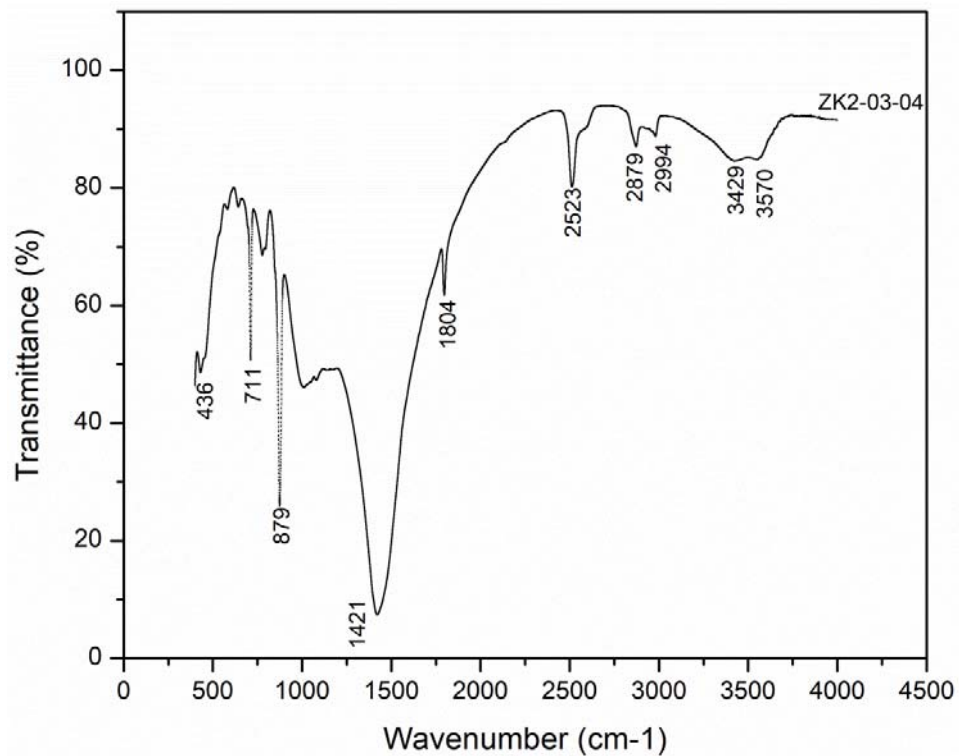


Fig 3.2. FTIR spectrum of bulk material fracture infill rock (ZK2)

The FTIR spectrum of fracture infill rock ZK2 is typical for high content of carbonate minerals which was identified as calcite under XRD-measurement. The calcite bands are range from 711 to 2994  $\text{cm}^{-1}$ . Signs of quartz and K-feldspars are found at Si–O frame work and Si-O bending regions.

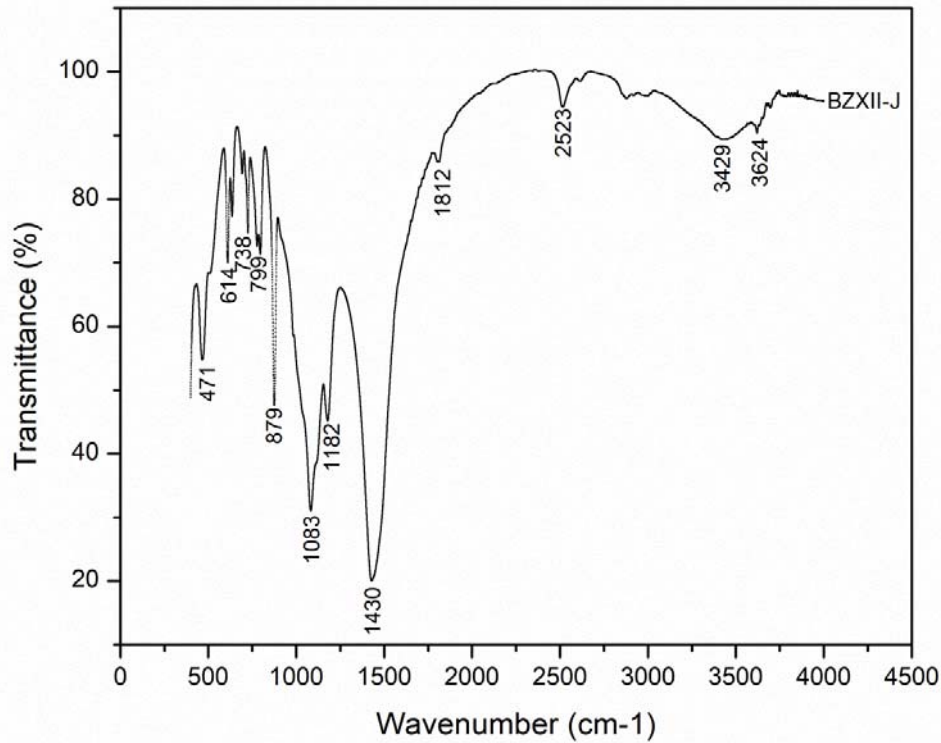


Fig 3.3. FTIR spectrum of bulk material from breccia rock (BZII-J)

The bulk material of breccia rock is characterized by carbonate (calcite, ankerite, dolomite) due to presence of bands at 879, 1403, 1812, 2523  $\text{cm}^{-1}$ , and quartz at 799  $\text{cm}^{-1}$ . The vibration of Si-O stretching at 3429, 3624  $\text{cm}^{-1}$  and Si-O bending at 1038  $\text{cm}^{-1}$  are ascribed to feldspar. Moreover, barite is identified by strong peaks at 614  $\text{cm}^{-1}$  (Ba-S-O polyhedral stretching which is the sheet structure of barite minerals), shoulder at 1050  $\text{cm}^{-1}$  (triple asymmetric S-O stretching and  $\text{SO}_4^{2-}$  tetrahedral stretching), a share vibration at 1182  $\text{cm}^{-1}$  with feldspar shows the asymmetric and bond vibration.

In general, the assignments and identification of mineralogical phases under investigation of infrared spectra are in good agreement with the observations in thin section and XRD-measurement (Tab 1.1).

### 1.2.3 Polarized Microscopy

Optical microscopy (polarized light microscopy) studies on the interaction of light with minerals, usually involving visible light and non-opaque minerals. This is a powerful method for analyzing minerals and understanding their texture in details. The polarizing microscope polarizes the light from light source and allows it to pass through the rock material, where the light is refracted by the crystalline structure of the mineral. In birefringent minerals the

polarized beam is split into two beams with a fast and slow direction. The optical path difference finally causes interference colors under crossed polarizers. The interference colors can be produced together with the color (pleochroism) of a mineral. Its refractive index, cleavage, and other criteria are used to identify minerals in a thin section. Additionally, this method allows defining the microstructure, and the alteration history of rocks. In this study, nine representative rock samples from URL Kurt and Bukov (bulk rock, veins, fracture infill) and URL Kurt (bulk rock, fracture fillings) (Table 1.1) were analyzed at the Technical Petrology Lab (Technical University Darmstadt).

### ***Granite from URL Kurt***

Texturally, the granites are phaneritic, and their grain size varies from medium- to coarse-grained. The majority of the grains are subhedral to euhedral therefore representing a hypidiomorphic texture (Fig 4.1, 4.2, 4.3). The rock is primarily composed of feldspar (plagioclase, K-feldspar (microcline)) and quartz, while minor to accessory minerals are represented by opaques, titanite, and apatite. Magmatic amphibole and mica are missing in the rocks. Epidote, chlorite, sericite, and calcite are found as alteration products after primary phases. Plagioclase and microcline are mostly subhedral to euhedral lath-shaped with large grain sizes in comparison with other minerals. Both feldspars are intensively altered to fine-grained sericite. Otherwise, some microcline grains appear fresh but microcracks (mostly parallel to cleavages) are filled by sericite or calcite. Quartz is found less common in comparison with feldspar. It appears with an anhedral shape and abundant microcracks are developed. Growth of calcite and epidote is found in veins and voids of the rock (Fig 4.1A, 4.1D, 4.1F, 4.3C, 4.3C, 4.3D). Epidote is yellowish green with weak pleochroism, shows strong positive relief and mainly equant crystals. Apatite is enclosed in quartz and K-feldspar grains (Fig 4.2E). Completely chloritized biotite occurs in trace amount (Fig 4.1C, 4.2C). At the depth of 914m, fractures in the granite are filled by scapolite (Fig 4.2A)

In general, optical microscopy observations of the granitic and granitic dyke rocks indicate moderate to strong hydrothermal alteration of primary granites. The original mineralogical composition of these hydrothermally altered granite is mostly transformed to other phases, i.e. scapolites in fractures and veins, whereas calcite, epidote, sericite, Fe-oxides appears both in fractures and/or grew on primary minerals.

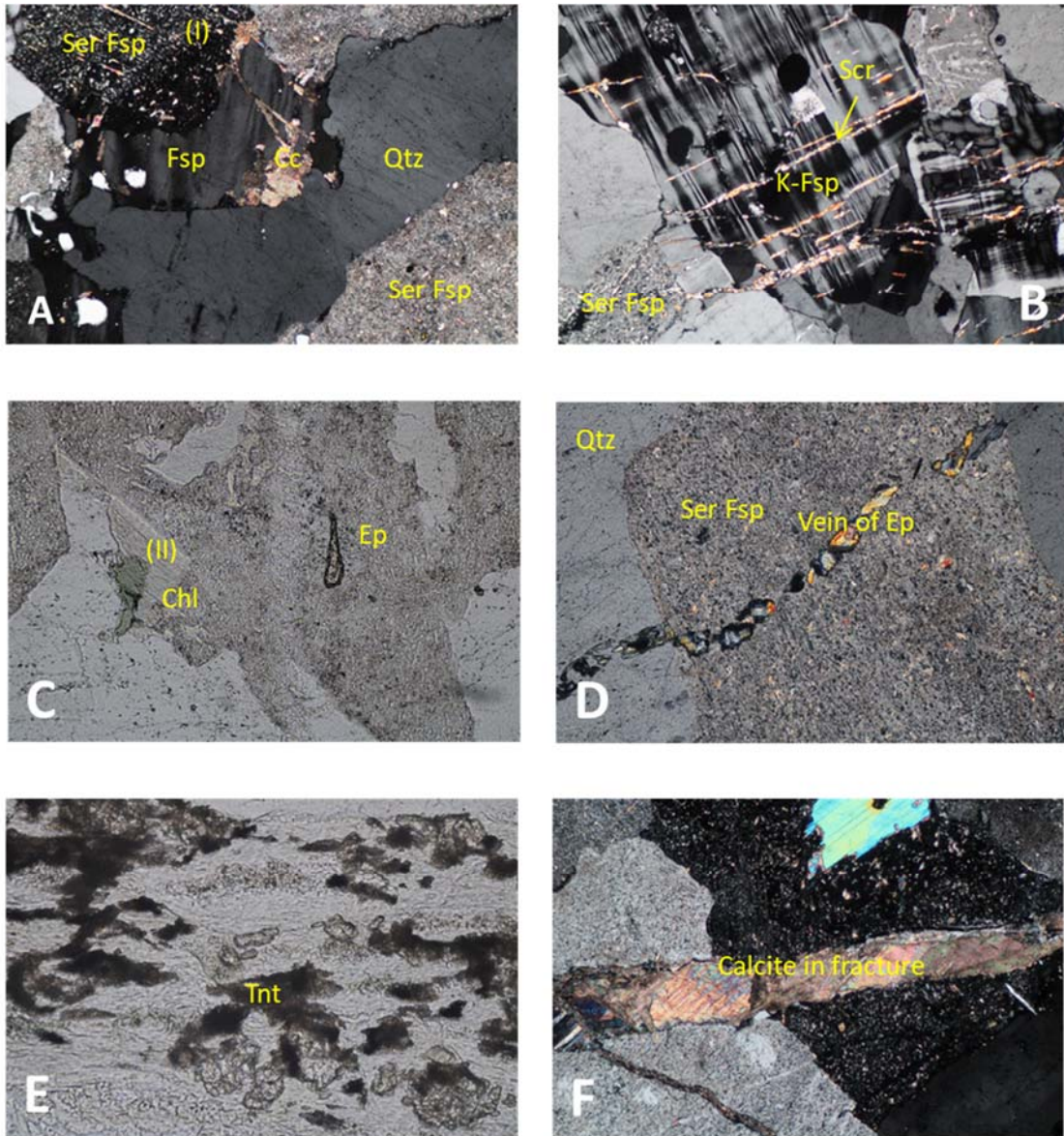


Fig 4.1. Microphotographs of representative textures of granite 458 m, URL Kurt. *Qtz* quartz, *Bt* biotite, *Chl* chlorite, *Ill* illite, *Plag* plagioclase, *Cc* carbonate minerals (in the XRD study detected as calcite), *ser Plag* sericitized plagioclase, *Kfs* K-feldspar, *Ttn* titanite, *Ep* epidote, *Cal* calcite, growth of sericite on feldspar (I) and chlorite on biotite (II)

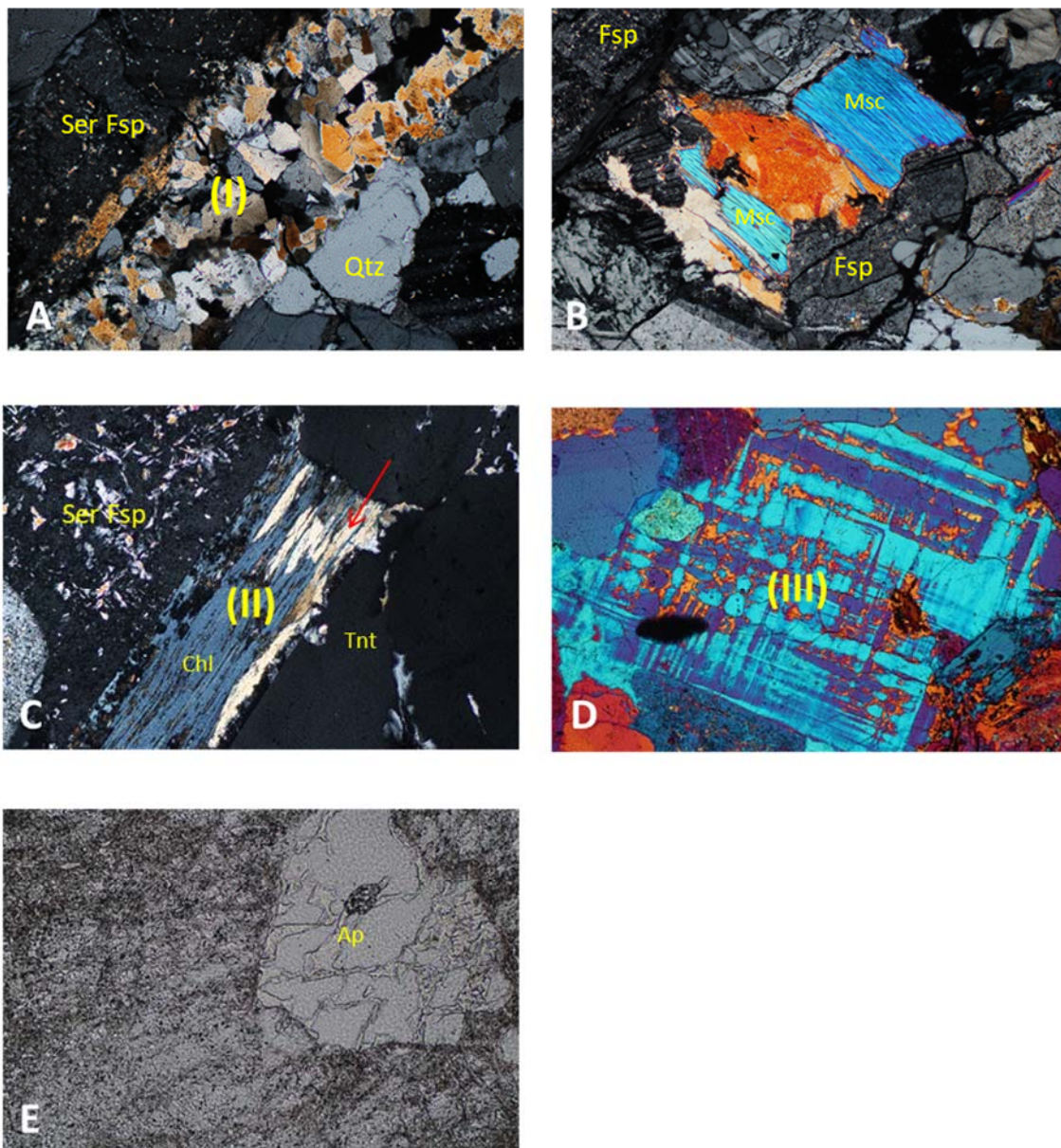


Fig 4.2. Microscopic observation of thin section from granite 954 m, URL Kurt. *Qtz* quartz, *Chl* chlorite, *Fsp* feldspars, *Cc* carbonate minerals, *Ap* Apatite, *Ser Fsp* sericized feldspars, (I) scapolite in filled fracture, (II) chloritization of biotite, (III) albitization of K-feldspar (image with crossed polarizers and inserted gypsum plate)

### **Granitic dykes from URL Kurt**

The granitic dyke samples are characterized by fine-grained euhedral minerals, with a few remains of phenocrysts (Fig 4.4, 4.5). They are composed of equi-granular quartz, plagioclase, and K-feldspar, while chlorite, sericite, epidote, carbonate, and actinolite occur in variable amounts as alteration products. Plagioclase and microcline are mostly subhedral. However, they are completely pseudomorphed either by sericite, chlorite or carbonate or a mixture of sericite and carbonate. Traces of albitization of plagioclase are found (Fig 4.4F). Sericite and carbonate filled microcracks and/or grew replace feldspar minerals. It is frequently observed pale yellow elongated subhedral actinolite grains (Fig 4.4B) occur as an essential product of altered minerals in this sample. The association of actinolite with

chlorite, epidote and quartz indicates formation temperatures above 280 °C and boiling in the geothermal system. Accessory chlorite and epidote are present together with trace amounts of calcite in the studied samples. Their size distribution is almost similar to that of actinolite. A conspicuous feature of the investigated samples is scapolite veins (Fig. 4.4D) which are probably a product of the alteration of feldspar. Scapolite grains appear as fine-grained, anhedral to subhedral crystals. In general, the granitic dyke rocks are mainly composed of quartz, pseudomorphosed feldspar, actinolite, chlorite, epidote, carbonate as a product of an intense propylitic alteration at high to intermediate temperatures and a low fluid/rock-ratio.

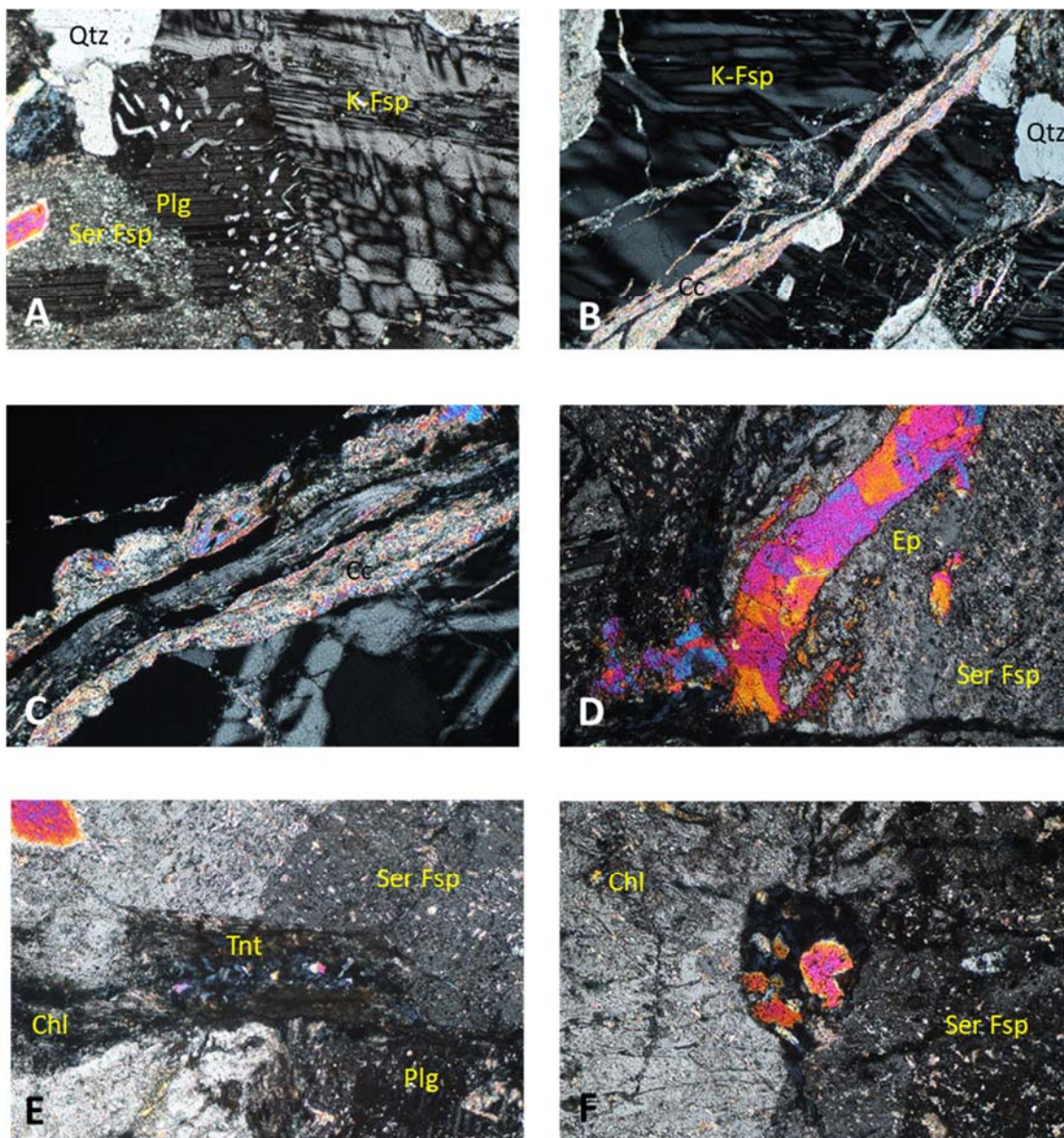


Fig 4.3. Microscopic observation of thin section from granite 954 m, URL Kurt, *Qtz* quartz, *Chl* chlorite, *Fsp* feldspars, *Plg* plagioclase, *Tnt* titanite, *Ep* Epidote, *Cal* carbonate minerals (in the XRD study detected as calcite), *Ser Fsp* sericitized feldspars, (A) partly sericitized plagioclase in contact with fresh K-feldspar (microcline), (B) calcite veins and veinlets in K-feldspar, (C) calcite and sericite in a vein in K-feldspar, (D) secondary epidote in a sericitized plagioclase, (E) association of sericitized plagioclase with chlorite and titanite

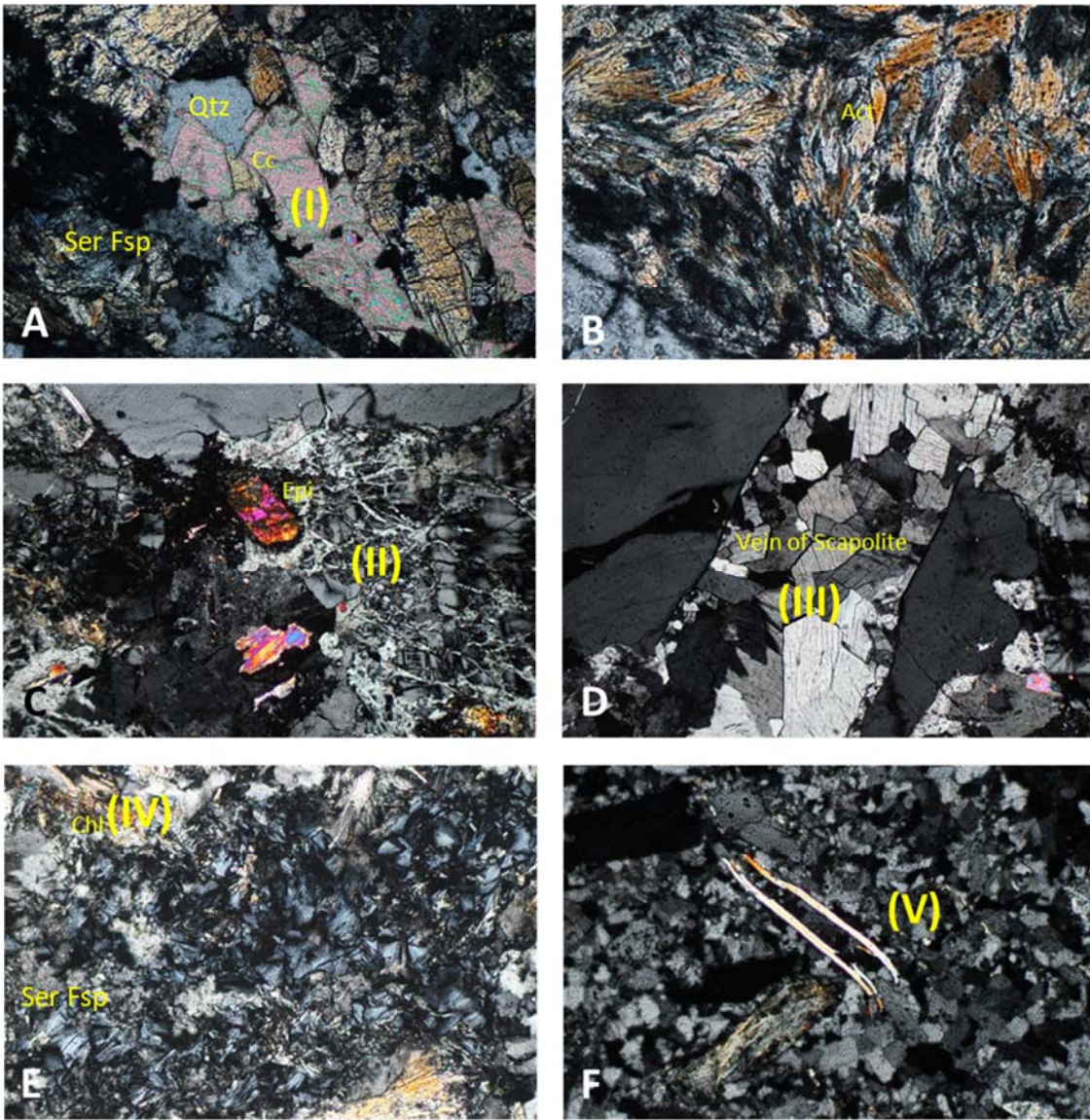


Fig. 4.4. Microscopic observation of thin section from granitic dyke-639m-01, URL Kurt shows propylitic alteration with assemblages of *Act* Actinolite, *Chl* chlorite, *Fsp* feldspars, *Cc* carbonate (in the XRD study detected as calcite), *Ser Fsp* sericized feldspars, (I) carbonate in voids, (II) Epidote embedded in K-feldspar, microcracks in K-feldspar are filled by carbonate and sericite (III) fracture-filled vein of scapolite, (IV) replacement of biotite by chlorite, (V) albitization of feldspar

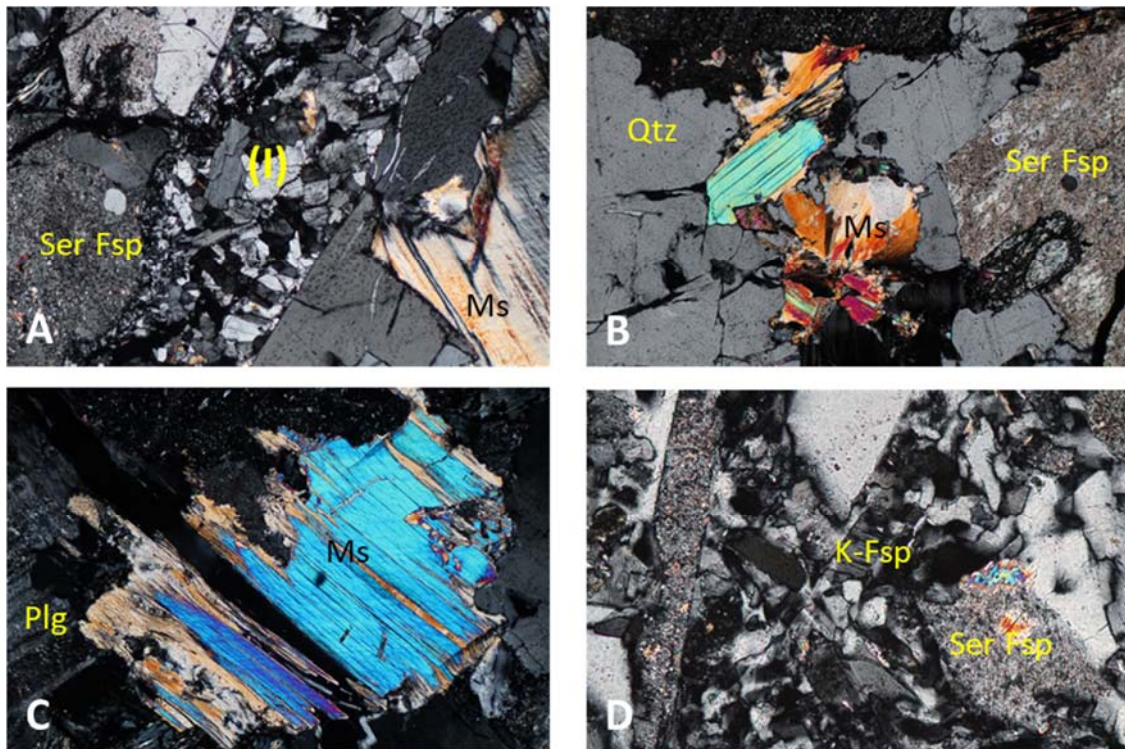


Fig 4.5. Microscopic observation of thin section from granite dyke-639m-03, URL Kurt shows propylitic alteration with assemblages of Fe-phylosilicate *Ap* Apatite, *Chl* chlorite, *Fsp* feldspars, *Cc* carbonate minerals (in the XRD study detected as calcite), *Ser Fsp* sericitized feldspars, (*I*) scapolite in filled fracture

### ***Metamorphosed S8 and S8 carbonate fracture filling from URF Burkov***

The study of two S8 rock samples by optical microscopy (Fig 4.6, 4.7) clearly indicates a significant grain size reduction. The rocks are extremely altered with abundant newly formed clay minerals as chlorite and sericite (lately identified as illite from XRD-data). Quartz and feldspar (plagioclase and K-feldspar) are the main constituents of the original rock. Single fresh crystals of biotite are rare because the original biotite was nearly completely transformed to chlorite (Fig. 4.6B, 4.7D). Intense alteration of plagioclase and K-feldspar to sericite is observed (Fig 4.6A, 4.6C). Carbonate (dolomite, calcite) and Fe-oxides crystallized from hydrothermal solutions which penetrated into microveins crosscutting the rock (Fig, 4.6A, 4.7) and/or replace K-feldspar grains and hence act as alteration products after primary phases. Euhedral apatite is associated with chloritized biotite (Fig 4.7E). The microstructure and mineral association suggests that sample S8 is a cataclasite that is composed of subangular rock fragments including quartz and feldspar.

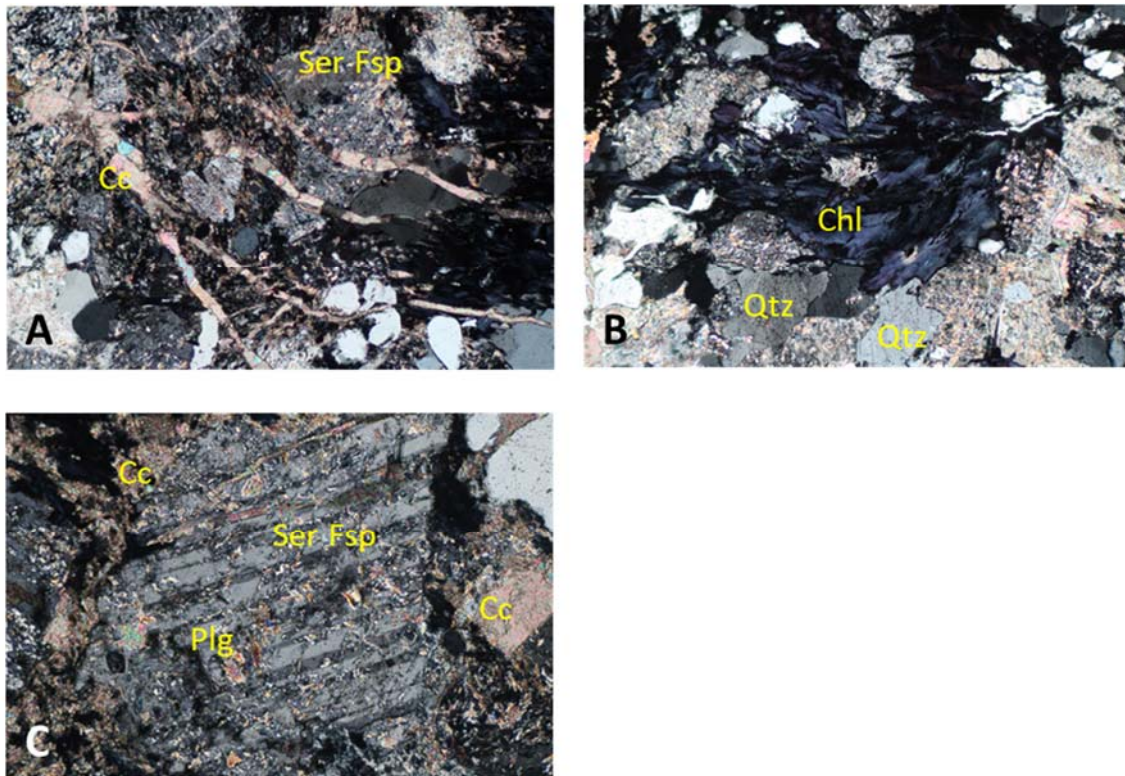


Fig. 4.6 Microscopic observation of thin section from carbonate fracture filling S8, URF Bukov shows hydrothermal transformation and a cataclastic microstructure. *Qtz* quartz, *Plg* Plagioclase, *Chl* chlorite, *Cal* carbonate minerals (in the XRD study detected as calcite), *Ser Fsp* sericitized feldspars, (A) calcite in veins cut through sericitized plagioclase and quartz, (B) sheets of chlorite with abnormal blue interference colors between sericitized feldspar and quartz

#### **Fracture filling ZK2 from URL Burkov**

Under the microscope, the fracture fillings of the rocks from Bukov are mainly composed of quartz, feldspar, calcite and mica (Fig 4.8, 4.9). They are characterized by variable grain sizes and crystal habits. Calcite and feldspar (plagioclase and K-feldspar) appear anhedral to subhedral with coarser grain sizes compared to euhedral quartz. Rutile, chlorite, and Fe-oxides are found as accessories and occur as minor phases in fractures. There are three types (generations) of calcite: small anhedral calcite that crystallized in voids and is associated with fine-grained plagioclase and quartz (Fig 4.9D), coarse-grained euhedral platy calcite occurring together with euhedral quartz and plagioclase (Fig 4.8C, 4.9A, 4.9B), and calcite in veins cutting through grains of feldspars (Fig 4.8D). Chlorite occurs in aggregates and probably replaces primary minerals (biotite) (Fig 4.9E). The growth of small euhedral crystals of quartz (Fig 4.9A, 4.9B) suggests a younger generation of this phase. Traces of rutile (associated with chlorite) and Fe-oxides are also found (Fig 4.8F, Fig. 4.9C).

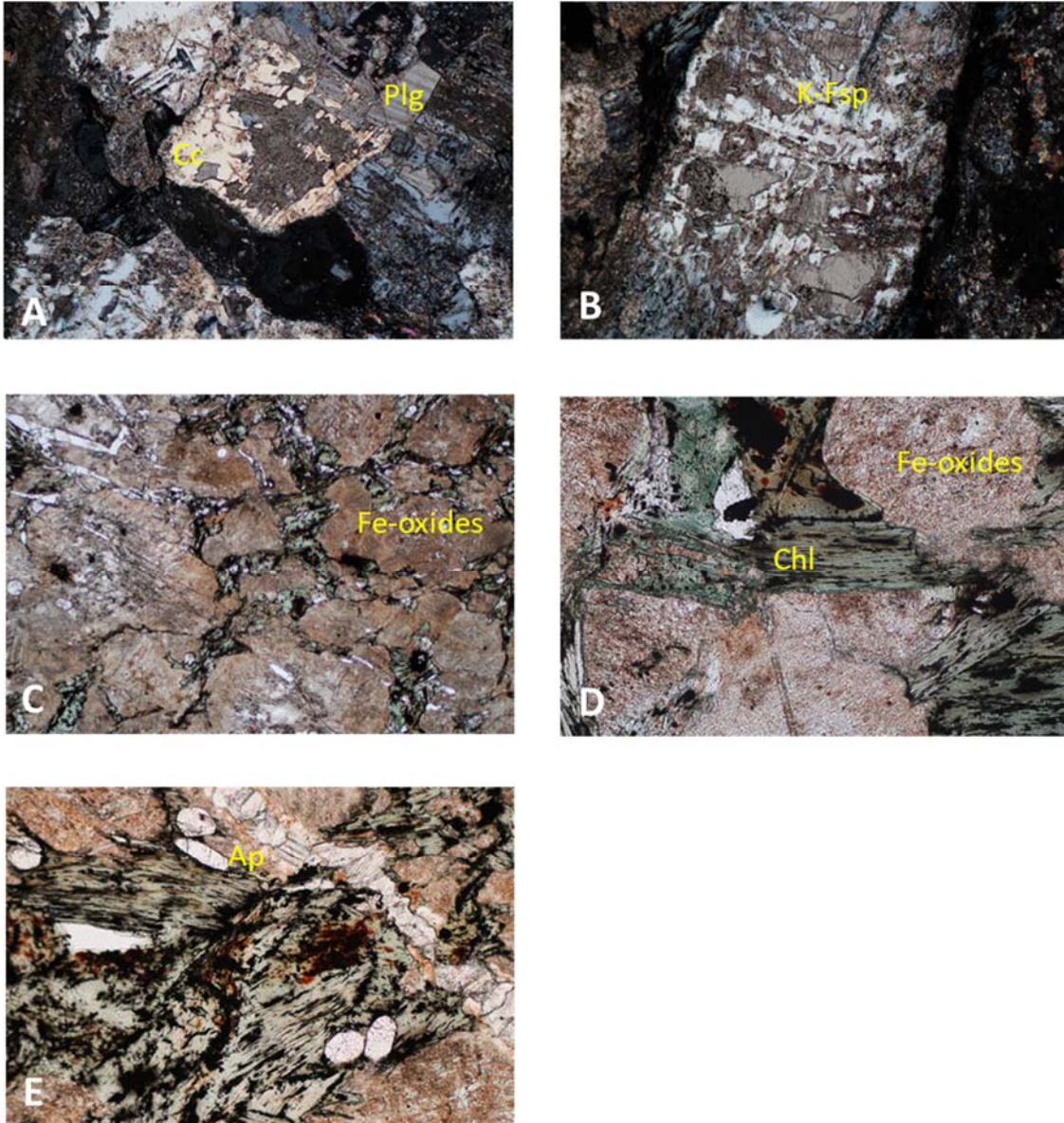


Fig. 4.7 Microscopic observation of thin section from S8, URF Bukov shows extreme hydrothermal transformation. (A) Growth of calcite at the expense of plagioclase, (B) altered K-feldspar (sericitization and albitization), (C) feldspars stained with Fe-oxides/hydroxides, (D) complete chloritization of biotite, (E) euhedral crystals of apatite associated with completely chloritized biotite

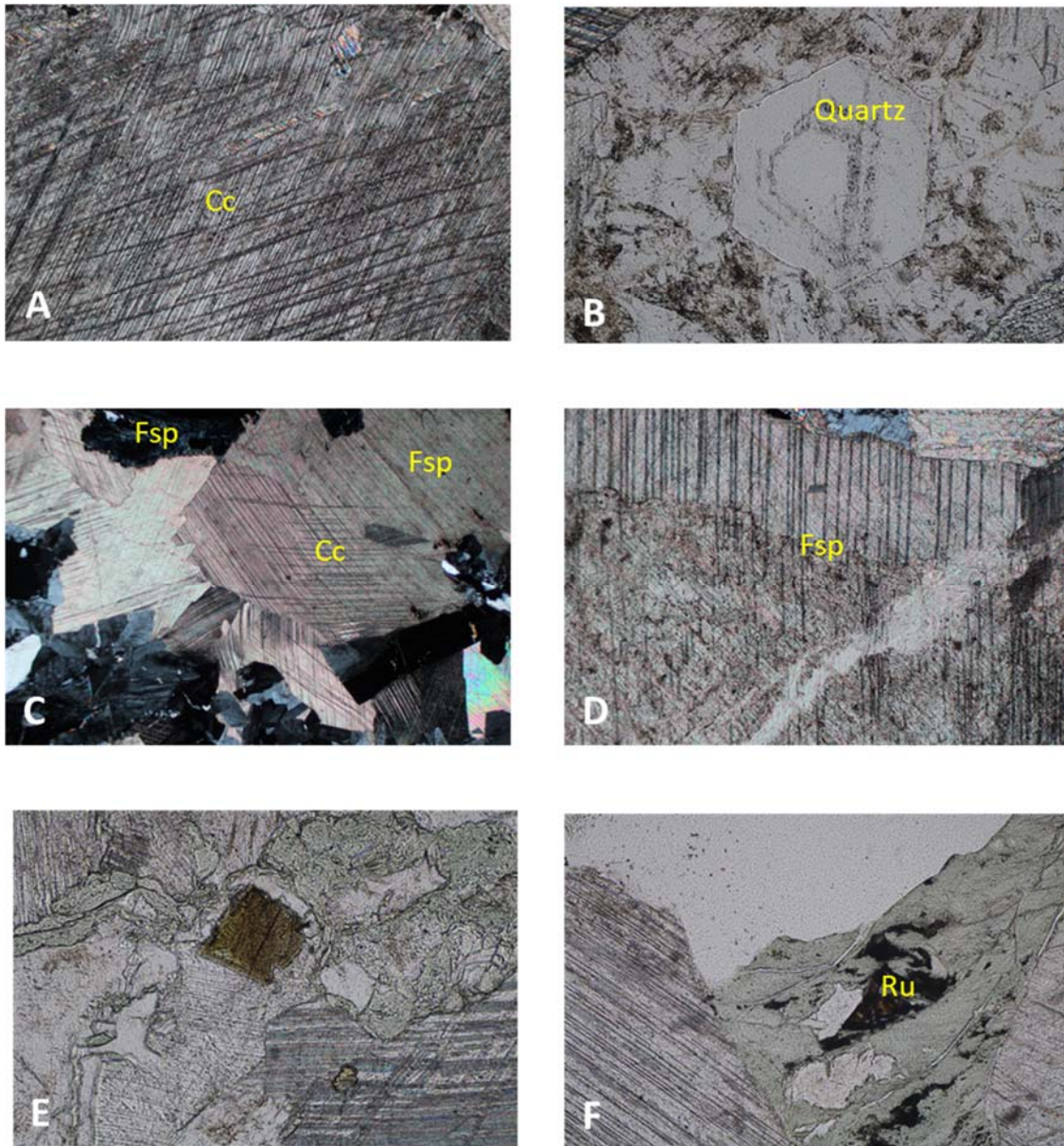


Fig 4.8. Microscopic observation of thin section of fracture filling ZK2-02, URF Bukov shows main composition of calcite, feldspar, and quartz and traces of chlorite and rutile, *Rt* Rutile, *Qtz* quartz, *Fsp* feldspars, *Cal* carbonate minerals (in the XRD study detected as calcite), (B) euhedral zoned quartz (D) 3 generations of calcite.

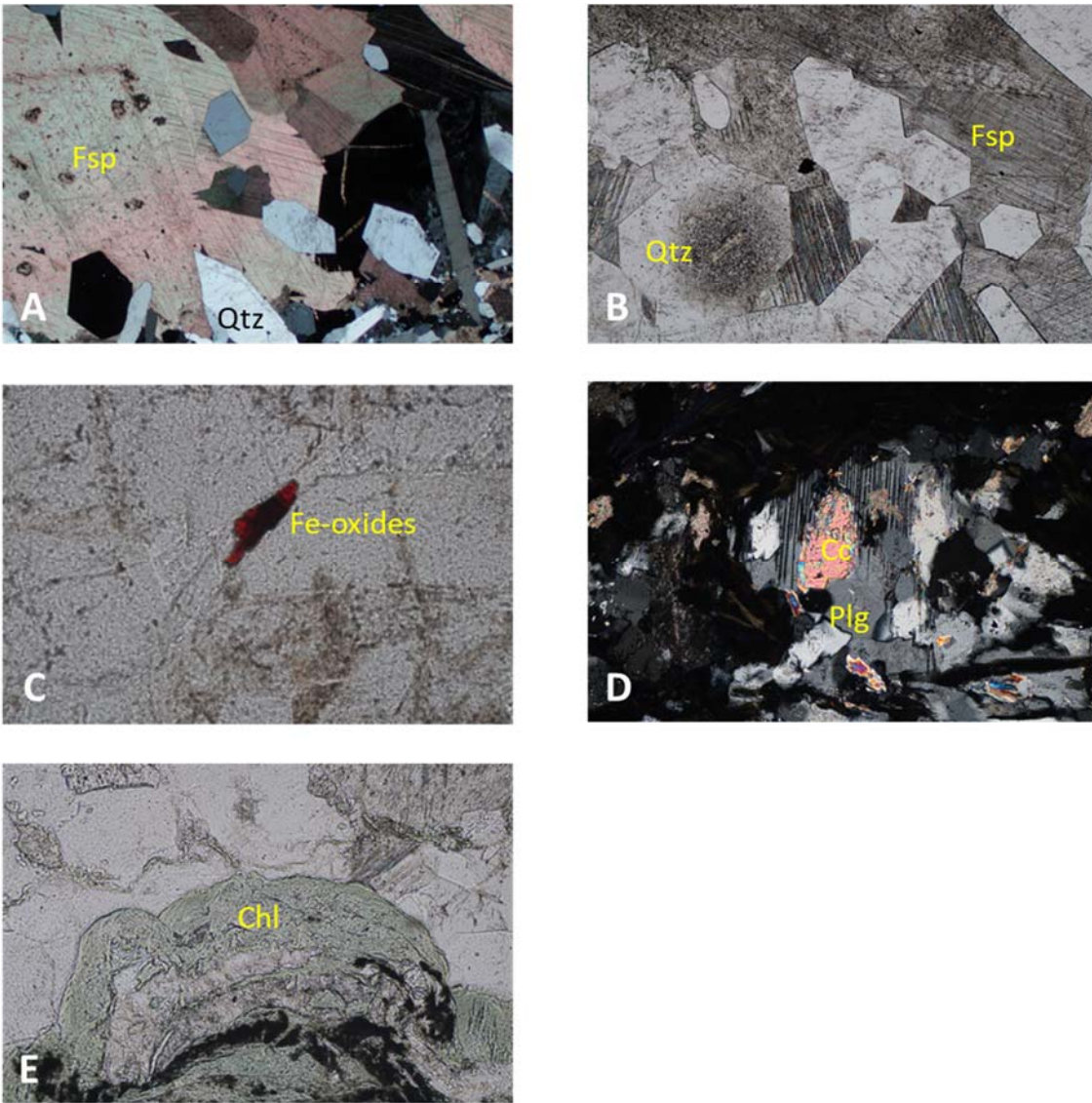


Fig 4.9 Microscopic observation of thin section of fracture filling ZK2-02, URF Bukov shows main composition of calcite, feldspar, quartz, calcite, Feoxides, *Qtz* quartz, *Fsp* feldspars, *Plg* plagioclase, *Cal* carbonate minerals (in the XRD study detected as calcite), (A,B) euhedral quartz (D) growth of calcite in plagioclase, (E) aggregate of chlorite

#### 1.2.4 Optical Cathodoluminescence Imaging

Three representative carbonate-bearing rocks from URF Bukov were selected and investigated with a cathodoluminescence microscope (hot cathode HC3-LM-Simon-Neuser CL microscope at the Geowissenschaftliches Zentrum der Georg-August-Universität Göttingen. Three images of the same spot including transmitted light (TL), transmitted light with crossed polarizers (POL), and CL were taken with a magnification of 5x or 10x with a Kappa DX 40C Peltier-cooled camera. The microscope operated at conditions of 14 kV acceleration voltage and a beam current of <1 mA, corresponding to 20-40  $\mu\text{A}/\text{mm}^2$  beam current density.

##### ***Bulk material of fault breccia (BZ-XII-J)***

An association of carbonate, quartz, and calcite replacing feldspar is observed under crossed polarizers (POL) in this sample (Fig 5.1). XRD results (Tab 2.1) have confirmed the occurrence of dolomite, ankerite, barite and small amounts of calcite in the sample. Patches /layers of quartz (late) brecciated and intruded the carbonates. They are characterized as low temperature  $\alpha$ -quartz due to their non-luminescence (Ramseyer et al., 2018). This indicates that quartz is a younger generation compared to calcite (B3.1, B4.1). The thin sections exhibit a reddish orange luminescence of carbonate and show distinct compositional changes in the form of CL banding. A growth zonation of carbonate is observed in veinlets (A5.1, A6.1). According to Morad et al. (2012), the development of carbonate banding most likely develops from fracture growth and marks the expansion of the fractures. The carbonate of the hydrothermal system was then precipitated within the opening voids and fractures. Such banding reflects movement within the geothermal system and aperture growth along the fractures (Huntington et al., 2015).

##### ***Carbonate fracture filling S8***

Veins of carbonate which is identified as calcite in the X-ray diffractogram (Tab. 2.1) are often found in quartz in this specimen (Fig 5.2). The host quartz is characterized by dark greyish blue luminescence colors with zones of non-luminescing bands. Based on Ramseyer et al. (2018), this quartz is classified as low temperature  $\alpha$ -quartz which is very common in authigenic quartz overgrowths, fracture fillings or euhedral vein crystals. The CL colors are inhomogeneously distributed within the carbonates. The larger part of the vein carbonate is non-luminescent. On the other hand, the veinlets and “fillings” exhibit orange CL, and relics of carbonate are characterized by red CL. The red CL probably hints to strong alteration of dolomite crystals with partly preserved growth zones (A3.2).

##### ***Fracture filling ZK2***

The fracture filling of sample ZK2 is characterized by dark red to bright red CL colors of massive carbonate (calcite as shown in Tab 2.1). The carbonates contain newly formed

aggregates or single crystals of euhedral quartz. The quartz shows very dark greyish blue CL colors and growth zoning.

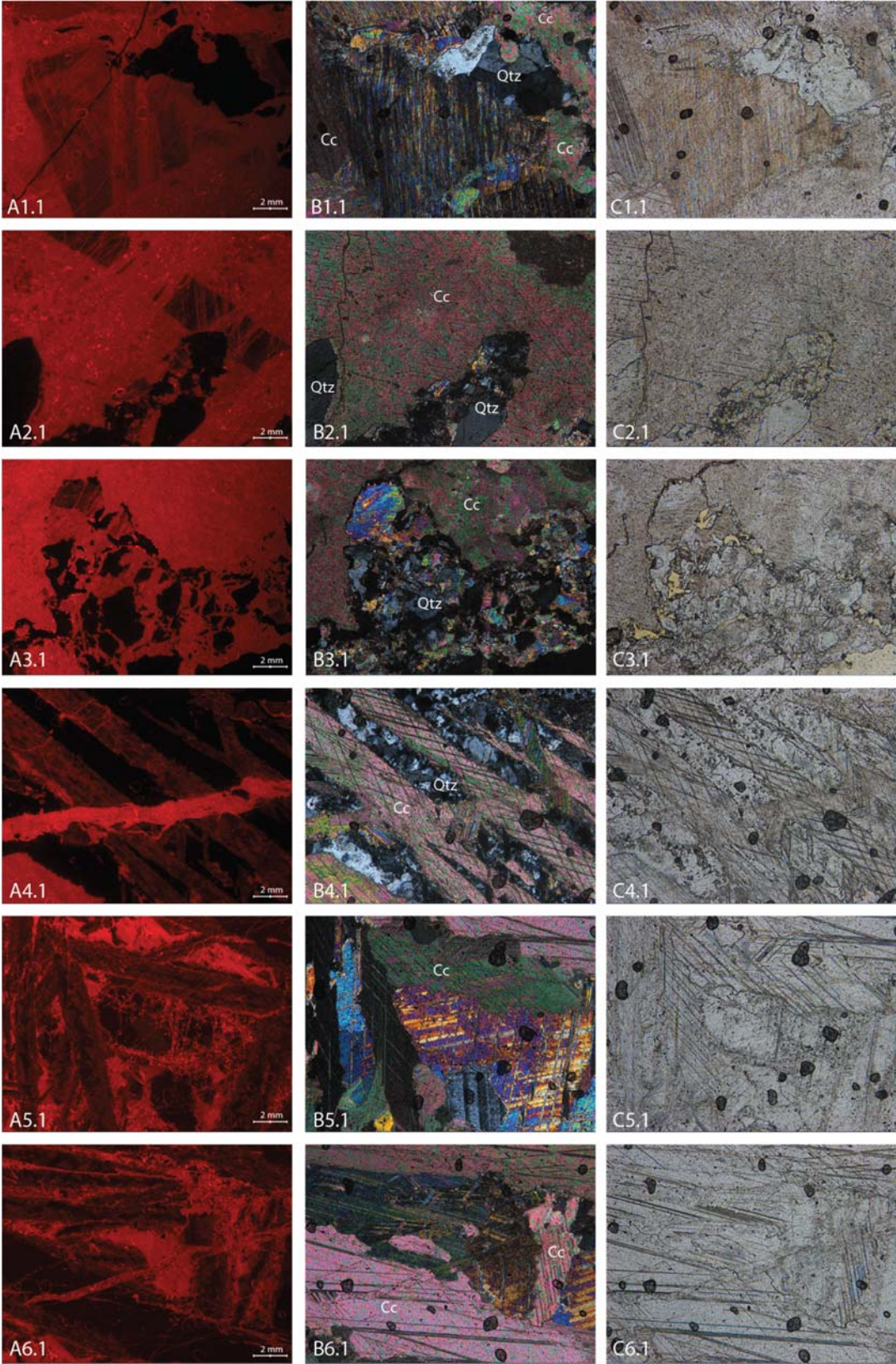


Fig 5.1. Cathodoluminescence images (column A), transmitted light images with crossed polarizers (column B), and transmitted light images (column C) of sample BZ-XII-J08

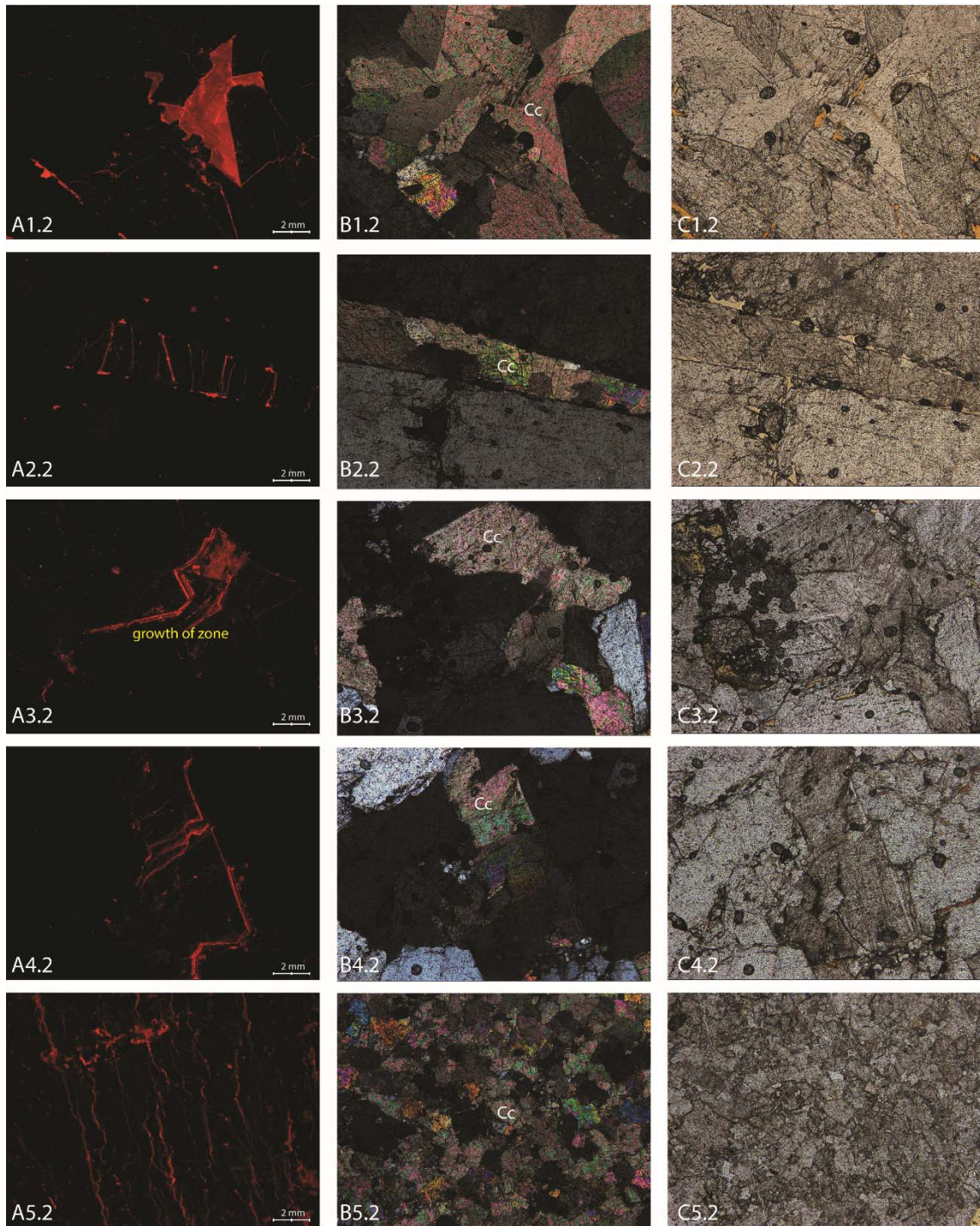


Fig 5.2 Cathodoluminescence images (column A), transmitted light images with crossed polarizers (column B), and transmitted light images (column C) of carbonate fracture filling S8 (S8.9)

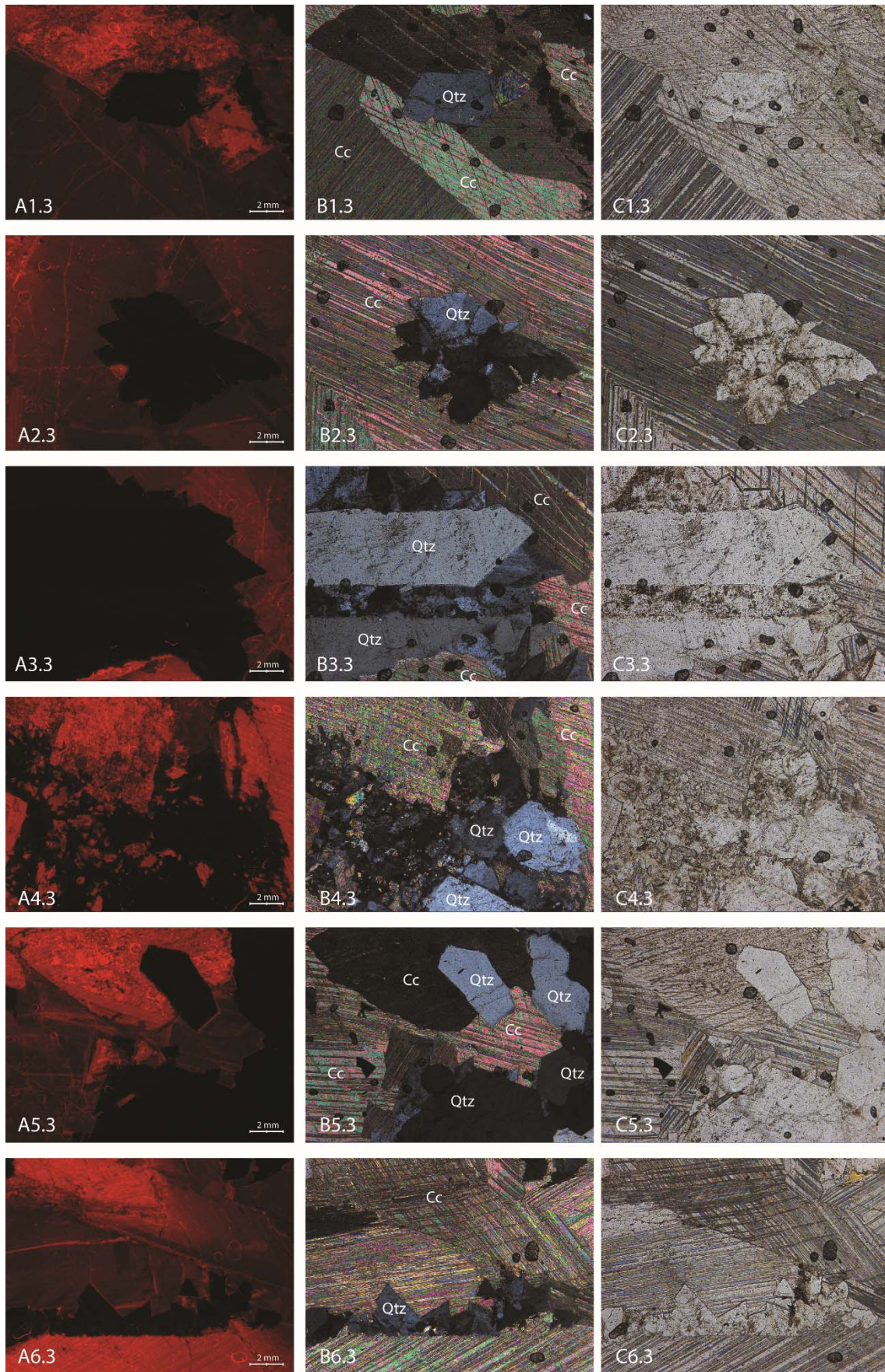


Fig 5.3 Cathodoluminescence images (column A), transmitted light images with crossed polarizers (column B), and transmitted light images (column C) of calcite in fracture filling of sample ZK2

In general, carbonates (calcites) in different rocks of URF Bukov are typically characterized by yellow to orange CL colors (Sun and Hanson, 1975, Habermann et al. 2000, Götze 2012). Figures 5.1, 5.2, and 5.3 show the youngest carbonate generation that latter resulting from fracturing (McNamara et al, 2016). The other carbonate grains revealed dull or purple/blue CL (non-luminescence) to dark orange/red CL colors that represent an older generation of carbonate in fractures, and voids. They are crosscut by younger fractures that are hard to recognize without CL microscopy (A4.1, A1.2, A6.2). The carbonates show textural growth and chemical zoning visible in a variation of CL intensity and colors. Yellow/orange CL colors in calcite due to activator  $Mn^{2+}$  in calcite (Lapiente et al. 2000; Pagel et al. 2000), whereas red CL is a response to the amount of  $Fe^{2+}$  (Long and Agrell, 1965, Gorobets and Walker, 1995). However, the variation of Mn in calcite is not necessarily correlated to the intensity of CL because it could be reduced by quenching of Fe (Mason, 1987), while other trace elements including Zn and Pb do not activate the CL or affect its intensity even at low concentration (Budd et al., 2000). Therefore, the lack of CL intensity in veins, which are cross-cut by the younger generation, is most likely due to a reduction of Mn concentration and/or increase in Fe amount. This latter is supported by the presence of newly formed Fe oxides in the rocks (Fig 4.6). Concerning the formation mechanism of hydrothermal calcite, Lohmann and Walker (1989) mentioned that a high Fe contents in calcites, characterized by strong intensity of dark red to purple/blue CL, are a product of a recrystallization process. The comparison between CL and TL images confirms that Fe-bearing calcites are products from the alteration of host minerals such as Fe-bearing mica and feldspar. On the other hand, the lower intensity of orange to red CL colors in calcite that was precipitated in veins, and voids, is due to the circulation of hydrothermal fluids through the system. The detected relics of dolomite in CL images (but not in XRD- data) indicate complete transformation of dolomite to calcite in this rock.

In addition, the detection of growth zones in carbonate minerals by CL analysis suggests different successive stages of calcite growth in samples from URF Bukov (samples BZXII-J08 and S8-09). The growth zoning of calcite is characterized by different luminescence intensities and sharp contacts between the individual zones (A1.1-A6.1 and A3.2 to A5.2, A1.3, A2.3, A5.3, and A6.3). Otherwise, there are several calcite grains lacking detectable zoning bands (A4.3) and some grains show irregular variations of the CL intensity, especially orange CL colors of calcite in veins and voids of S8-09.

### **1.2.5 Scanning Electron Microscopy (SEM-EDX)**

The scanning electron microscopy (SEM) using a FEI Quanta 400 ESEM FEG instrument (FEI, Eindhoven, the Netherlands) which equipped with energy-dispersive X-ray detector (Oxford, Oxfordshire, UK) at Institute of Applied Geosciences, TU-Darmstadt, Germany. The analyses were implemented manually, referred to as operator-controlled scanning electron microscopy (SEM) instrument. The acceleration voltage of 15 kV and a sample chamber pressure of around  $1 \times 10^{-5}$  mbar were used. The Oxford software Aztec was used for single

EDX-point and EDX-Mapping to control the measurement. Each measurement was measured with 5s to 10s of counting time for X-ray microanalysis.

Four rock samples in URL Kurt and 6 rock materials from URF Bukov were investigated detail in phases, crystal forms, texture of rocks. The minerals phases are clearly identified basing the crystal forms and chemical measurement of individual measured spot from EDX, therefore it is no need to do further EDX-mapping for the rocks.

Under SEM-investigation, feldspars, quartz and biotite (Fig 6.1) are still found as main phases of granitic rocks from URL Kurt. The primary smooth quartz grain show no dissolution features. In the granitic dyke materials, it is very often to observe spherical form of the feldspar (plagioclase and K-feldspar), quartz, carbonate and clay minerals which appeared cloudy on the surface of the rocks. The growth of sericite on the grain of feldspar which are embedded between original quartz is observed in Fig 6.1D and appears in microcrystal forms. Polycrystalline scapolite filled the fractures and veins (Fig 6.1F), they display no detectable crystallographic relationship with primary phases and shows clearly cleavage at (100) and (110). In addition, pyrite is detected in the rocks with the framboidal form.

The observation of host rocks of hydrothermal metamorphosed S8 from SEM-images is shown in Fig 6.2. There is no sign of quartz dissolution basing the form and surface of the exposed grains and reaches into the grain interior in the sample. Similarly, feldspars also display unchanged in form and morphology. Otherwise, the development of microcrystal of calcite on surface of different grains is observed clearly. The EDX-measurements show quartz and feldspar are below calcite layer. The other calcite grew in the veins and crosscut the primary rock forming minerals.

Thin section of fracture filling rocks of ZK2 samples were produced for investigation of CL-measurement and now confirmed by SEM (Fig 6.3 C). The rocks are composed of quartz, calcite, chlorite, titanite and  $\text{TiO}_2$ . K-feldspar enclosed with calcite in Fig 6.3A. Their morphology is almost not changed. The edges are still sharp and crystal faces well developed without any dissolution features and K-feldspar grain is surrounded by calcite. Chlorite developed on the rims of calcite which show clearly sheet form of clay mineral group, no primary mica grain found in sample. The EDX measurements indicate significant high concentration of K in chlorite together with Mg and Fe (App 2.3). Quartz crystals are embedded into calcite background, 200 – 400  $\mu\text{m}$  in diameter sized, anhedral and often show sharp boundary with calcite (Fig 6.3 B). In addition, titanite and  $\text{TiO}_2$  are also observed (Fig.6.3D). The EDX-measurements (App 2.4) has shown the development of  $\text{TiO}_2$  in the center and titanite in the rims, it suggests a migration of Ca and Si from titanite together with hydrothermal fluids and the rest of Ti stays in center of the particle as  $\text{TiO}_2$ .

The mineralogical composition in breccia fault under SEM-observation is consistent with polarized microscopy, CL and XRD-results (Fig 6.4). Large apatite (ca. 3m  $\mu\text{m}$ ) is surrounded by carbonate and barite (white small grains) distributed widely on the surface of rocks. Some carbonate grains are very large (up to 30  $\mu\text{m}$  in size) and enclosed other carbonate phases.

Carbonate crystals are well crystallizing form in thin section. The EDX-mesurements indicated that the rocks composed large barite, dolomite, and ankerite (App 2.5) but only some grains are calcite.

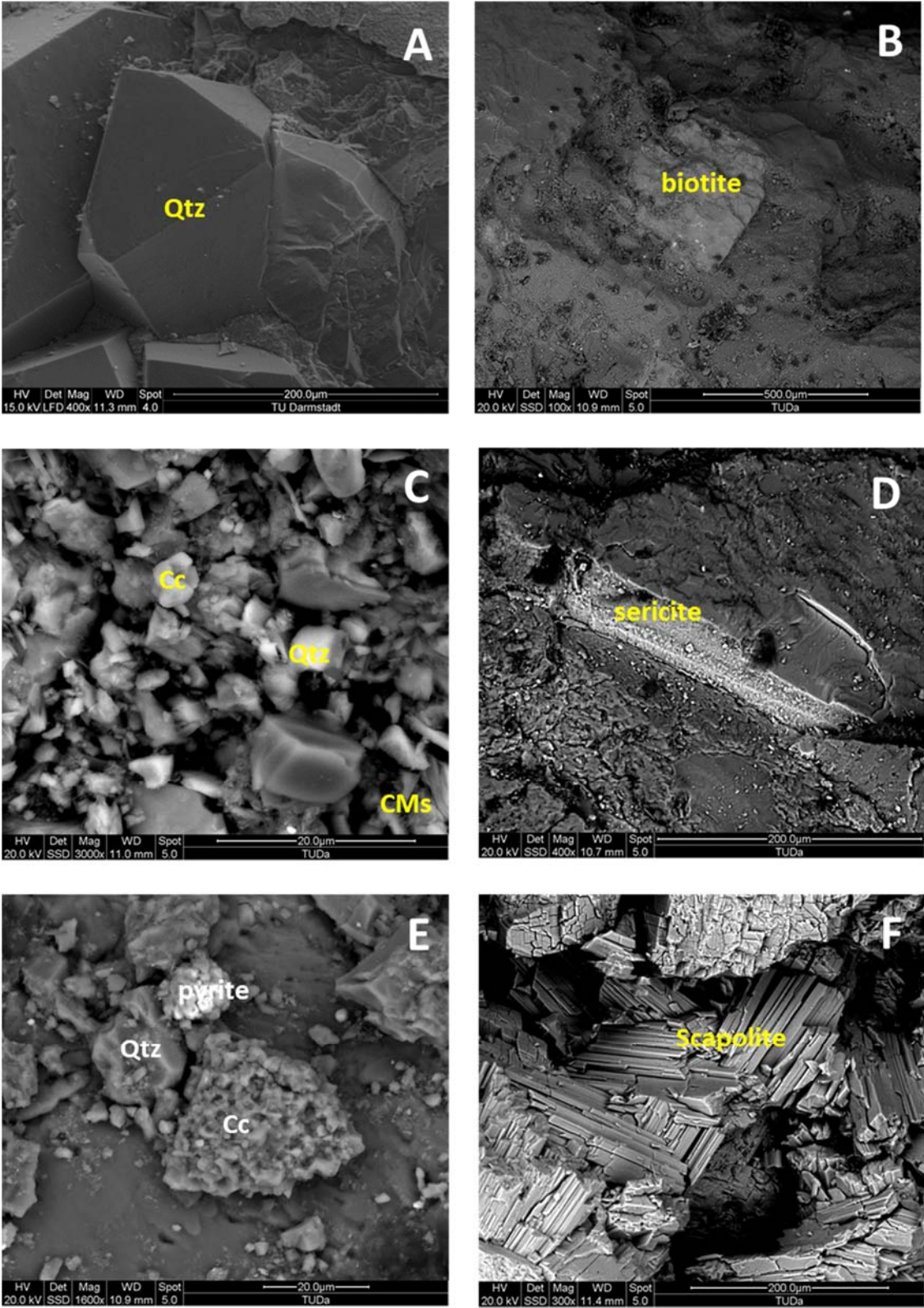


Fig. 6.1. SEM-images of granitic and their dykes, (A) primary quartz (Qtz), (B) primary biotite embedded in quartz and feldspar, (C) cloudy small grains of calcite (Cc), quartz (Qtz), and clay minerals (CMs) are appeared

on surfaces of rocks, (D) sericitization of feldspar between primary feldspar and quartz, (E) Association of framboidal pyrite, quartz, calcite (F) growth of scapolite in fractures and veins.

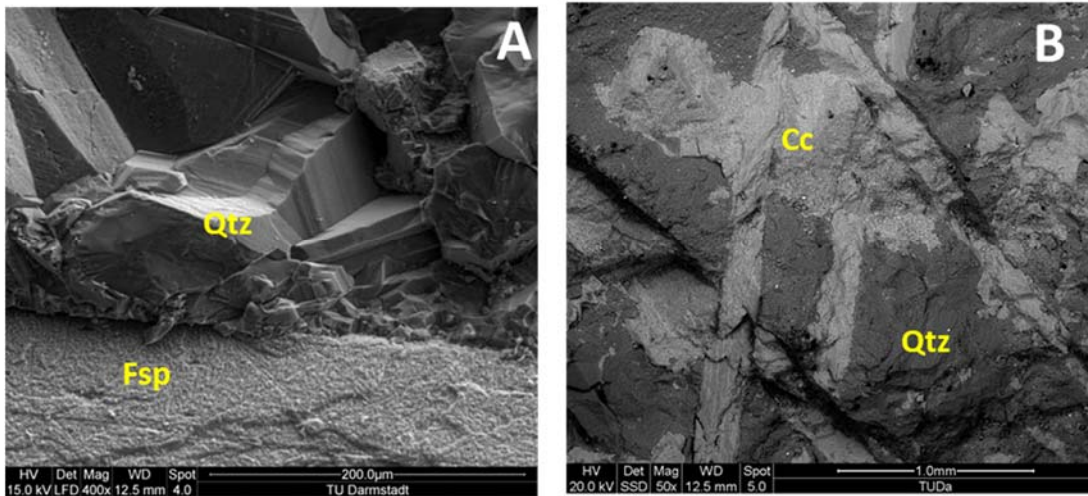


Fig. 6.2. SEM-images of hydrothermal cataclasite S8, (A) primary quartz (Qtz) and feldspar (Fsp), (B) development of calcite (Cc) vein on the surface of quartz grains (Qtz) and on veins

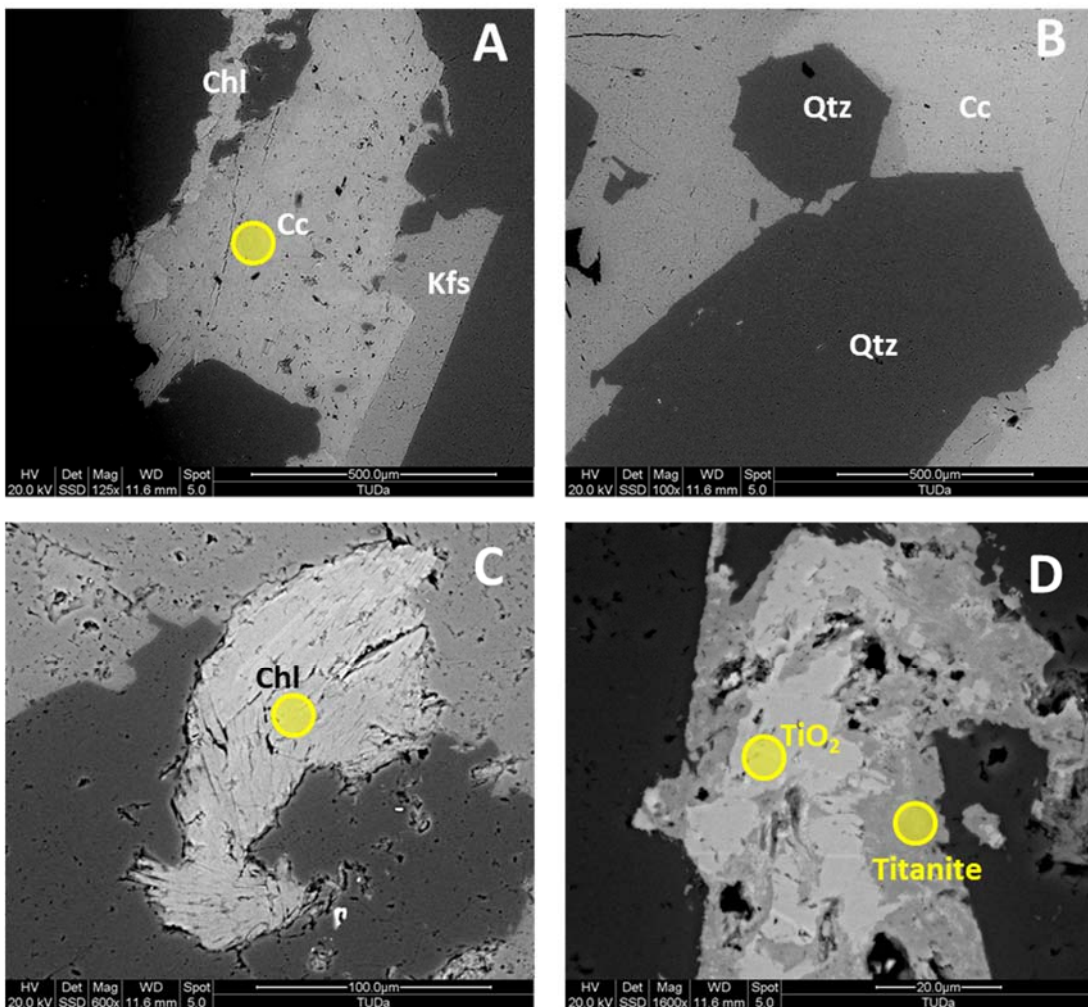


Fig. 6.3. SEM-images of fracture filling ZK2 from thin-section, Cc carbonate minerals (calcite), Qtz quartz, Kfs K-feldspar. Circle symbol is spot of EDX-measurement (App 2)

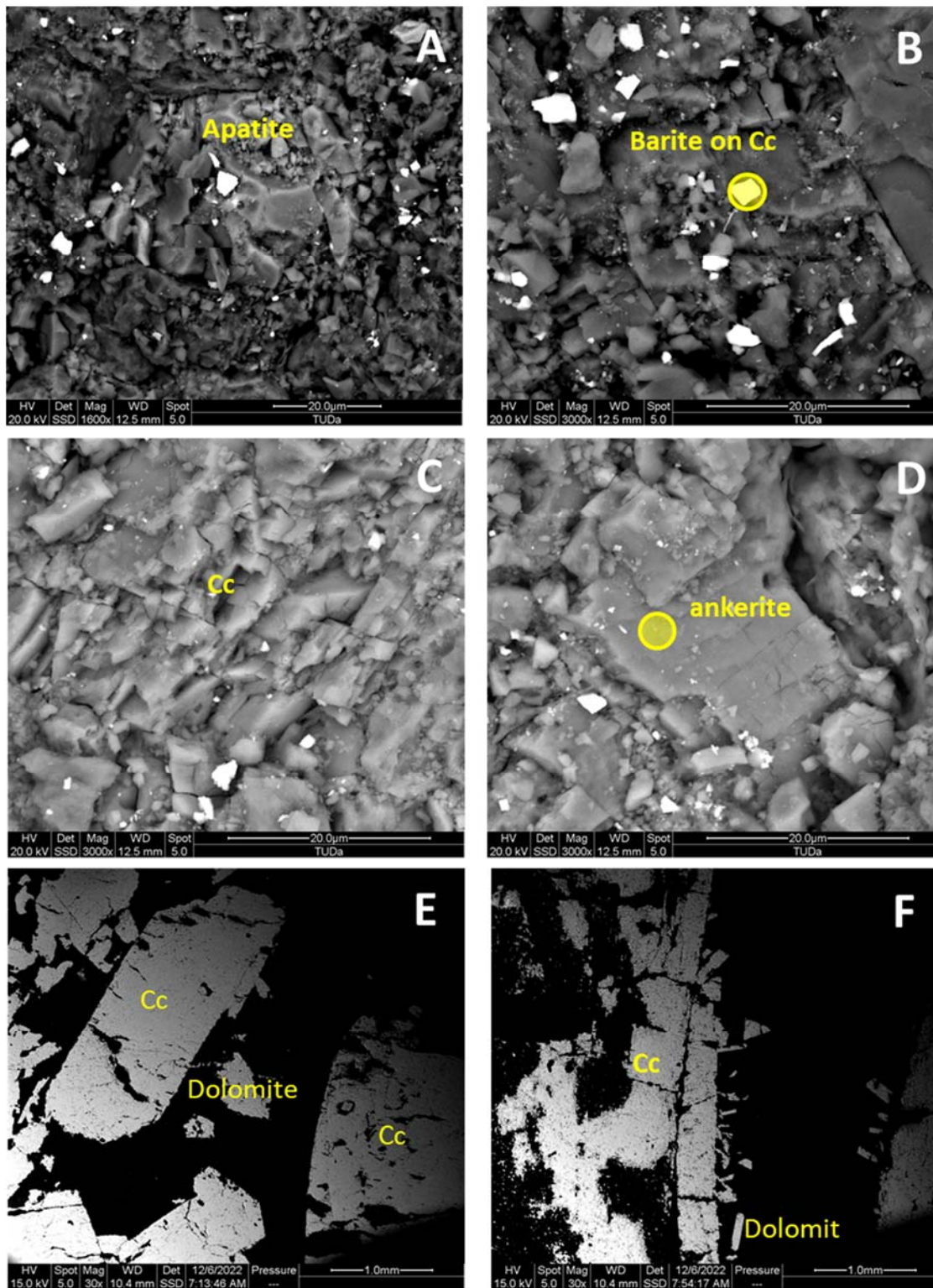


Fig. 6.3. SEM-images of fracture filling ZK2 from hand specimens (A-D) images from thin-section (E, F), Cc carbonate minerals (calcite, ankerite, dolomite), Qtz quartz, Kfs K-feldspar. Circle symbol is spot of EDX-measurement (App 2)

## **Chapter 2. Mineralogy and alteration of host rocks in hydrothermal systems**

The mineralogical compositions of the samples investigated in two locations are described in detail in previous chapters and summarized in Tab 2.1. The rocks are strongly hydrothermally altered. Primary minerals of the original rock (educt) remain partly preserved contrasting with the abundant formation of secondary minerals indicating different transformation processes which occurred in the rocks during hydrothermal events.

### **2.1 Granite and granitic dyke rocks in URL Kurt**

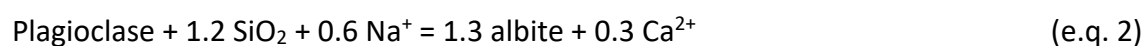
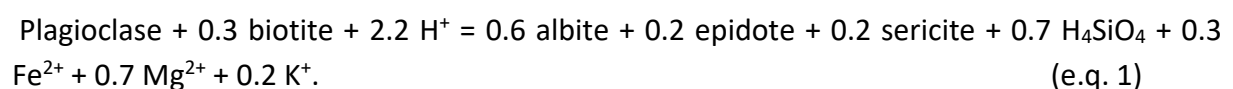
Modal determinations of studied rocks in Kurt under polarized microscopy and combined with XRD- and FTIR-data indicates granitoid rock compositions. The primary magmatic minerals were fractured as mesoscopic, observed by brittle fractures and mineralized vein (1 - 1.7 cm) systems (Fig 2.1). The rocks are composed of plagioclase, K-feldspar, quartz, biotite, muscovite, epidote, and trace amounts of titanite and apatite (Tab. 2.1). K-feldspar and plagioclase occur widely but they both show evidence of intensive alteration to illite or calcite, although some fresh microcline crystals are still observed. The quartz grains display a strong undulate extinction and numerous micro cracks (brittle fractures). Rare coarse crystals (1-3 mm) of muscovite occur freshly (Fig 4.5C), contrasting to biotite, which are extensively chloritized (Fig 4.2C, 4.3E). Fracture gauche and vein systems are filled by scapolite (Fig. 4.4 D, 4.5A) instead of calcite as previously assumed on the hand specimens. It is in agreement with the negative reaction with acid HCl 1M test as described previously. Under microscopy observation, scapolite does not show any reaction precursor of magmatic minerals indicating an authigenic formation of scapolite from which are probably products of precipitation from allochthonous fluids. Otherwise, other small cracks such as veinlets, micro cracks and voids are filled by carbonate (calcite), and illite (Fig 4.1B, 4.1F, 4.6A). Furthermore, micro crystals of calcite and illite are found as partial transformed phases of magmatic plagioclase, microcline, and sometimes mica (muscovite), but also pseudomorphic feldspar. The occurrence of secondary pale yellow to pale green euhedral polygonal grained epidote are apparently found not only in veins (Fig 4.1D, 4.3D) but also in voids (Fig. 4.4C) of the granitoid rocks. They are associated with calcite, but occur together with chloritized biotite and contact with sericitized feldspar. Growth of albite on K-feldspar and plagioclase crystals is also observed (Fig 4.2D, 4.4F). All the observations indicated a diffusion transformation process of saussuritization and albitization of plagioclase in low

grade alteration system with high aH<sub>2</sub>O and suggested a formation of newly phases in microstructure of host minerals (eg. formation of illite or calcite in cleavages of feldspars).

Petrological and mineralogical results have revealed that instead of carbonates, scapolite was detected with different analytical methods in large fractures and vein (0.2 – 1mm) of granitic rock sample in Kurt. Otherwise, calcite and illite are found as microcrystals in veins, veinlets, microcracks or voids on the surface of original magmatic crystals of the rocks. The lack of direction and/or arrangement of cleavage direction under polarized microscopy observation probably showed a precipitation of scapolite during the move of fluids. Growth of epidote in veins is observed in coarse crystal form. Another population of calcite and sericite is observed as replacements of primary feldspar (plagioclase, and K-feldspar). In general, numerous secondary minerals are detected in granite and granitic dyke rock hand specimens of URL Kurt including scapolite, white mica (illite detected with XRD-analysis), carbonate (calcite detected with XRD-analysis, Tab. 2.1), epidote, chlorite, albite as hydrothermal alteration products. The secondary mineral assemblages (Fig 4.2, 4.3, 4.4, 4.6, 4.7) indicate different rock transformation processes as scapolitization, albitization, saussuritization, chloritization. They are the main alteration form of the saussuritization, sericitization and de-carbonatization of primary minerals. In the hydrothermal system, the observed alteration paragenesis is controlled by different geochemical compositions and temperatures of hydrothermal fluids. The succession of alteration assemblages in the rocks of URL Kurt showed that – the first alteration event was probably controlled by late magmatic metasomatism at > 400 °C by magmatic hydrothermal volatils. The temperature was then dropped from approximately 400 to 200 °C during magma cooling or a late stage of magma penetration from an independent hydrothermal event and the fluid was therefore controlled diffusion of rocks (Tulloch, 1982; Frey et al., 1991; Eliasson, 1993; Freiburger et al., 2001; Drake et al., 2009). The latter process may be indicated by an allochthonous fluid composition allowing the formation of CaO rich minerals together with CaO from primary orthoclase.

Scapolite appears largely in fractures of the granitic dyke specimen, they are lined with magmatic quartz and sericitized feldspars (Fig 4.2A, 4.4D, 6.1F). In bulk rocks, they were detected as trace amounts of marialite in XRD-measurements (Tab 2.1). Scapolite is mostly found proximal to magmatic intrusions and interpreted to be formed during metasomatic processes of epithermal contact metamorphism (Orville, 1975; Newton and Goldsmith,

1975; 1976, Deer et al., 2013). The formation of scapolite can be sequentially or contemporaneously related to other metasomatic processes as albitization with presence of saline fluids (Nijland and Touret, 2001). The microscopic observations indicate a fluid controlled metasomatism and the volatiles were expelled during the intrusion of the granite (auto-metasomatism, uralitization) or crystallization happened from volatiles of other proximal magmatic intrusions (Einaudi et al., 1981). In most of the case, plagioclase transformed to marialite (scapolitization) through the interaction between plagioclase with fluids containing Cl<sup>-</sup>, CO<sub>2</sub>, SO<sub>3</sub>, and Na<sup>+</sup> (Strauss, 2003), this interpretation is comparable with Ellis (1978) and Vanko and Bishop (1982) who stated that the crystallization of marialite occurs at high NaCl activity (Ellis, 1978, Vanko and Bishop, 1982). The Cl<sup>-</sup> rich scapolite may be a reaction product from an external NaCl source (allochemical) or can be originated from Cl<sup>-</sup> in the volatile phase while Na was product from the altered plagioclase and in competition with the formation of albite. Finally, the formation temperature of scapolite needs to be high, as Orville (1975) found in their experiment, the NaCl-rich scapolite was synthesized at temperatures of 750 °C at low to high pressures. Otherwise, Vako and Bishop (1982) compared the formation of mirialitic scapolite in field studies and under laboratory conditions concerning the metasomatic alteration of feldspar (plagioclase) predicting a formation temperature at around 400 °C. It is suggested in this study, that the fractures and veins were prior formed and scapolite crystallization filling them later during the metasomatic activities at ca. 400 °C. To support this idea, the assemblage of albite, epidote, chlorite and white mica (illite) in the presence of relicts of magmatic plagioclase and biotite has suggested consequently albitization, saussuritization, and sericitization of plagioclase in presence of magmatic fluids that occurred contemporaneously during the cooling of granitic rocks. Due to the synchronous paragenesis of alteration processes a minimum and maximum temperature estimate of 200 to 400 °C (Seki 1972; Bird and Helgeson, 1981; Eggleton and Banfield, 1985; Rochelle et al., 1989) is proposed. The petrographic observation of sericitization and saussuritization and the paragenesis of alteration minerals in granite and granite dykes specimens in URL Kurt can be explained with two alteration processes (Eliasson, 1993), according to the first equation of Ferry (1979):



The second equation showed a replacement of albite for plagioclase (albitization) following a mechanism of alkaline ion exchange between fluid and feldspar phases (Orville, 1963). This is a reaction between plagioclase, quartz and Na from a NaCl-solution (Ferry, 1979) and originated from a metasomatic aluminosilicate reaction with an albite exsolution (Engvik et al., 2008).

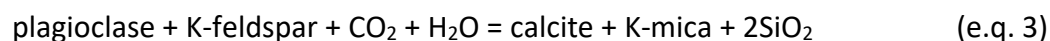
As mentioned above, the NaCl-rich brines probably formed syngeneic with the albite and scapolite formation that exsolved from catalytic acting volatiles of granitic magma (Hay et al., 1988) or external sources (Barton and Johnson, 1996) as migrating fluids at condition of 350-450 °C (Nijland and Touret, 2001). The excess amount of Fe from the first reaction was probably incorporated in the lattice structure of the fracture filling epidote or or co-precipitate during the albitization reaction (Putnis et al., 2007). Although epidote is the main accompanied product in saussuritization reaction (Ferry, 1979), the observation of epidote in veins and veinlets are often formed from local hydrothermal fluids and released by hydrothermal alteration products of plagioclase, pyroxenes and amphiboles mineral breakdown in the surrounding rocks at 220 °C (Castelli et al., 1998; Brunsmann et al., 2001).

In almost all of the thin section, primary biotite mostly disappears and is replaced by chlorite but some grains are found without alteration (Fig 6.1B). According to Schmidt et al. (2018), the transformation process of biotite to chlorite firstly occurs at the rims and cleavage faces of the biotite grain, where the reaction begins and gradually migrates deeper into the center with time (Gastuche, M.C., 1963, Nagy, K.L.; 1995). The fully transformation reaction of biotite to chlorite happens at 210-230 °C as final stage by releasing K<sup>+</sup>, SiO<sub>2</sub>(aq) and minor amount of Al<sup>3+</sup> after going through intermediate phases of hydrobiotite, vermiculite, and corrensite (Cathelineau, 2008, Schmidt et al., 2018, Abdul-Latif and Weaver, 1969; Nagy and Lasagy, 1992).

White mica is identified from XRD-measurement as illite (as clay mineral) and muscovite (well-ordered structure and coarse grains), illite is widely distributed as alteration products of plagioclase in the URL rocks. The sericitization process forming illite in plagioclase is predominately found at crystal edges and alters the inner part of the mineral along the mineral cleavage. This happens also through the pores in the plagioclases (Que and Allen, 1996) which are simultaneously with the formation of chlorite and epidote. Several studies have indicated that well-ordered illite stable at temperatures at the range of 200 – 300 °C (Velde, 1985; Hedenquist and Noel, 1995) and the last mixed-layer smectite will disappear at

300 °C (Ferreiro Mählmann, 1994, 1996; Ferreiro Mählmann et al., 2012). Magmatic K-feldspar (mostly altered to sericite as observed under the microscopy) in the granite rocks were sericitized at temperatures higher than 200 °C (Sass et al., 1987). It is well known as products from lower temperatures during diagenesis and very low-grade metamorphism in granite rocks (Ferreiro Mählmann, 1996, 2001) and meta-sedimentary rocks in the laumontite and heulandite facies (Schmidt et al., 1997). In addition, the sericitization probably has occurred after intrusion or during cooling and solidification of the granite (Que and Allen, 1996; Nguyen-Thanh et al., 2021), but as indicated above, also much later during diagenesis. Concordantly, the detection of zeolites (laumontite, heulandite, and clinoptilolite) in granite rocks of URL Kurt indicates low-pressures at temperatures <230 °C for heulandite (Liou, 1971) and for laumontite at < 2.5 kbar lower than 280 °C (Schmidt et al. 1997). This is consistent with zeolite occurrences in active geothermal regions (Kusakabe, 1980). The lack of data from non-altered granite and the diagenetic-metamorphic history of the hydrothermal altered host rocks have limited the interpretation of the hydrothermal fluids but it seems that this is the most possible reason for high amount of OH bearing minerals as zeolite and clay minerals in the rocks.

Calcite microcrystals widely distributed in veins and veinlets of the rocks. They also replaced the magmatic -feldspar (e.g orthoclase, plagioclase). Carbonate phases are both stable over the broad range of temperature (160 – 300 °C) (Keith and Muffler, 1978; Tulloch, 1982; Simons and Christenson, 1993; 1994) and newly formed by replacement of rock forming minerals, plagioclase and orthoclase in the case calcite is formed at low temperatures through hydrolysis reactions involving calcium-silicate minerals in interaction with sub-boiling fluids with a high CO<sub>2</sub> activity (Simmons and Christenson, 1993):



The co-existence of newly formed illite and carbonate in the rocks (Fig. 4.3C) has confirmed the formation temperature of those phases.

In summary, the granite rock and granite dyke rock specimens of URL Kurt are very strongly hydrothermally altered at high temperatures during metasomatism and followed by processes during magma cooling at lower temperature, probably also burial diagenetic conditions. If the drilling prospect may verify this scenario we propose that the rocks were firstly brittle deformed to create fractures and veins prior to hydrothermal fluid circulations. In a mineralized aquatic fluid system, precipitation and recrystallization in the fractures

occurred and filled by different secondary minerals as scapolite was found at heavily fractured sites and calcite and epidote precipitated in veins. Otherwise, crystallization of microcrystals of illite, chlorite and calcite replaced magmatic minerals of mica and feldspars following the same hydrolysis mechanism. The protolith polygonal granular grained not ordered, hiatal and hypidiomorphic magmatic structure and grain micro-structure of the granite rocks are generally preserved. Specifically magmatic feldspars are frequently completely pseudomorphically replaced but quartz is still coarse-grained and appeared as intragranular at interstitial of the old structure.

The fracture filling mineralogy and crystallization sequences indicated the successive lowering of the temperature of hydrothermal fluids. The mean temperature of > 400 °C in geothermal systems for an association of epidote + albite + K-feldspars (microcline) + chlorite + quartz and precipitation of scapolite in altered granites show a lower greenschist facies mineralogy. The formation of calcite and zeolites is interpreted to be concerned with the final low temperature stage (< 280 °C) during a high water rock interaction, expected to be related to a hydrothermal system.

## **2.2 Rocks in URF Bukov**

The cataclasite S8 and tectonic breccia BZXII-J are characterized by complex textures with abundant fractures and dykes together with a system of veins and voids between the rocks. Under hydrothermal conditions, the mineralogical composition of the cataclasite S8 shows a strong hydrothermal alteration. Strong reaction with HCl 1M with support of other analyses indicates the occurrence of macroscopic large crystals of calcite in fracture fillings S8 and ZK12 specimens. Otherwise, fault breccia BZXII-J sample is composed of dolomite, ankerite, and small amount of calcite (Tab. 2.1).

In the thin sections the granular polygonal microstructure of the cataclastic fractured educt rock S8 is still preserved. Remains of primary magmatic minerals as biotite and feldspar (plagioclases and K-feldspar) are evidenced but altered by newly growth of chlorite, calcite, illite and quartz. Microcrystals of carbonates (mainly calcite) crystallized in the veins and microcracks of (Fig 4.6A) or replaced feldspars crystals together with some white mica (Fig. 4.7A). In addition, development of very dense sericitized feldspars microcrystals (Fig. 4.6C) occurred together with chloritized biotite in voids and replacing biotite (Fig 4.6B, 4.7D) is also observed. The additional secondary minerals of Fe-oxides, actinolite and apatite were

also detected in the rock (Fig. 4.7). The metamorphosed cataclasite S8 is composed of transformed new clay mineral assemblages of illite and chlorite, which is significantly different from the composition of original rock. Hydrothermal fluid circulation along the failure zone is probably responsible for extreme alteration of cataclasite. It was reflected by transformation of original biotite to chlorite, feldspar to illite and formation of carbonate (dolomite and calcite) and new formation of Fe-oxides. In general, the neo-formed mineral assemblages which replaced magmatic educt minerals and precipitated in cracks or veins of S8 host rock specimens allow estimating the alteration temperatures of about 300 to 500 °C through transformation process of chloritization, sericitization, carbonization of primary rock forming minerals. Otherwise, the formation of Fe-oxides is part of the retrograde at the final low temperature stage of the water-rock interaction at lower temperature of 150 – 250 °C when the fractures were fully filled and the wall rock was cooled (Eliasson, 1993). The colorless in tiny euhedral prismatic elongate crystal form of apatite distributed widely in the S8 rock. The lack of isotopic dating data has limited the interpretation of apatite formation in this study but they are commonly accessory mineral in magmatic rocks but is also formed in hydrothermal condition (Chew and Spiking, 2015; Webster et al., 2009; Protwatke and Klemme, 2006). Otherwise, the association of anhedral apatite with chloritized biotite (Fig. 4.7E) has suggested a record of hydrothermal fluid interactions during mineralization.

Going more in detail regarding the fracture fillings of S8 from core samples (Fig 1.1B) and fracture filling ZK2 (Fig 1.1E), the mineralogical composition of both rocks are different. Fracture filling S8 contains only calcite and quartz, whereas calcite, feldspar, chlorite and titanite are found in fracture filling ZK2. Dark green chlorite is largely widespread between host rocks and carbonate fillings forming the selvage. This was observed in two large surfaces in the ZK2 specimen (Fig 1.1E). Microscopically in the thin section, calcites show sharp contacts with the host rocks or crosscutting older vein generations and voids of the rocks (Fig. A2.1, A4.1, A5.1, A6.1) but carbonates in fracture fillings of S8 and ZK2 are characterized by large blocky grains of calcites up to several centimeters.

Fillers in fault breccia (BZXII-J) are composed of different kinds of carbonates including calcite, ankerite, and dolomite together with quartz, barite and trace of pyrite (Tab 2.1). The detection of low temperature quartz ( $\alpha$ -quartz) proved epi-hydrothermal conditions during formations, very different to magmatic intrusion temperatures. The habitus was anhedral during crystallization but lately brecciated and posterior the fragments cemented by carbonate minerals. Carbonates in fault breccia (BZXII-J) appear with the main habitus of

blocky to platy dolomite, ankerite, calcite and cloudy microcrystals of barite. They are crosscut by a younger vein generation with low temperature  $\alpha$ -quartz (Fig 4.9, 5.3).

In contrast to calcites in veins or microcracks of granite in URL Kurt and metamorphosed S8, carbonates in fractures and dykes filling of S8, ZK2 and fault breccia rocks developed differently. Brittle deformations resulted in formation of fractures and fracture zones that allowed fluids to circulate through the bedrock. A sharp temperature-pressure gradient may have allowed boiling in the fluids (Simmons et al. 2005). The boiling fluids encouraged the precipitation of pseudomorphs carbonate crystals at 300 – 400 °C fractures and open voids upon loss of  $\text{CO}_3^{2-}$  (Simmons and Christenson, 1994):



The occurrence of quartz, carbonate minerals such as calcite ( $\text{CaCO}_3$ ), ankerite ( $\text{CaFe}(\text{CO}_3)_2$ ), siderite ( $\text{FeCO}_3$ ), dolomite ( $\text{CaMg}(\text{CO}_3)_2$ ) in the tectonic breccia BZXII-J sample is normally found at epi- to mesothermal conditions at intermediate pressures and temperatures of 300 to 400 °C, which suggested to the presents of magmatic-hydrothermal conditions (Möller et al., 1979; 1984). Including all possible temperature estimates shown in chapter 2.2 the formation of secondary alteration and precipitated minerals found in both host rocks (metamorphosed cataclasite and breccia) in URF Bukov a precise determination is not possible. The processes described were formed in a large range of temperatures but low pressure conditions.

In conclusion, tectonic structures, mineralogical composition and crystal microstructures of primary and secondary minerals of investigated rock specimens have suggested the effects of chemical composition of hydrothermal fluids as well as their circulation through fracture systems on primary rocks. In addition, the migration of fluids along tectonic failures in cataclasite metamorphosed rocks of Bukov has controlled either interaction between fluid and rock or caused variable types and distribution patterns of transformation of primary minerals. The alteration intensities of rocks in both locations observed in thin sections indicated large-scale fluid-rock interactions (Putnis et al., 2007). The highest temperatures originated from the intrusion of magma and cooling temperatures combined with fluid distribution, they both intensified the alteration processes of rocks in Kurt. Dependent on the time, water activity and kinetic of reaction, the mineralogical composition of magmatic rocks also determines the type of transformation, for example, biotite in granite is easily transformed to chlorite, thus, biotite chloritization promotes the intensification of

saussuritization of plagioclase because this process provides the necessary  $K^+$  and  $Fe^{2+}$  to the system (Janeczek, 1994). Furthermore, released  $K^+$  from the chloritization of biotite also contributes to the formation of secondary K-feldspar (probably secondary sanidine, as detected by XRD, see Tab. 2.1) in the hydrothermal system of granite, in particular a high  $a+K/a+H$  (Freiberger et al., 2001) is postulated. Otherwise, carbonate in large fractures and dykes were precipitated according to equation 4 at ca. 300 °C to 400 °C in S8 and BZXII-J rocks. The coexistence of  $\alpha$ -quartz and carbonate with the predominance of carbonate over  $\alpha$ -quartz in the fracture filling of ZK2 sample indicated a deposition of two minerals at temperatures below 150 °C (Sharp et a., 1965).

### **Chapter 3. Relation between mineralogical transformation processes and trace elements**

Pervasive fluid circulation systems can extend throughout the crust and are also responsible for several generations of the most important ore deposits, including traces and rare earth elements (REEs). The present study shows hydrothermal activities are usually associated with the formation of new minerals that are characterized by the fluid infiltration and replacement of successive minerals. Unfortunately, the chemical compositions of trace and rare elements (REEs) are missing in the work. Therefore, in this chapter the trace and REEs elements composition of the altered rocks are not mentioned but literatures are reviewed to find the relation between hydrothermal alteration processes of primary granitic rocks (URL Kurt) and formation of carbonate in metamorphosed cataclasite and breccia (URF Bukov) as well as calcite fracture fillings of them.

In granitic rocks, REEs are mainly hosted in impurities like apatite, titanite, and allanite (Clark, 1981, Dahlquist, 2002). They are not significantly affected during the alteration supporting the immobile behavior of REEs on the whole rock scale (Sandström et al., 2008). Otherwise, the other major minerals as feldspar also display large variation of trace elements composition which is mostly consistent with processes of fractional crystallization (Kontonikas-Charos et al., 2017). They are enriched Rb, Li, Cs and accompanied by a low K/Rb, Ba/Rb, Eu/Eu\* and K/Cs ratios (Dostal and Chatterjee, 2010). The concentration of REEs trend of hydrothermal feldspars in primary granite rock is largely inherited from the igneous feldspars they replace or convert (Kontonikas-Charos et al., 2017). Depending on the reaction mechanisms, REEs concentration can be changed, for example, REEs remain at the site of the reaction front in case reactions form hydrothermal feldspar that take place via coupled dissolution-precipitation. This indicates the fluids responsible for replacement of albite to plagioclase (Kontonikas-Charos et al., 2017). Otherwise, the recrystallization process causes a loss of trace elements, particularly Fe, Ti, and also REEs to the fluids (Parson et al., 2009). The assemblage of K-feldspar + sericite + chlorite of albitization within the hydrothermal system which eventually replaces plagioclase may trap REEs from igneous plagioclase but the concentration could be lowered due to the solubility and remobilization of REEs from albite to form other REE-bearing minerals (Kontonikas-Charos et al., 2017).

REEs are potentially mobile during hydrothermal alteration due to fluids movement, and most of the trivalent REE will be removed from the system during K-silicate alteration (Alderton et al., 1980), small decrease in the Eu content in the altered rock, especially sericitic alteration (Alderton et al., 1980, Sandström et al., 2008). The loss in Eu concentration is also related to the saussuritization of plagioclase because of concurrent release of Ca since  $\text{Eu}^{2+}$  replaced for Ca in the plagioclase lattice (Sun et al., 1975). The oxidation of  $\text{Ce}^{3+}$  to  $\text{Ce}^{4+}$  is attributed to a less mobilization of  $\text{Ce}^{2+}$  in comparison with other REEs which migrated into adjacent chlorite grains during the coeval chloritization of biotite (Sandström et al., 2008).

During and after hydrothermal alteration of biotite to chlorite, major elements of primary biotite such as Fe, Mg, Al, and Ni are mostly retained in secondary chlorite, whereas hydrothermal fluids transferred other elements of Co, Ga, Mn, and Zn to chlorite as well as Sc, Sr, Si, V, Li, K, Nb, Ba, Rb, Ti, Cl, Na, Sn, Cu from the biotite mostly transport and enter to another bearing trace elements phases but not chlorite during chloritization (Xiao and Chen, 2020). This has explained the reduction of light REEs but gain of heavy REE during chloritization (Sandström et al., 2008). In addition, the reformation of scapolite from alteration of feldspar is also another factor controls the behavior of trace and REEs elements in altered granitic rocks because scapolite contains main chemical composition of Al, Ca, Na, C, Cl, and S, and enriched B, Be, Ga, Li, Sr, and Pb and especially richer in B, Be, Li, and Pb.

Since long, hydrothermal carbonates such as calcites have used as petrogenetic proxy due to high potential of bearing trace element and rare earth elements (REEs), despite they are characterized by a much simpler crystal-chemical structure but can incorporate a wide range of trace and rare earth element (REE) composition (Rimstidt et al, 1998, Zhong and Mucci, 1995, Barker and Cox, 2011). A number of studies have worked on quantitative fields and experimental studies to archive the chemistry of the fluids where carbonates have precipitated basing geochemical characteristics of hydrothermal calcite, trace and REE elements composition (Wogelius et al., 1997, Barker and Cox, 2011). The growth of zone in calcites from CL colors reflected the variation of trace metals (Fe, Mn) from studied rocks but the other elements, such as Mg, Sr, Y and some of the REEs, can also be incorporated into carbonate minerals by different processes including isomorphic substitution and surface absorption (Veizer, 1983, Zhong and Mucci, 1995). Therefore, besides main and minor elements, the trace element chemistry of hydrothermal calcites needs further research on carbonate in rocks of URF Bukov. In addition, the later formation of  $\alpha$ -quartz in fracture filling is observed together with carbonates. As mentioned above they were both formed at

low temperature (<300 °C) and the content of Al in hydrothermal  $\alpha$ -quartz can be reached as high as 4000 ppm with different trace elements as Ti, K, Li, Ba, Na, Ca, Sb, Sr, Rb, Ga, Ge, As, and Cs (Rusk et al., 2008).

In general, in natural system, hydrothermal processes have led to the fractionation of the heavy and light REEs which are mostly occurred in REE ore minerals (bastnäsite – Ce, parasite-Ce, synchysite-Ce, monazite-Ce, xenotime-Y and non-REE minerals that contain low appreciable concentrations of REEs (Migdisov et al., 2020). Therefore the geothermal systems are most important resources of trace and REEs elements, the lack of geochemistry of rocks in this study has limited the understand on different hydrothermal alteration processes of precursor minerals as feldspar (albite, plagioclase, K-feldspar), mica (muscovite, biotite) to newly phases, which is believed to have strongly relation to behaviors and concentration of trace and REE elements of rocks in frame of hydrothermal system.

# Chapter 4. Sub-cores of elevated temperature experiments

## 4.1. Sub-core drillings

The obtained sub-cores from 5 crystallized rocks of URL Kurt and Bukov with cylindrical shape (0.5 cm × h cm, d × h, while h is variable from sample to sample due to inhomogeneity of host rock) are drilled. Their drilled locations are presented in Fig 9.1 and 9.2. The sub-cores are further investigated on porosity, density and  $\mu$ CT before doing thermal treatment experiments.

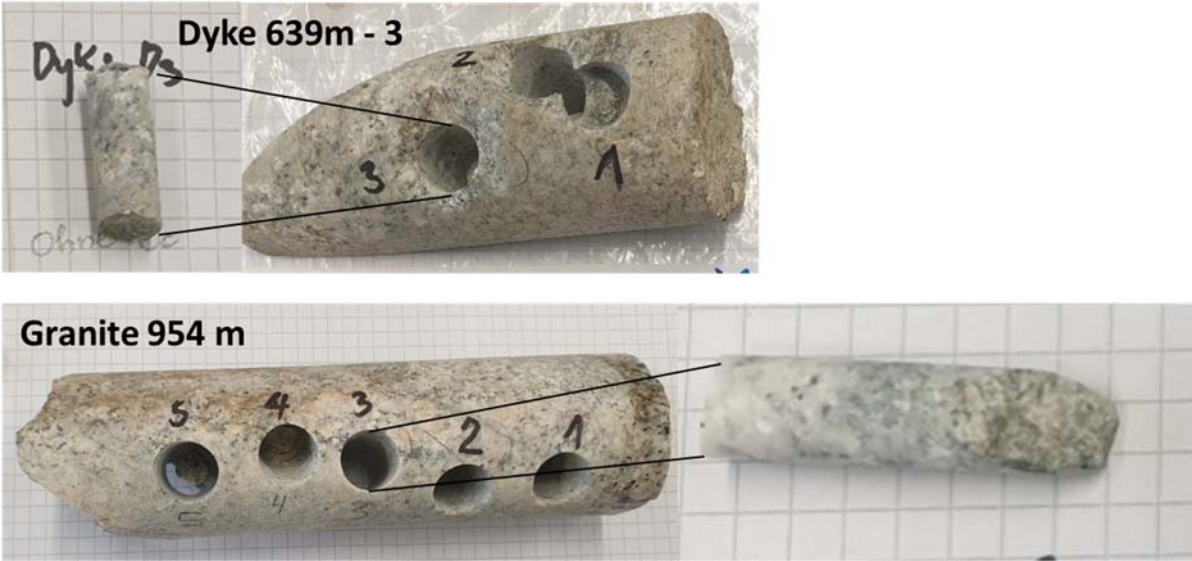


Fig 9.1. Location of sub-cores (left) in core rocks of URL Kurt and sub-cores (right) for further measurements (porosity, density, and  $\mu$ CT)

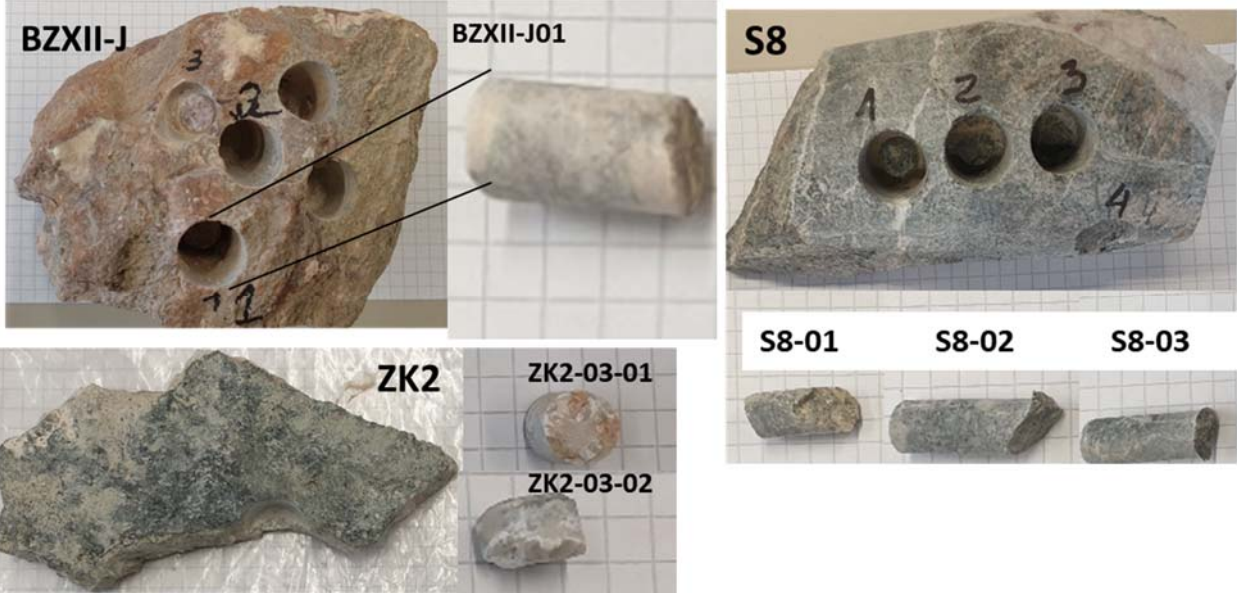


Fig 9.2. Location of sub-cores in hand specimens of URF Bukov and sub-cores for further measurements (porosity, density, and  $\mu$ CT)

## 4.2. Porosity and density of sub-core materials

The porosity and density of 8 sub-cores materials from altered crystalline rocks in URL Kurtz and URF Bukov were analyzed before sending for elevated temperature experiments. The measurement was implemented by Helium pycnometer Accupyc 1330 at TU-Darmstadt. The principle of the method basing helium pycnometer measurement by general gas law:

$$p_1(V_1 - V_p) = p_2(V_2 - V_p)$$

The instrument works with two chambers of known volume  $V_1$  and measured pressure  $p_1$ . Here, the sample chamber is filled with helium, and the volume of the sample  $V_p$  is unknown. When expanding into an expansion chamber, a new pressure  $p_2$  is established in the two connected chambers with volume  $V_2$  (Fig 10.1).

The powder pycnometer measures the volume of the DryFlo through piston travel and measuring chamber area at a defined compression force. Two measuring passes are necessary, once without sample and once with sample.

For a high accuracy measurement, the sample should be in plugs max.  $\varnothing$  4cm, h 3.0/ blocks max. 2.5x2.5 cm h 3.0 cm/ small hand pieces), and must be placed in the drying oven at 105° C after sawing until the weight is constant (approx. 1d). Then store in the desiccator (always take only 1 specimen for measurement). For comparative examinations of several specimens, care should be taken, if possible, to ensure that the specimens are similar in shape and size.

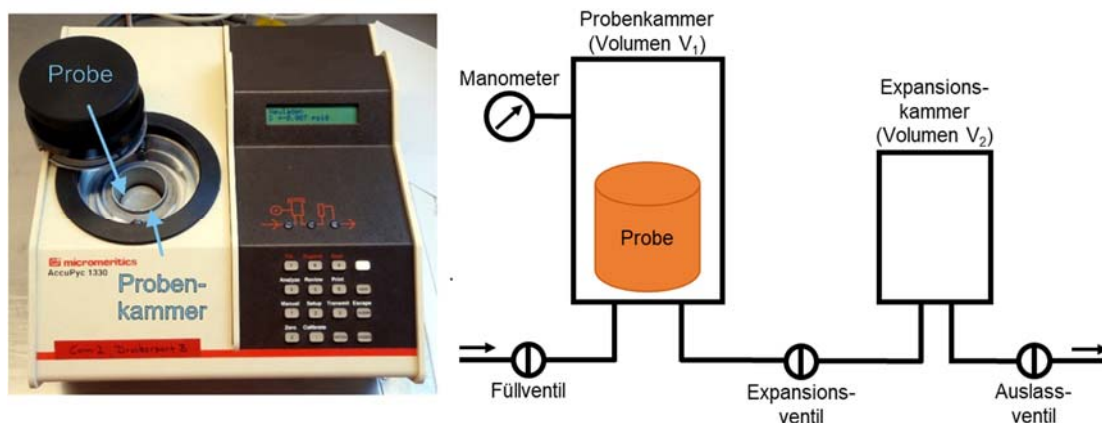


Fig 10.1 Functionality illustration of AccuPyc GeoPyc Mhi 20180102

The inhomogeneity and instability of rocks have limited the size and form of the sub-cores. The uncompleted forms sub-cores were conducted in triplicate for S08-01, BZXII-J01 and two times for BZXII-J03. Unfortunately the porosities of these measurements for sub-cores are variable and could not be used.

Tab 10.1 Porosity and density of sub-core materials from

Location	Samples	Density (g/cm <sup>3</sup> )	Porosity (%)
URL Kurtz	Granite-954m	2.6385	3.036
	Dyke 639m	2.6203	2.903
URF Bukov	S08-01_I01	2.6693	0.214
	S08-01_I02	2.6693	2.117
	S08-01_I03	2.6693	4.254
	S08-02	2.701	4.075
	S08-03	2.7171	2.869
	BZXII-J01-I01	3.2628	6.458
	BZXII-J01-I02	3.2628	18.004
	BZXII-J01-I03	3.2628	0.0173
	BZXII-J02	2.8405	4.282
	BZXII-J03-I01	3.4763	0.226
BZXII-J03-I02	3.4763	3.511	

### 4.3. Structural investigation of sub-cores by $\mu$ CT

Further structures of three whole rocks and 8 sub-cores from hand rocks were investigated using  $\mu$ CT. They were scanned with an X-ray microtomography (Xradia Versa 520, Zeiss, Oberkochen, Germany). The scanning was conducted at a voltage of 80 keV and power of 7 W. A total of 1601 projections for each sub-core were taken at an exposure time of 1 s with no filter. The 3D reconstruction achieved a field of view of 10 mm.

Due to flawlessness during scans, three whole rock specimens were selected for  $\mu$ CT to find the suitable measured parameters for sub-cores samples. Each rock was scanned at high and low quality. Unfortunately, the size of the sample was too big, so the fracture filling ZK2 could be partly scanned. The  $\mu$ CT-scans are shown in Fig. 11.1 - 11.3 and Appendix 3. The total rocks show different tones of brightness in their grains which probably introduced different kinds of minerals in the rock. Unfortunately it is impossible to identify the link between them but the amount in vol% of each colour tone is subtracted and shown in Tab 1.11. Besides, the fissures are observed apparently in the rocks. They are filled by air that indicates those fissures are probably formed lately in the manufacturing processes.

Tab 1.11. Analysis parameter in different tone brightness (mineral phases) from  $\mu$ CT-scans

Rock	Phase	Amount (Vol%)	Voxels	Total Voxels	Total Vol (cm <sup>3</sup> )	Observations
Kurt Granite	Darkest	18.94	60480100	319393126	21.22	
	Light	68.91	220107344			
	Very light	9.19	29345432			Mostly around the bright spots
	Bright spots	2.96	9460250			Mostly small spots
Bukov ZK2	Dark	37.65	58560200	155527956	10.33	
	Light	48.63	75637152			
	Bright	13.71	21330604			Looks like grains in flat conglomerates
Dyke 639	Darkest	1.77	5819017	328926723	21.85	This is just an air-filled fissure
	Dark	76.84	252759760			Undefined minerals
	Light	18.48	60789280			Mostly around the bright spots
	Bright spots	2.91	9558666			Small bright isolated spots

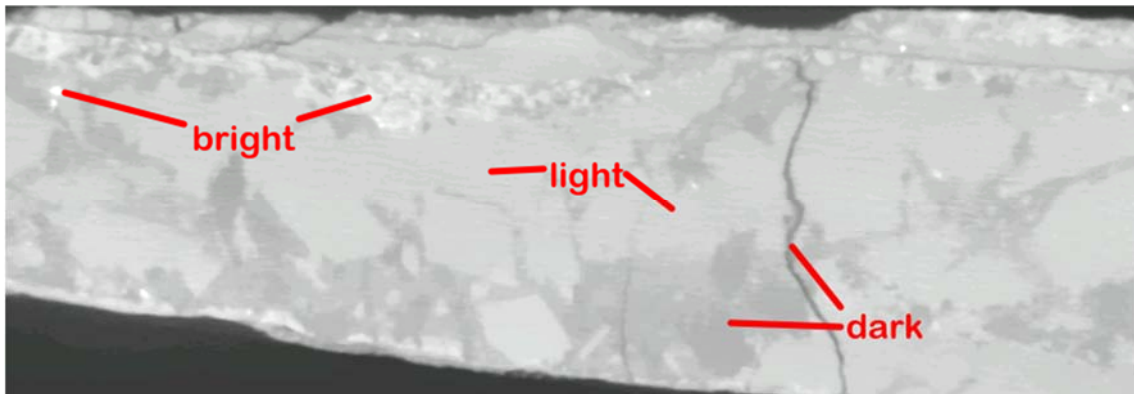


Fig. 11.1.  $\mu$ CT-scans of ZK2 samples (URF Bukov) with tone of brightness as described in tab. 11.1

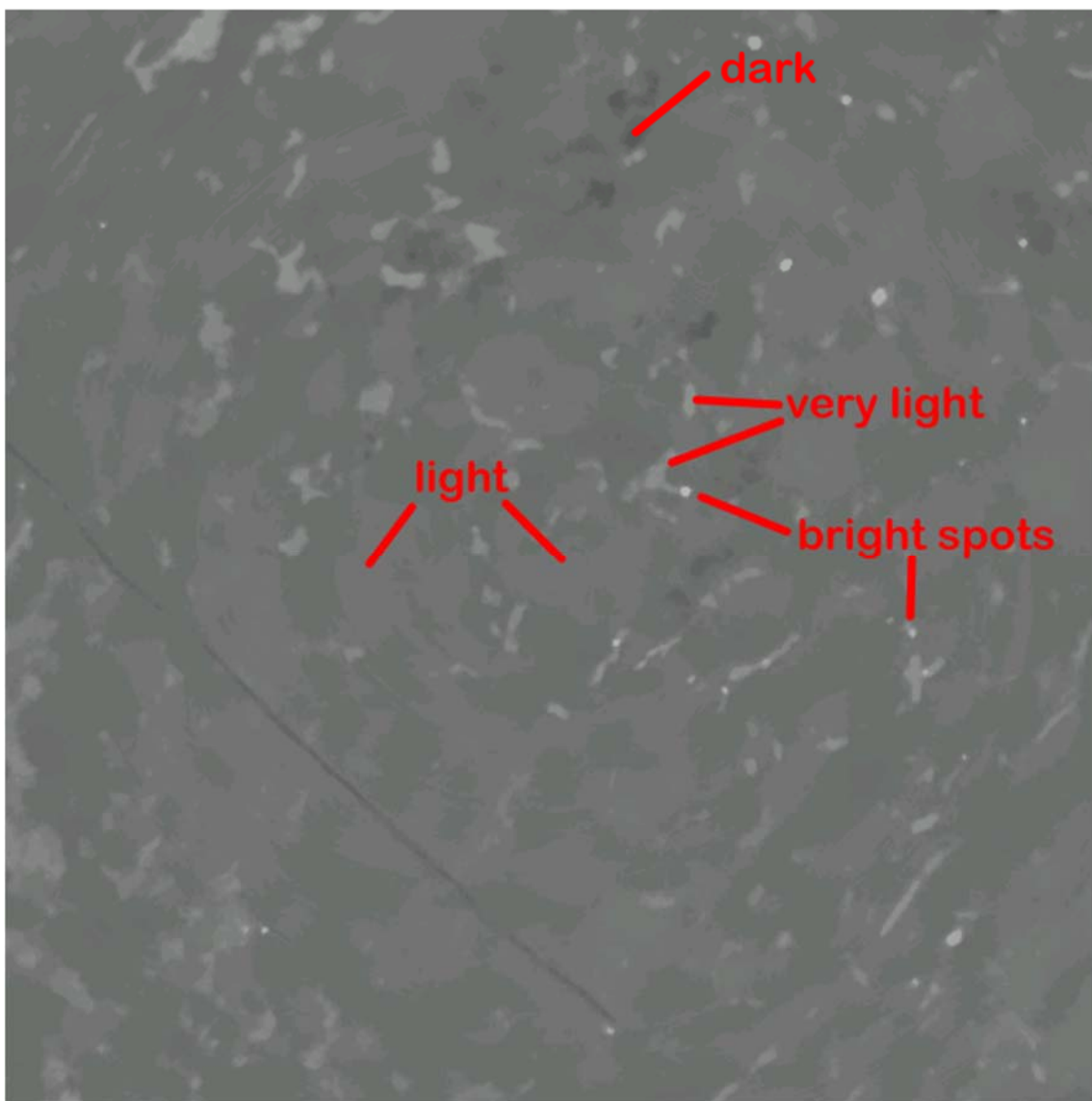


Fig. 11.2  $\mu$ CT-scans of granite 954 m (URL Kurt) with tone of brightness as described in tab. 11.1

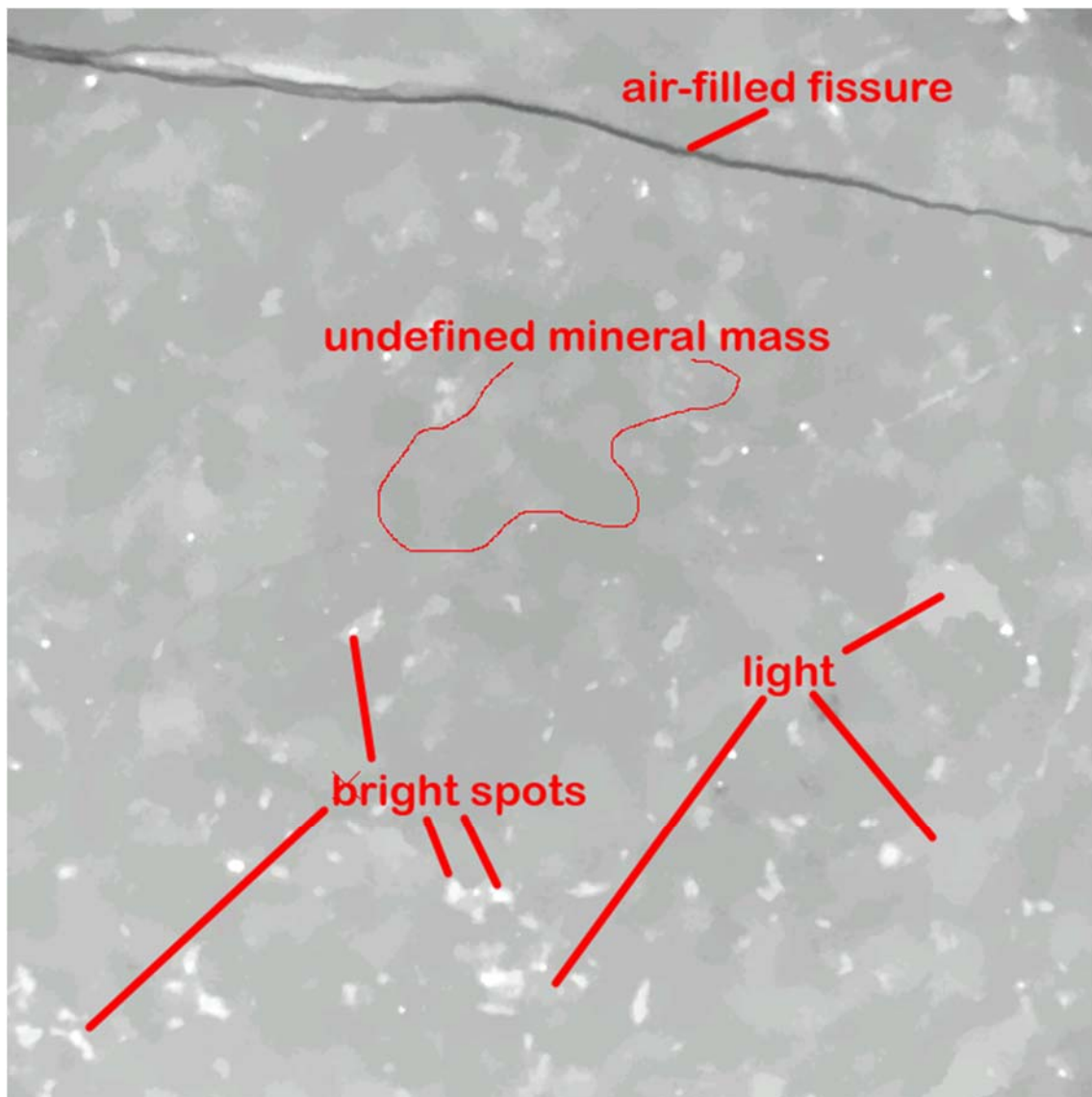
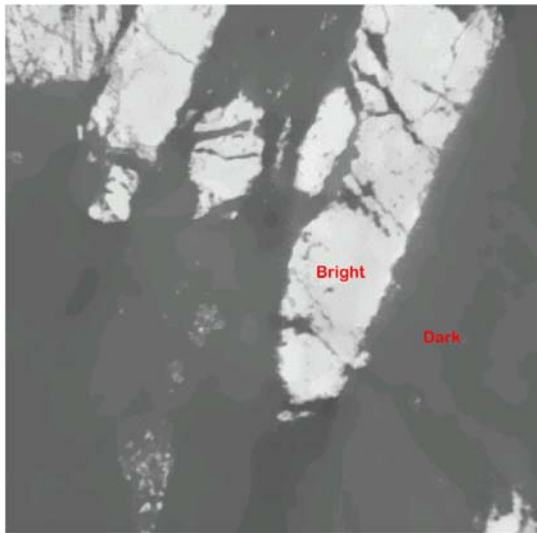
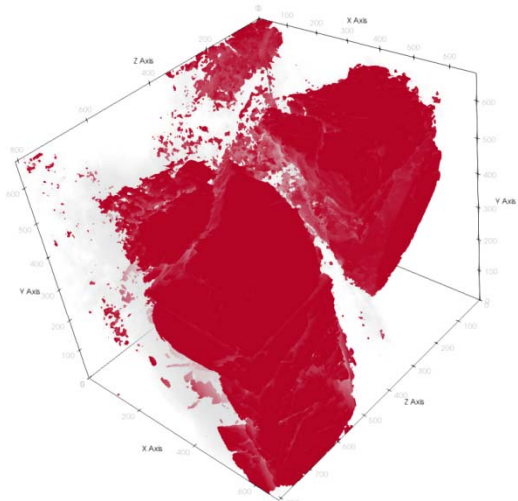


Fig. 11.3  $\mu$ CT-scans of granitic dyke 639 m (URL Kurt) with tone of brightness as described in tab. 11.1

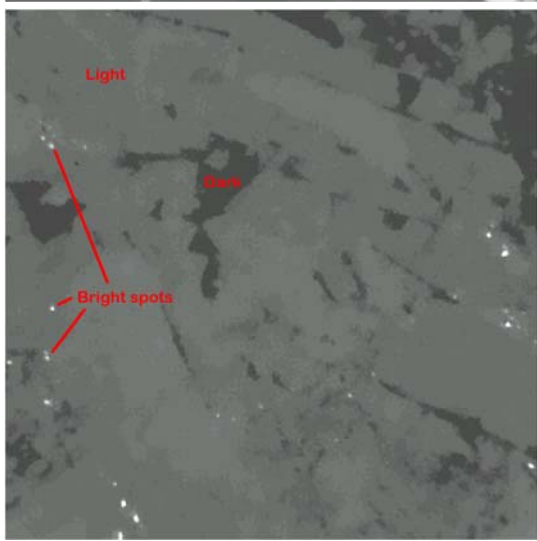
As mentioned previously, the sub-cores will be used as starting materials of elevated temperature experiments. The 8 subcores were scanned and tomographic images showing the structure of the subcore with distinctive phases that are equal to bright tones in the scans. Further information about the separated phases and their distribution over the subcores are coming soon together with reaction products. Therefore, the interpretation of scans for 8 subcores are still suspended although the  $\mu$ CT-scans of sub-cores are completely done.



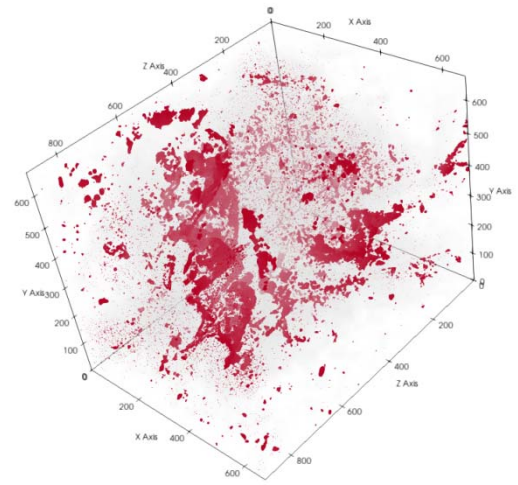
A



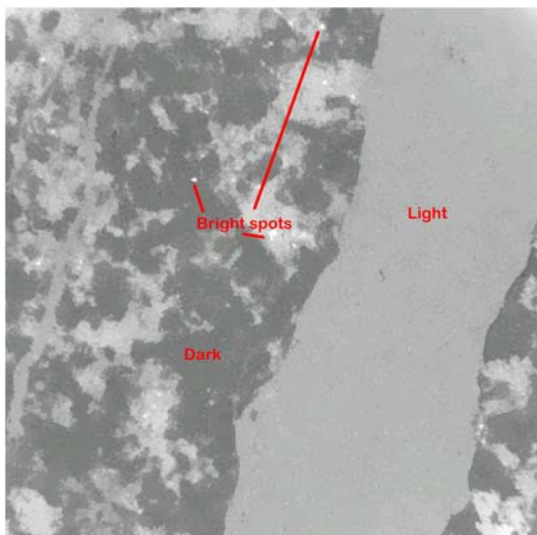
B



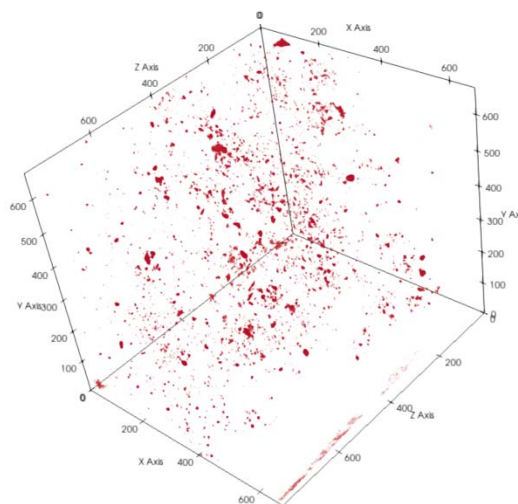
C



D



E



F

Fig. 11.4.  $\mu$ CT-scans (left) mineral phases with different brightness and 3-D tomographic images (right) from BZXII-J01\_A (A) and 3-D tomographic images of bright phases (B); BZXII-J02\_B (C) and 3-D tomographic images of bright spots (D); S8-1A (E) and 3-D tomographic images bright spots.

## Chapter 5. Summary and Conclusions

Fracture systems are commonly observed in granitic crystalline rocks of URL Kurt, South Korea and metamorphosed rocks (S8) in URF Bukov, Czech including fracture fillings (ZK2) and fault breccia rocks (BZXII-J).

The petrology and mineralogy of the whole altered rocks and their fracture fillings in both locations are characterized by different petrological and mineralogical analysis methods.

The protolith texture of altered granite and granitic dykes rocks in URL Kurt is generally preserved and characterized by coarse grained of phaneritic igneous rocks and composed mostly of quartz, plagioclase, feldspars and mica (muscovite and biotite). The original minerals are pseudomorphically replaced by new phases of sericite, calcite, chlorite or act as filler in veins, veinlets or microcracks between and/or in primary crystals. The fracture network systems in rocks are characterized by the light color, generally a few millimeters wide, occurring beside the fracture planes. They are filled by fine- to medium-grained of secondary minerals. The primary minerals are strongly altered by hydrothermal alteration. The most diagnostic mineralogical features within the altered rocks are:

- (1) The Transformation of K-feldspar to illite, calcite, saussuritic pseudomorphs (albitization)
- (2) The transformation of biotite to chlorite (chloritization)
- (3) The recrystallization of scapolite from feldspar (plagioclases) in the main fractures systems of rocks
- (4) The crystallization of scapolite from plagioclase in main fractures systems
- (5) The neoformation of calcite and epidote in veinlets, cracks and voids of rocks

The association of quartz, K-feldspar (microcline), sericite, albite (saussurite), chlorite, and epidote mineralogy of the altered granite allow to estimate the alteration temperatures of the rocks in the range of ca 200 to 400 °C. The appearance of scapolite in large fractures suggested a metasomatic condition at the beginning of the alteration process with temperature up to 400 °C. The detection of zeolite (trace amounts that detected by XRD-measurement), clay (illite, chlorite), and microcrystal of calcite formation are related to the final low temperature stage (tentatively in the range of <200 °C) of the interaction between hydrothermal fluids and rocks. Therefore, the assemblages of secondary minerals and their crystallization sequences reflect the lowering of the temperature of the hydrothermal fluids.

The mineralogy of the host rock metamorphosed cataclasite S8 is characterized quartz, feldspar (plagioclase) as primary minerals but calcite, illite, chlorite, Fe-oxides, actinolite are found as secondary minerals. It indicated a strong alteration of host rock under hydrothermal alteration. The mineralogical characteristics of altered rocks are quite similar to altered granitic rocks of URL Kurt that indicated a temperature of hydrothermal fluids in the range of 200 - 400 °C.

- (1) Chloritization of biotite to chlorite
- (2) Albitization of feldspars
- (3) Sericitization of K-feldspars
- (4) Newly growth of microcrystal carbonates (calcite) from plagioclases
- (5) Formation of Fe-oxides probably from alteration of secondary chlorite to muscovite and hematite.

The fracture fillings of S8, ZK2 and fault breccia BZXII-J are characterized by mostly large granular crystals of calcite which indicated a formation of them at high temperature of boiling hydrothermal fluids when they penetrated to previous fractures of the rocks (300 – 400 °C). Otherwise, the development of calcite in veins and veinlets suggested lower temperatures of fluids together with growth of calcite on primary feldspars (<200 °C).

The characterization of rocks allows expecting the degree of alteration of rocks which gives the possibility to estimate physico-chemical properties of rocks. The porosity and sorption are two important factors of host rocks in EBS because they represent the permeability and capabilities for retention of radionuclides transported in the fracture ground water of engineered barrier systems (EBS). In addition, the porosity and mineralogical composition of rocks are identified as the density of rocks. The lower density of rocks is a consequence of alteration of primary rocks and/or newly formation of secondary rocks especially clay minerals (illite, chlorite) under hydrothermal conditions. The combination between low density of newly formed minerals with fracture and vein systems allow the expected result of lowering density and increase porosity of rock after thermal treatment but increase the sorptive property of rocks due to higher amount of clay minerals.

The primary minerals and transformation processes as well as secondary minerals in hydrothermal systems are expected to have a high potential of rare and REEs elements. The geochemistry and isotope geochemistry as well as geological settings of rocks are missing. It has limited the explanation about the origin of fractures or vein rocks in two areas as well as further understanding about the record hydrothermal fluid interactions during mineralization and alteration. Therefore, it is necessary to do further geochemistry and isotope geochemistry investigation of the investigated rocks.

The subcores samples were selected for further structural investigation using  $\mu$ CT. Tomographic images reveal the structure of subcores with different mineral phases by different tones of brightness. The linkage between mineral phases and their brightness in  $\mu$ CT-scans as well as volume of fissures are still processing and it will be more effective to compare with reaction products after experiments.

## Chapter 6. References

- Abdul-Latif, N. A., and Weaver, C. E., 1969, Kinetics of Acid-Dissolution of Palygorskite (Attapulgitite) and Sepiolite: *Clays and Clay Minerals*, v. 17, p. 169-178.
- Adler, H. H., and Kerr, P. F., 1963, Infrared spectra, symmetry and structure relations of some carbonate minerals: *American Mineralogist*, v. 48, no. 7-8, p. 839-853.
- Alderton, D. H. M., Pearce, J. A., and Potts, P. J., 1980, Rare earth element mobility during granite alteration: Evidence from southwest England: *Earth and Planetary Science Letters*, v. 49, no. 1, p. 149-165.
- Balan, E., and Klopogge, J. T., 2017, Chapter 2 - Theoretical Aspects of Infrared and Raman Spectroscopies, in Gates, W. P., Klopogge, J. T., Madejová, J., and Bergaya, F., eds., *Developments in Clay Science*, Volume 8, Elsevier, p. 6-33.
- Barker, S., and Cox, S., 2011, Oscillatory zoning and trace element incorporation in hydrothermal minerals: Insights from calcite growth experiments: *Geofluids*, v. 11.
- Barton, M., and Johnson, D., 1996, Evaporite-source model for igneous related Fe oxide-(REE-Cu-Au-U) mineralization: *Geology*, v. 24, p. 259-262.
- Bergmann, J., Friedel, P., and Kleeberg, R., 1998, BGMN—a new fundamental parameters based Rietveld program for laboratory X-ray sources, its use in quantitative analysis and structure investigations: *CPD Newsletter*, v. 20, no. 5.
- Bird, D. K., and Helgeson, H. C., 1980, Chemical interaction of aqueous solutions with epidote-feldspar mineral assemblages in geologic systems; 1, Thermodynamic analysis of phase relations in the system CaO-FeO-Fe: *American Journal of Science*, v. 280, no. 9, p. 907-941.
- Brunsmann, A., Franz, G., and Erzinger, J., 2001, REE mobilization during small-scale high-pressure fluid–rock interaction and zoisite/fluid partitioning of La to Eu: *Geochimica et Cosmochimica Acta*, v. 65, p. 559-570.
- Budd, D., Hammes, U., and Ward, W., 2000, Cathodoluminescence in Calcite Cements: New Insights on Pb and Zn Sensitizing, Mn Activation, and Fe Quenching at Low Trace-Element Concentrations: *Journal of Sedimentary Research*, v. 70.
- Castelli, D., Rolfo, F., Compagnoni, R., and Xu, S., 1998, Metamorphic veins with kyanite, zoisite and quartz in the Zhu-Jia-Chong eclogite, Dabie Shan, China: *Island Arc*, v. 7, no. 1-2, p. 159-173.
- Cathelineau, M., 2018, Cation site occupancy in chlorites and illites as a function of temperature: *Clay Minerals*, v. 23, no. 4, p. 471-485.
- Clarke, D. B., 1981, The mineralogy of peraluminous granites; a review: *The Canadian Mineralogist*, v. 19, no. 1, p. 3-17.
- Dahlquist, J. A., 2002, Mafic microgranular enclaves: early segregation from metaluminous

- magma (Sierra de Chepes), Pampean Ranges, NW Argentina: *Journal of South American Earth Sciences*, v. 15, no. 6, p. 643-655.
- Deer, W. A. F., Howie, R. A., and Zussman, J., 2013, *An Introduction to the Rock-Forming Minerals*, Mineralogical Society of Great Britain and Ireland.
- Doebelin, N., and Kleeberg, R., 2015, Profex: a graphical user interface for the Rietveld refinement program BGMN: *Journal of Applied Crystallography*, v. 48, no. 5.
- Dostal, J., and Chatterjee, A. K., 2010, Lead isotope and trace element composition of K-feldspars from peraluminous granitoids of the Late Devonian South Mountain Batholith (Nova Scotia, Canada): implications for petrogenesis and tectonic reconstruction: *Contributions to Mineralogy and Petrology*, v. 159, no. 4, p. 563-578.
- Drake, H., Tullborg, E.-L., and Page, L., 2009, Distinguished multiple events of fracture mineralisation related to far-field orogenic effects in Paleoproterozoic crystalline rocks, Simpevarp area, SE Sweden: *Lithos*, v. 110, p. 37-49.
- Einaudi, M. T., Meinert, L. D., and Newberry, R. J., 1981, Skarn Deposits, *in* Skinner, B. J., ed., *Seventy-Fifth Anniversary Volume*, Society of Economic Geologists, p. 0.
- Eliasson, T., 1993, *Mineralogy, geochemistry and petrophysics of red coloured granite adjacent to fractures* SVENSK KÄRNBRÄNSLEHANTERING AB SWEDISH NUCLEAR FUEL AND WASTE MANAGEMENT CO BOX 5864 S-102 48 STOCKHOLM.
- Ellis, D. E., 1978, Stability and phase equilibria of chloride and carbonate bearing scapolites at 750°C and 4000 bar: *Geochimica et Cosmochimica Acta*, v. 42, no. 8, p. 1271-1281.
- Eggleton, R. A., and Banfield, J. F., 1985, The alteration of granitic biotite to chlorite: *American Mineralogist*, v. 70, no. 9-10, p. 902-910.
- Engvik, A. K., Putnis, A., Fitz Gerald, J. D., and Austrheim, H. k., 2008, Albitization of granitic rocks: the mechanism of replacement of oligoclase by albite: *The Canadian Mineralogist*, v. 46, no. 6, p. 1401-1415.
- Farmer, V. C., and Russell, J. D., 1964, The infra-red spectra of layer silicates: *Spectrochimica Acta*, v. 20, no. 7, p. 1149-1173.
- Ferreiro Mählmann, R., 1994, Zur Bestimmung von Diagenesehöhe und beginnender Metamorphose - Temperaturgeschichte und Tektogenese des Austroalpins und Südpenninikums in Vorarlberg und Mittelbünden.
- Ferreiro Mählmann, R., 1996, Das Diagenese-Metamorphose-Muster von Vitritreflexion und Illit-"Kristallinität" in Mittelbünden und im Oberhalbstein. Teil 2: Korrelation kohlenpetrographischer und mineralogischer Parameter.
- Ferreiro Mählmann, R., 2001, Correlation of very low grade data to calibrate a thermal maturity model in a nappe tectonic setting, a case study from the Alps: *Tectonophysics*, v. 334, no. 1, p. 1-33.
- Ferreiro Mählmann, R., Bozkaya, Ö., Potel, S., Le Bayon, R., Šegvić, B., and Nieto, F., 2012,

- The pioneer work of Bernard Kübler and Martin Frey in very low-grade metamorphic terranes: paleo-geothermal potential of variation in Kübler-Index/organic matter reflectance correlations. A review: *Swiss Journal of Geosciences*, v. 105, no. 2, p. 121-152.
- Ferry, J., 1979, Reaction mechanisms, physical conditions, and mass transfer during hydrothermal alteration of mica and feldspar in granitic rocks from south-central Maine, USA: *Contributions to Mineralogy and Petrology*, v. 68, p. 125-139.
- Freiberger, R., Hecht, L., Cuney, M., and Morteani, G., 2001, Secondary Ca-Al silicates in plutonic rocks: Implications for their cooling history: *Contributions to Mineralogy and Petrology*, v. 141, p. 415-429.
- Frey, M., Capitani, C. D., and Liou, J. G., 1991, A new petrogenetic grid for low-grade metabasites: *Journal of Metamorphic Geology*, v. 9, no. 4, p. 497-509.
- Gastuche, M., 1963, The octahedral layer: *Clays and Clay Minerals*, v. 12, p. 471-493.
- Goko, K., 2000, Structure and hydrology of the Ogiri field, West Kirishima geothermal area, Kyushu, Japan: *Geothermics*, v. 29, p. 127-149.
- Gorobets, B., and Walker, G., 1995, Origins of luminescence in minerals: a summary of fundamental studies and applications: *Advance Mineralogy*, v. 2, p. 138-146.
- Götze, J., 2012, Application of Cathodoluminescence Microscopy and Spectroscopy in Geosciences: *Microscopy and Microanalysis*, v. 18, no. 6, p. 1270-1284.
- Habermann, D., Neuser, R. D., and Richter, D. K., 2000, Quantitative High Resolution Spectral Analysis of Mn<sup>2+</sup> in Sedimentary Calcite, *in* Pagel, M., Barbin, V., Blanc, P., and Ohnenstetter, D., eds., *Cathodoluminescence in Geosciences*: Berlin, Heidelberg, Springer Berlin Heidelberg, p. 331-358.
- Hay, S., Hall, J., Simmons, G., and Russell, M., 1988, Sealed microcracks in the Lewisian of NW Scotland: A record of 2 billion years of fluid circulation: *Journal of The Geological Society - J GEOL SOC*, v. 145, p. 819-830.
- Hedenquist, J., and White, N., 1995, Epithermal gold deposits. Styles, characteristics and exploration: *Society of Economic Geologists, Newsletter*, v. 23, p. 1, 9-13.
- Henley, R. W., and Ellis, A. J., 1983, Geothermal systems ancient and modern: a geochemical review: *Earth-Science Reviews*, v. 19, no. 1, p. 1-50.
- Huntington, K., Sumner, K., Camp, E., Cladouhos, T., Uddenberg, M., Swyer, M., and Garrison, G., 2015, Assessing past fracture connectivity in geothermal reservoirs using clumped isotopes: proof of concept in the Blue Mountain Geothermal field, Nevada USA.
- Tulloch, J. A., 1982 Mineralogical observations on carbonate scaling in geothermal wells at Kawerau and Broadlands, *in* *Proceedings Proceedings of the New Zealand Geothermal Workshop (Proc N Z Geotherm Workshop*, p. 131-134

- Moore, D. M ; Reynold, R. C., Jr. 1997. X-Ray Diffraction and the Identification and Analysis of Clay Minerals, 2nd ed. xviii + 378 pp. Oxford, New York: Oxford University Press. ISBN 0 19 508713 5: Geological Magazine, v. 135, no. 6, p. 819-842.
- Janeczek, J., 1994, The effect of aluminous titanite on the biotite-chlorite and amphibole-chlorite reactions: European Journal of Mineralogy, v. 6, no. 5, p. 623-625.
- Keith, T. E. C., and Muffler, L. J. P., 1978, Minerals produced during cooling and hydrothermal alteration of ash flow tuff from Yellowstone drill hole Y-5: Journal of Volcanology and Geothermal Research, v. 3, no. 3, p. 373-402.
- Kontonikas-Charos, A., Ciobanu, C. L., Cook, N. J., Ehrig, K., Krneta, S., and Kamenetsky, V. S., 2018, Rare earth element geochemistry of feldspars: examples from Fe-oxide Cu-Au systems in the Olympic Cu-Au Province, South Australia: Mineralogy and Petrology, v. 112, no. 2, p. 145-172.
- Kusakabe, H., 1982, An interpretation of zeolitic zoning around kuroko ore deposits on the basis of hydrothermal experiments: Mining Geology, v. 32, no. 6, p. 435-442.
- Lapiente, M. P., Turi, B., and Blanc, P., 2000, Marbles from Roman Hispania: stable isotope and cathodoluminescence characterization: Applied Geochemistry, v. 15, no. 10, p. 1469-1493.
- Larkin, P., 2011, Instrumentation and Sampling Methods. In book: Infrared and Raman Spectroscopy p. 27-54.
- Liou, J. G., 1971, P—T Stabilities of Laumontite, Wairakite, Lawsonite, and Related Minerals in the System  $\text{CaAl}_2\text{Si}_2\text{O}_8\text{-SiO}_2\text{-H}_2\text{O}$ : Journal of Petrology, v. 12, no. 2, p. 379-411.
- Lohmann, K. C., and Walker, J. C., 1989, The  $\delta^{18}\text{O}$  record of Phanerozoic abiotic marine calcite cements: Geophysical Research Letters, v. 16, no. 4, p. 319-322.
- Long, J. V. P., and Agrell, S. O., 1965, The cathodoluminescence of minerals in thin section: Mineralogical magazine and journal of the Mineralogical Society, v. 34, no. 268, p. 318-326.
- Mason, R. A., 1987, Ion microprobe analysis of trace elements in calcite with an application to the cathodoluminescence zonation of limestone cements from the Lower Carboniferous of South Wales, U.K: Chemical Geology, v. 64, no. 3, p. 209-224.
- McNamara, D. D., Lister, A., and Prior, D. J., 2016, Calcite sealing in a fractured geothermal reservoir: Insights from combined EBSD and chemistry mapping: Journal of Volcanology and Geothermal Research, v. 323, p. 38-52.
- Migdisov, A., Xu, H., Williams-Jones, A., and Brugger, J., 2020, The REEs in Hydrothermal Systems, p. 1-12.
- Morad, S., Al-Aasm, I. S., Nader, F. H., Ceriani, A., Gasparrini, M., and Mansurbeg, H., 2012, Impact of diagenesis on the spatial and temporal distribution of reservoir quality in the Jurassic Arab D and C members, offshore Abu Dhabi oilfield, United Arab

- Emirates: *GeoArabia*, v. 17, no. 3, p. 17-56.
- Möller, P., Morteani, G., and Dulski, P., 1984, The origin of the calcites from Pb-Zn veins in the Harz Mountains, Federal Republic of Germany: *Chemical Geology*, v. 45, no. 1, p. 91-112.
- Möller, P., Morteani, G., Hoefs, J., and Parekh, P. P., 1979, The origin of the ore-bearing solution in the Pb · Zn veins of the western Harz, Germany, as deduced from rare-earth element and isotope distributions in calcites: *Chemical Geology*, v. 26, no. 3, p. 197-215.
- Nagy, K. L., 1995, Dissolution and precipitation kinetics of sheet silicates: *Reviews in Mineralogy and Geochemistry*, v. 31, no. 1, p. 173-233.
- Nagy, K. L., and Lasaga, A. C., 1992, Dissolution and precipitation kinetics of gibbsite at 80°C and pH 3: The dependence on solution saturation state: *Geochimica et Cosmochimica Acta*, v. 56, no. 8, p. 3093-3111.
- Newton, R. C., and Goldsmith, J. R., 1975, Stability of the scapolite meionite ( $3\text{CaAl}_2\text{Si}_2\text{O}_2 \cdot \text{CaCO}_3$ ) at high pressures and storage of  $\text{CO}_2$  in the deep crust: *Contributions to Mineralogy and Petrology*, v. 49, no. 1, p. 49-62.
- Newton, R. C., and Goldsmith, J. R., 1976, Stability of the end-member scapolites:  $3\text{NaAlSi}_3\text{O}_8 \cdot \text{NaCl}$ ,  $3\text{CaAl}_2\text{Si}_2\text{O}_8 \cdot \text{CaCO}_3$ ,  $3\text{CaAl}_2\text{Si}_2\text{O}_8 \cdot \text{CaSO}_4$ : *Zeitschrift für Kristallographie - Crystalline Materials*, v. 143, p. 333 - 353.
- Nguyen-Thanh, L., Mählmann, R. F., Hoang-Minh, T., Petschick, R., Reischmann, T., Nesbor, H.-D., Ruttman, M., and Fritsche, J.-G., 2021, Clay mineral formation in Permian rocks of a geothermal borehole at Northern Upper Rhine Graben, Germany: *International Journal of Earth Sciences*, v. 110, no. 4, p. 1415-1438.
- Nijland, T. G., and Touret, J. L. R., 2001, Replacement of graphic pegmatite by graphic albite-actinolite-clinopyroxene intergrowths (Mjåvatn, southern Norway): *European Journal of Mineralogy*, v. 13, no. 1, p. 41-50.
- Orville, P. M., 1963, Alkali ion exchange between vapor and feldspar phases: *American Journal of Science*, v. 261, no. 3, p. 201-237.
- Orville, P. M., 1975, Stability of scapolite in the system Ab-An-NaCl-CaCO<sub>3</sub> at 4 kb and 750°C: *Geochimica et Cosmochimica Acta*, v. 39, no. 8, p. 1091-1105.
- Ovenstone, J., Romani, J. O., Davies, D., and Silver, J., 2003, Topotactic crystallisation of calcite under hydrothermal conditions: *Journal of Materials Science*, v. 38, no. 12, p. 2743-2746.
- Pagel, M., Barbin, V., Blanc, P., and Ohnenstetter, D., 2000, Cathodoluminescence in Geosciences: An Introduction, *in* Pagel, M., Barbin, V., Blanc, P., and Ohnenstetter, D., eds., *Cathodoluminescence in Geosciences*: Berlin, Heidelberg, Springer Berlin Heidelberg, p. 1-21.

- Putnis, A., Hinrichs, R., Putnis, C., Golla-Schindler, U., and Collins, L., 2007, Hematite in porous red-clouded feldspars: Evidence of large-scale crustal fluid–rock interaction: *Lithos*, v. 95, p. 10-18.
- Que, M., and Allen, A. R., 2018, Sericitization of plagioclase in the Rosses Granite Complex, Co. Donegal, Ireland: *Mineralogical Magazine*, v. 60, no. 403, p. 927-936.
- Ramseyer, K., Baumann, J., Matter, A., and Mullis, J., 2018, Cathodoluminescence Colours of  $\alpha$ -Quartz: *Mineralogical Magazine*, v. 52, no. 368, p. 669-677.
- Rimstidt, J. D., Balog, A., and Webb, J., 1998, Distribution of trace elements between carbonate minerals and aqueous solutions: *Geochimica et Cosmochimica Acta*, v. 62, no. 11, p. 1851-1863.
- Rochelle, C. A., Milodowski, A. E., Savage, D., and Corella, M., 1989, Secondary mineral growth in fractures in the Miravalles geothermal system, Costa Rica: *Geothermics*, v. 18, no. 1, p. 279-286.
- Rusk, B. G., Lowers, H. A., and Reed, M. H., 2008, Trace elements in hydrothermal quartz: Relationships to cathodoluminescent textures and insights into vein formation: *Geology*, v. 36, no. 7, p. 547-550.
- Sandström, B., Annersten, H., and Tullborg, E.-L., 2008, Fracture-related hydrothermal alteration of metagranitic rock and associated changes in mineralogy, geochemistry and degree of oxidation: A case study at Forsmark, central Sweden: *International Journal of Earth Sciences*, v. 99, p. 1-25.
- Sass, B. M., Rosenberg, P. E., and Kittrick, J. A., 1987, The stability of illite/smectite during diagenesis: An experimental study: *Geochimica et Cosmochimica Acta*, v. 51, p. 2103-2115.
- Schmidt, R., Bucher, K., and Stober, I., 2018, Experiments on granite alteration under geothermal reservoir conditions and the initiation of fracture evolution: *European Journal of Mineralogy*, v. 30.
- Seki, Y., 1972, Lower grade stability limit of epidote in the light of natural occurrences: *Journal of the Geological Society of Japan*, v. 78, p. 405-413.
- Sharp, W. E., 1965, The deposition of hydrothermal quartz and calcite: *Economic Geology*, v. 60, no. 8, p. 1635-1644.
- Simmons, S. F., and Christenson, B. W., 1993, Towards a unified theory on calcite formation in boiling geothermal systems, *in Proceedings NZ Geothermal Workshop*, New Zealand, 1993.
- Simmons, S. F., and Christenson, B. W., 1994, Origins of calcite in a boiling geothermal system: *American Journal of Science*, v. 294, no. 3, p. 361.
- Sun, S. S., and Hanson, G. N., 1975, Origin of Ross Island basanitoids and limitations upon the heterogeneity of mantle sources for alkali basalts and nephelinites: *Contributions to*

Mineralogy and Petrology, v. 52, no. 2, p. 77-106.

Strauss, T. A. L., 2003, The geology of the Proterozoic Haveri Au-Cu deposit, Southern Finland [PhD thesis: Rhodes University.

Ufer, K., Kleeberg, R., Bergmann, J., Curtius, H., and Dohrmann, R., 2008, Refining real structure parameters of disordered layer structures within the Rietveld method: Zeitschrift fur Kristallographie Supplements, v. 2008.

Vanko, D. A., and Bishop, F. C., 1982, Occurrence and origin of marialitic scapolite in the Humboldt lopolith, N.W. Nevada: Contributions to Mineralogy and Petrology, v. 81, p. 277-289.

Veizer, J., 1983, Chemical diagenesis of carbonates: theory and application of trace element technique: Stable isotopes in sedimentary geology, v. 10, p. 3.1-3.100.

Velde, B. D., 1985, Clay minerals : a physico-chemical explanation of their occurrence 1985.

Wogelius, R. A., Fraser, D. G., Wall, G. R. T., and Grime, G. W., 1997, Trace element and isotopic zonation in vein calcite from the Mendip Hills, UK, with spatial-process correlation analysis: Geochimica et Cosmochimica Acta, v. 61, no. 10, p. 2037-2051.

Xiao, B., and Chen, H., 2020, Elemental behavior during chlorite alteration: New insights from a combined EMPA and LA-ICPMS study in porphyry Cu systems: Chemical Geology, v. 543, p. 119604.

Zhong, S., and Mucci, A., 1995, Partitioning of rare earth elements (REEs) between calcite and seawater solutions at 25 C and 1 atm, and high dissolved REE concentrations: Geochimica et Cosmochimica Acta, v. 59, no. 3, p. 443-453.

# Appendix

# Appendix 1. Refined parameters from Rietveld refinement for XRD-diffractogram from Profex-BGMN software

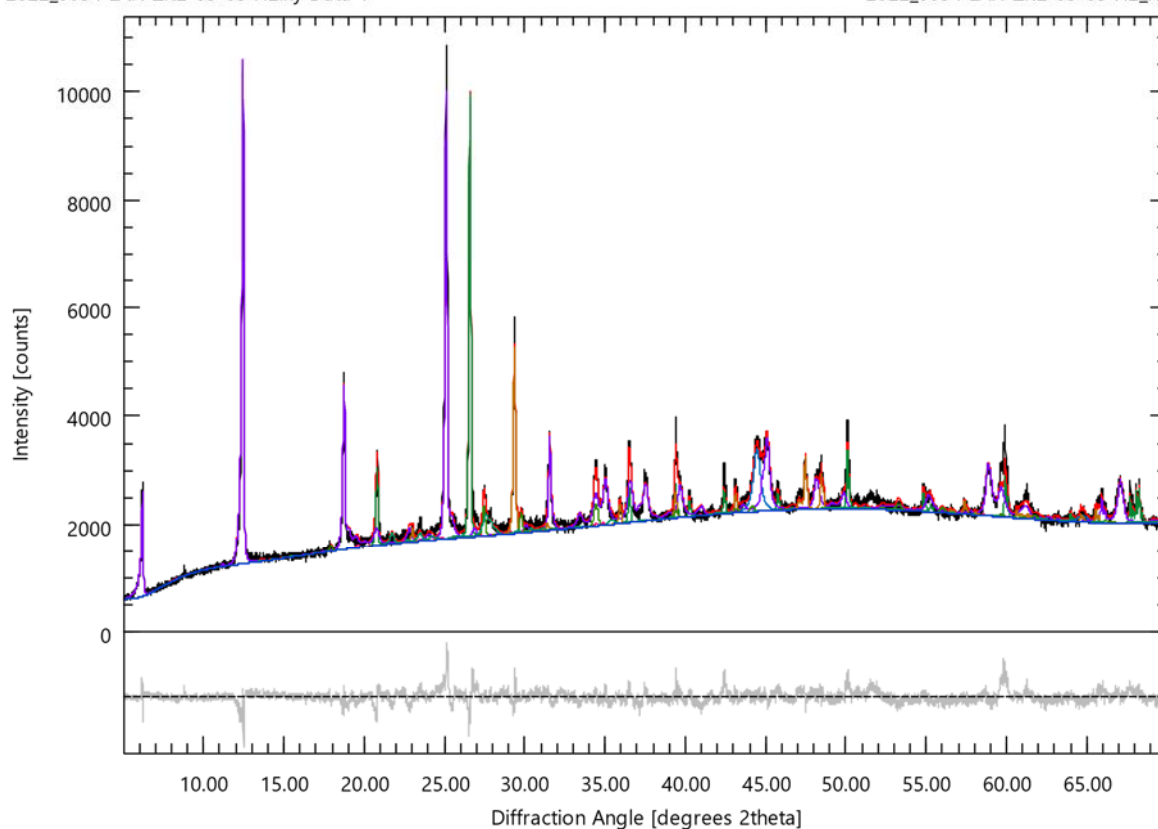
## Sample Information

ZK2-03-03 H2				
File Name	ZK2-03-03 H2_R06.dia			
Instrument configuration	PW1830_TU Darmstadt_adopted.geq			
Wavelength	CU (1.5406 Å)			
Directory	C:/Users/kasbo/Documents/Data_Laptop/Profex_data/BGE_Project/XRD_Profex_MUSE_Lan			
Date of Refinement	Dienstag Juli 26, 2022			
Operator	Kasbo			
Statistics	$R_{wp} = 4.42$	$R_{exp} = 2.21$	$\chi^2 = 4.0000$	GoF = 2.0000

## Diffraction Pattern

2022\_0054 LAN ZK2-03-03 H2.xy Data 1

2022\_0054 LAN ZK2-03-03 H2\_R06.dia



## Global GOALS

Parameter	Value	ESD
Qquartz	0.164	0.002
Qironalpha**	0.0373	0.0008
Qchlorite2b	0.564	0.005
Qmusc2m1	0.015	0.004
QCalcite	0.104	0.002

Qtitanite	0.042	0.002
Qanortk25	0.074	0.003
QSiO2p3221	0.000000	0.000000

*\*\* part of sample holder*

Local GOALs

**Quartz**

Parameter	Value	ESD
Refined composition	SI3 O6	
A	0.491438	
C	0.540681	
GrainSize(1,0,1)	1105	217

**Iron\_alpha**

Parameter	Value	ESD
Refined composition	FE2	
A	0.287854	

**CHLORITE\_Iib-2**

Parameter	Value	ESD
Refined composition	AL4.6820 FE3.9916 H16 MG6.0084 SI5.2480 O36	
A	0.53636	
B	0.92913	
C	1.425622	
BETA	96.998	

**MUSCOVITE\_2M1**

Parameter	Value	ESD
Refined composition	AL11.6800 FE0.3200 K4 SI12 O48	
A	0.525000	
B	0.90124	
C	2.10000	
BETA	96.0000	

**Calcite**

Parameter	Value	ESD
Refined composition	C6 CA6 O18	
A	0.498865	
C	1.706218	
GrainSize(1,1,1)	219	16

**Titanite**

Parameter	Value	ESD
Refined composition	CA4 SI4 TI4 O20	
A	0.75256	
B	0.86395	
C	0.70893	

BETA	127.274	
------	---------	--

#### Albite\_high\_K25

Parameter	Value	ESD
Refined composition	AL4 K1 NA3 SI12 O32	
A	0.823700	
B	1.29200	
C	0.713000	
ALPHA	92.27	
BETA	116.288	
GAMMA	90.7000	

#### SiO2p3221

Parameter	Value	ESD
Refined composition	SI3 O6	
A	UNDEF	
C	UNDEF	
GrainSize(1,1,1)	UNDEF	

#### Refined Chemical Composition

Phase	Phase Quantity (wt-%)	H (wt-%)	C (wt-%)	O (wt-%)	Na (wt-%)	Mg (wt-%)	Al (wt-%)	Si (wt-%)	K (wt-%)	Ca (wt-%)	Ti (wt-%)	Fe (wt-%)
Albite_high_K25	7,44	0,00	0,00	48,07	6,48	0,00	10,13	31,65	3,67	0,00	0,00	0,00
CHLORITE_Ilb-2	56,40	1,31	0,00	46,65	0,00	11,83	10,23	11,94	0,00	0,00	0,00	18,05
Calcite	10,38	0,00	12,00	47,96	0,00	0,00	0,00	0,00	0,00	40,04	0,00	0,00
Iron_alpha**	3,73	0,00	0,00	0,00	0,00	0,00	0,00	0,00	0,00	0,00	0,00	100,00
MUSCOVITE_2M1	1,51	0,00	0,00	48,17	0,00	0,00	19,77	21,14	9,81	0,00	0,00	1,12
Quartz	16,35	0,00	0,00	53,26	0,00	0,00	0,00	46,74	0,00	0,00	0,00	0,00
SiO2p3221	0,00	0,00	0,00	53,26	0,00	0,00	0,00	46,74	0,00	0,00	0,00	0,00
Titanite	4,18	0,00	0,00	40,81	0,00	0,00	0,00	14,33	0,00	20,45	24,42	0,00
Weighted total	99,99	0,74	1,25	46,01	0,48	6,67	6,82	17,65	0,42	5,01	1,02	13,93

\*\* part of sample holder

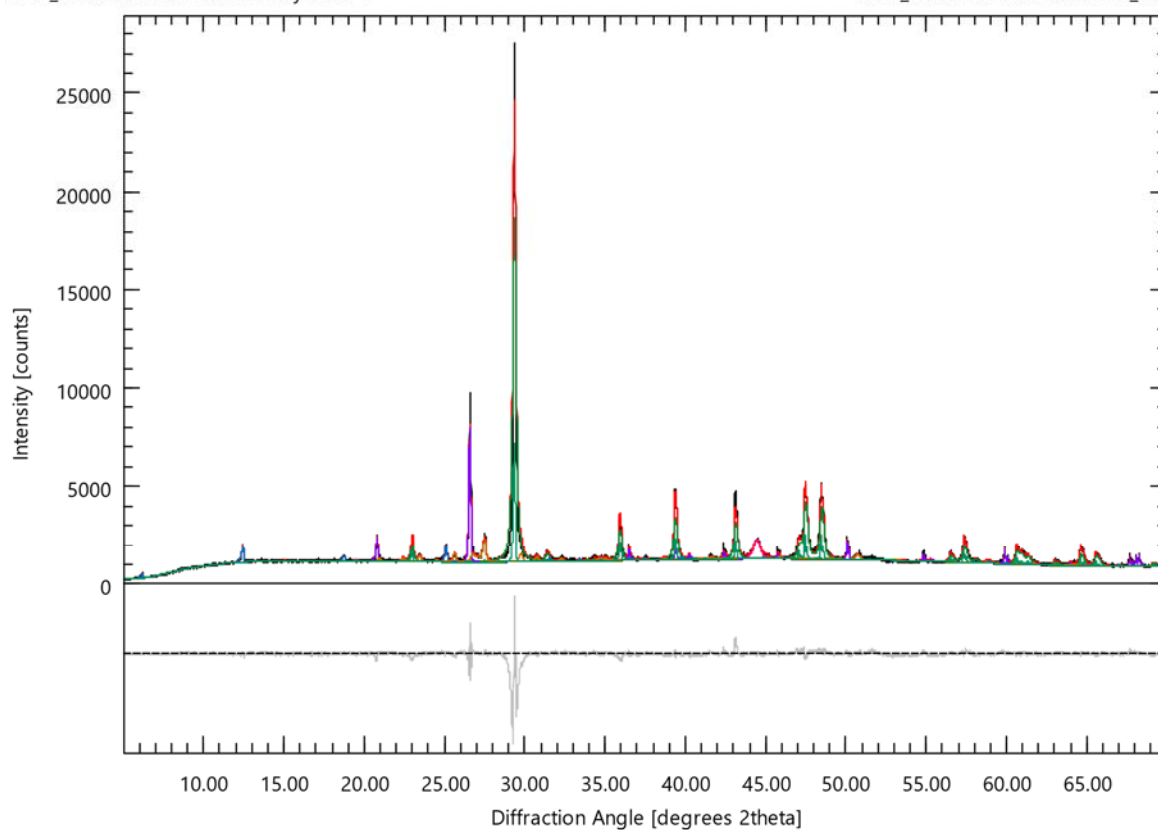
Sample Information

ZK2-03-04 H2				
File Name	ZK2-03-04 H2_R03a.dia			
Instrument configuration	PW1830_TU Darmstadt_adopted.geq			
Wavelength	CU (1.5406 Å)			
Directory	C:/Users/kasbo/Documents/Data_Laptop/Profex_data/BGE_Project/XRD_Profex_MUSE_Lan			
Date of Refinement	Sonntag Juli 31, 2022			
Operator	kasbo			
Statistics	$R_{wp} = 5.32$	$R_{exp} = 2.79$	$\chi^2 = 3.6359$	GoF = 1.9068

Diffraction Pattern

2022\_0055 LAN ZK2-03-04 H2.xy Data 1

2022\_0055 LAN ZK2-03-04 H2\_R03a.dia



Global GOALS

Parameter	Value	ESD
QCalcite	0.594	0.005
Qchlorite2b	0.043	0.003
Qquartz	0.1064	0.0009
Qironalpha**	0.0256	0.0004
Qmicroint2	0.106	0.003
Qtitanite	0.0048	0.0009
QCalciteMark	0.121	0.005

\*\* part of sample holder

Local GOALS

Calcite

Parameter	Value	ESD
Refined composition	C6 CA6 O18	
A	0.498792	
C	1.705319	
GrainSize(1,1,1)	50.27	

CHLORITE\_Iib-2

Parameter	Value	ESD
Refined composition	AL4.6820 FE3.7414 H16 MG6.2586 SI5.2480 O36	
A	0.53666	
B	0.9290	
C	1.42640	
BETA	97.0000	

Quartz

Parameter	Value	ESD
Refined composition	SI3 O6	
A	0.491532	
C	0.540723	
GrainSize(1,0,1)	ERROR	

Iron\_alpha

Parameter	Value	ESD
Refined composition	FE2	
A	0.287856	

MICROCLINE\_intermediate2

Parameter	Value	ESD
Refined composition	AL4 K4 SI12 O32	
A	0.85858	
B	1.30013	
C	0.71921	
ALPHA	89.977	
BETA	115.908	
GAMMA	90.3000	

Titanite

Parameter	Value	ESD
Refined composition	CA4 SI4 TI4 O20	
A	0.75273	
B	0.880100	
C	0.70377	
BETA	126.171	

Parameter	Value	ESD
Refined composition	C6 CA6 O18	
A	0.499075	
C	1.706610	
GrainSize(1,1,1)	ERROR	

#### Refined Chemical Composition

Phase	Phase Quantity (wt-%)	H (wt-%)	C (wt-%)	O (wt-%)	Mg (wt-%)	Al (wt-%)	Si (wt-%)	K (wt-%)	Ca (wt-%)	Ti (wt-%)	Fe (wt-%)
CHLORITE_IIb-2	4,29	1,31	0,00	46,95	12,40	10,30	12,01	0,00	0,00	0,00	17,03
Calcite	59,36	0,00	12,00	47,96	0,00	0,00	0,00	0,00	40,04	0,00	0,00
CalciteMark	12,10	0,00	12,00	47,96	0,00	0,00	0,00	0,00	40,04	0,00	0,00
Iron_alpha**	2,56	0,00	0,00	0,00	0,00	0,00	0,00	0,00	0,00	0,00	100,00
MICROCLINE_intermediate2	10,57	0,00	0,00	45,99	0,00	9,69	30,27	14,05	0,00	0,00	0,00
Quartz	10,64	0,00	0,00	53,26	0,00	0,00	46,74	0,00	0,00	0,00	0,00
Titanite	0,48	0,00	0,00	40,81	0,00	0,00	14,33	0,00	20,45	24,42	0,00
Weighted total	100,00	0,06	8,58	47,01	0,53	1,47	8,76	1,49	28,71	0,12	3,29

\*\* part of sample holder

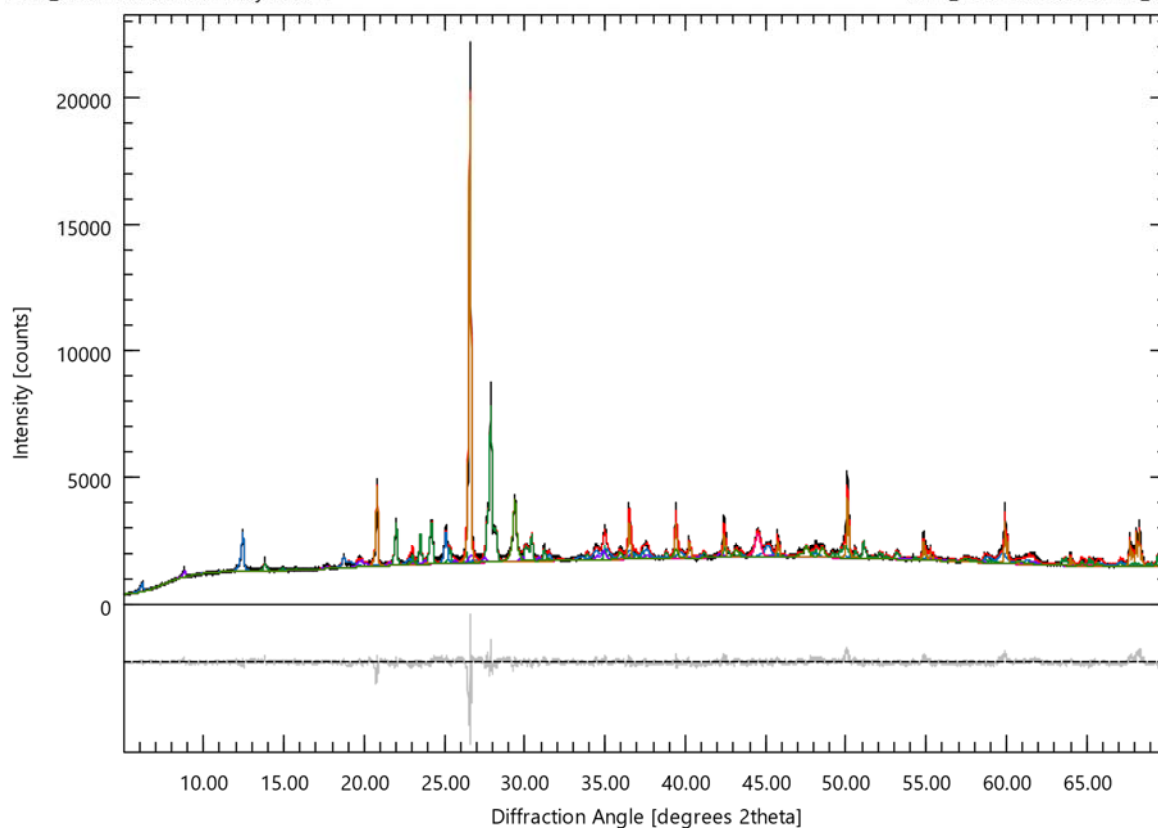
#### Sample Information

S8-6.2 H2	
File Name	S8-6.2 H2_R02.dia
Instrument configuration	PW1830_TU Darmstadt_adopted.geq
Wavelength	CU (1.5406 Å)
Directory	C:/Users/kasbo/Documents/Data_Laptop/Profex_data/BGE_Project/XRD_Profex_MUSE_Lan
Date of Refinement	Dienstag Juli 26, 2022
Operator	kasbo
Statistics	$R_{wp} = 4.64$ $R_{exp} = 2.37$ $\chi^2 = 3.8330$ $GoF = 1.9578$

Diffraction Pattern

2022\_0056 LAN S8-6.2 H2.xy Data 1

2022\_0056 LAN S8-6.2 H2\_R02.dia



Global GOALS

Parameter	Value	ESD
Qalbite	0.332	0.003
Qchlorite2b	0.191	0.004
QMuscovite2M1	0.081	0.004
Qironalpha**	0.0175	0.0004
Qquartz	0.285	0.002
QCalcite	0.094	0.002

\*\* part of sample holder

Local GOALS

**Plagioclase\_Albite**

Parameter	Value	ESD
Refined composition	AL4.3600 NA4 SI11.6400 O32	
A	0.814020	
B	1.279671	
C	0.715898	
ALPHA	94.2361	
BETA	116.6141	
GAMMA	87.8467	

**CHLORITE\_Iib-2**

Parameter	Value	ESD
Refined composition	AL4.6820 FE5.2520 H16 MG4.7480 SI5.2480 O36	
A	0.53634	

B	0.92775	
C	1.42633	
BETA	96.874	

#### Muscovite2M1

Parameter	Value	ESD
Refined composition	AL11.6800 FE0.3200 K2.4000 SI12 O48	
A	0.52112	
B	0.90116	
C	2.00162	
BETA	94.5000	
GrainSize(1,0,0)	179	55

#### Iron\_alpha

Parameter	Value	ESD
Refined composition	FE2	
A	0.287505	

#### Quartz

Parameter	Value	ESD
Refined composition	SI3 O6	
A	0.4914982	
C	0.540736	
GrainSize(1,0,1)	1028	109

#### Calcite

Parameter	Value	ESD
Refined composition	C6 CA6 O18	
A	0.498668	
C	1.70439	
GrainSize(1,1,1)	48.9	

#### Refined Chemical Composition

Phase	Phase Quantity (wt-%)	H (wt-%)	C (wt-%)	O (wt-%)	Na (wt-%)	Mg (wt-%)	Al (wt-%)	Si (wt-%)	K (wt-%)	Ca (wt-%)	Fe (wt-%)
CHLORITE_IIb-2	19,07	1,27	0,00	45,19	0,00	9,05	9,91	11,56	0,00	0,00	23,01
Calcite	9,40	0,00	12,00	47,96	0,00	0,00	0,00	0,00	0,00	40,04	0,00
Iron_alpha**	1,75	0,00	0,00	0,00	0,00	0,00	0,00	0,00	0,00	0,00	100,00
Muscovite2M1	8,06	0,00	0,00	50,13	0,00	0,00	20,57	22,00	6,13	0,00	1,17
Plagioclase_Albite	33,22	0,00	0,00	48,83	8,77	0,00	11,22	31,18	0,00	0,00	0,00
Quartz	28,50	0,00	0,00	53,26	0,00	0,00	0,00	46,74	0,00	0,00	0,00
Weighted total	100,00	0,24	1,13	48,57	2,91	1,73	7,28	27,66	0,49	3,76	6,24

\*\* part of sample holder

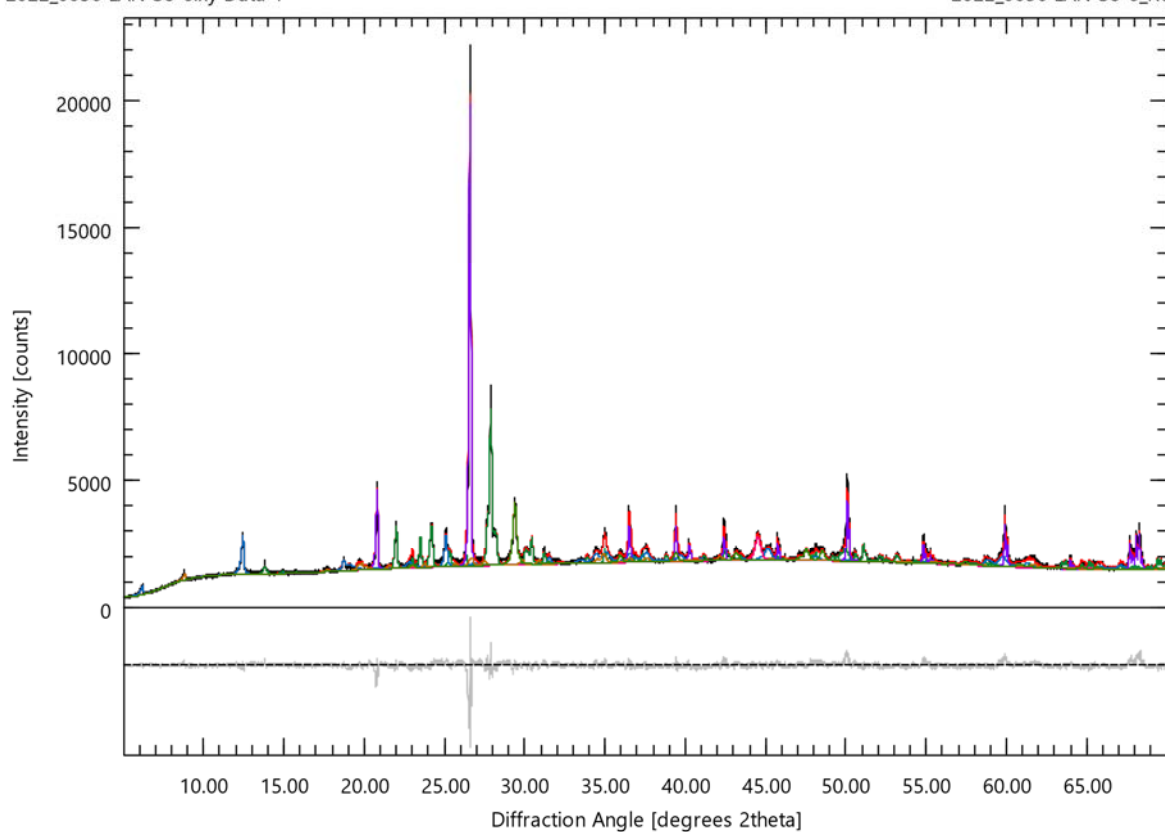
Sample Information

S8-6				
File Name	S8-6_R02.dia			
Instrument configuration	PW1830_TU Darmstadt_adopted.geq			
Wavelength	CU (1.5406 Å)			
Directory	C:/Users/kasbo/Documents/Data_Laptop/Profex_data/BGE_Project/XRD_Profex_MUSE_Lan			
Date of Refinement	Dienstag Juli 26, 2022			
Operator	kasbo			
Statistics	$R_{wp} = 4.64$	$R_{exp} = 2.37$	$\chi^2 = 3.8330$	GoF = 1.9578

Diffraction Pattern

2022\_0056 LAN S8-6.xy Data 1

2022\_0056 LAN S8-6\_R02.dia



Global GOALS

Parameter	Value	ESD
Qalbite	0.332	0.003
Qchlorite2b	0.191	0.004
Qquartz	0.283	0.002
Qironalpha**	0.0174	0.0004
QMuscovite2M1	0.082	0.004
QCalcite	0.094	0.002

\*\* part of sample holder

Local GOALS

Plagioclase\_Albite

Parameter	Value	ESD
Refined composition	AL4.3600 NA4 S111.6400 O32	

A	0.814021	
B	1.279669	
C	0.715898	
ALPHA	94.2355	
BETA	116.6143	
GAMMA	87.8471	

#### CHLORITE\_Iib-2

Parameter	Value	ESD
Refined composition	AL4.6820 FE5.2286 H16 MG4.7714 SI5.2480 O36	
A	0.53633	
B	0.92775	
C	1.42633	
BETA	96.875	

#### Quartz

Parameter	Value	ESD
Refined composition	SI3 O6	
A	0.4914982	
C	0.540736	
GrainSize(1,0,1)	1024	108

#### Iron\_alpha

Parameter	Value	ESD
Refined composition	FE2	
A	0.287506	

#### Muscovite2M1

Parameter	Value	ESD
Refined composition	AL11.6800 FE0.3200 K2.4000 SI12 O48	
A	0.52114	
B	0.90114	
C	2.00160	
BETA	94.5000	
GrainSize(1,0,0)	169	49

#### Calcite

Parameter	Value	ESD
Refined composition	C6 CA6 O18	
A	0.498670	
C	1.70439	
GrainSize(1,1,1)	48.5	

#### Refined Chemical Composition

Phase	Phase Quantity (wt-%)	H (wt-%)	C (wt-%)	O (wt-%)	Na (wt-%)	Mg (wt-%)	Al (wt-%)	Si (wt-%)	K (wt-%)	Ca (wt-%)	Fe (wt-%)
CHLORITE_Iib-2	19,12	1,27	0,00	45,22	0,00	9,10	9,92	11,57	0,00	0,00	22,92

Calcite	9,40	0,00	12,00	47,96	0,00	0,00	0,00	0,00	0,00	40,04	0,00
Iron_alpha**	1,74	0,00	0,00	0,00	0,00	0,00	0,00	0,00	0,00	0,00	100,00
Muscovite2M1	8,15	0,00	0,00	50,13	0,00	0,00	20,57	22,00	6,13	0,00	1,17
Plagioclase_Albite	33,23	0,00	0,00	48,83	8,77	0,00	11,22	31,18	0,00	0,00	0,00
Quartz	28,35	0,00	0,00	53,26	0,00	0,00	0,00	46,74	0,00	0,00	0,00
Weighted total	99,99	0,24	1,13	48,57	2,91	1,74	7,30	27,62	0,50	3,76	6,22

*\*\* part of sample holder*

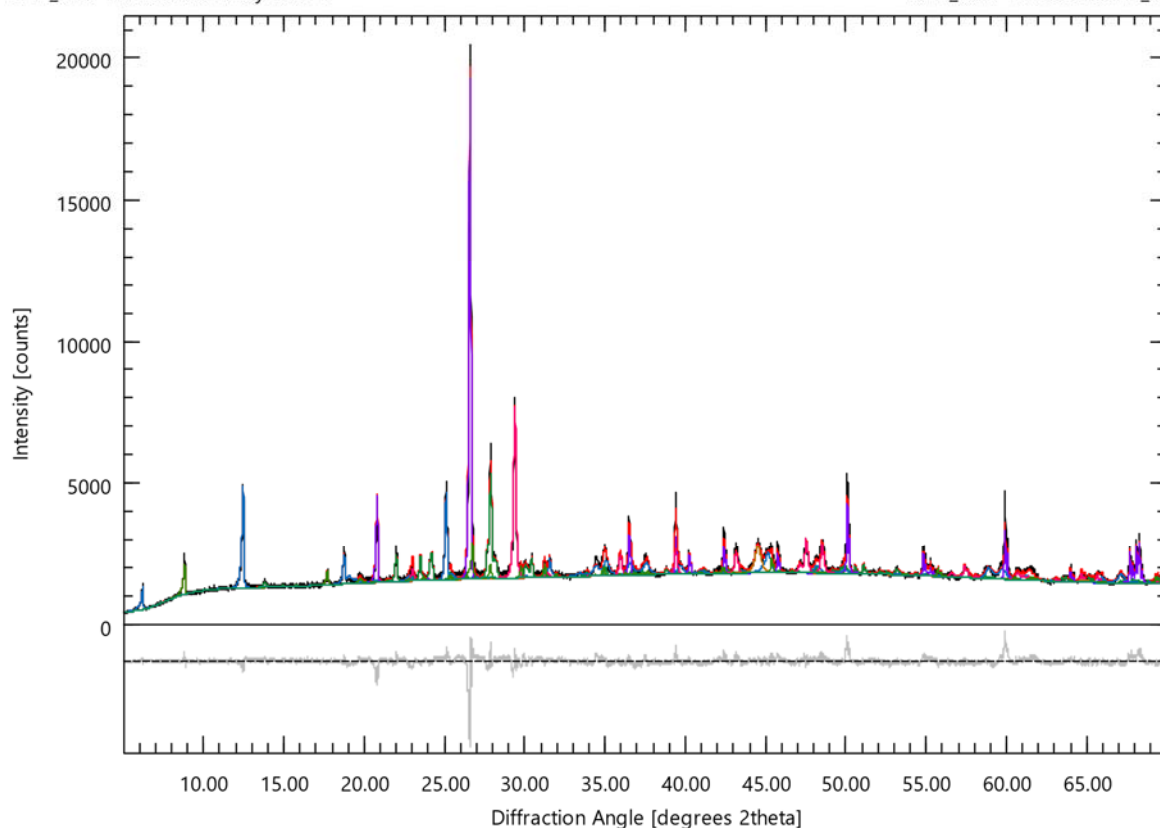
Sample Information

S8-7.3 H2				
File Name	S8-7.3 H2_R02.dia			
Instrument configuration	PW1830_TU Darmstadt_adopted.geq			
Wavelength	CU (1.5406 Å)			
Directory	C:/Users/kasbo/Documents/Data_Laptop/Profex_data/BGE_Project/XRD_Profex_MUSE_Lan			
Date of Refinement	Dienstag Juli 26, 2022			
Operator	kasbo			
Statistics	$R_{wp} = 5.28$	$R_{exp} = 2.41$	$\chi^2 = 4.7999$	GoF = 2.1909

Diffraction Pattern

2022\_0057 LAN S8-7.3 H2.xy Data 1

2022\_0057 LAN S8-7.3 H2\_R02.dia



Global GOALS

Parameter	Value	ESD
Qalbite	0.192	0.003
Qchlorite2b	0.246	0.004
Qquartz	0.276	0.002
Qcalcite	0.172	0.002
Qironalpha**	0.0216	0.0005
Qmusc2m1	0.082	0.003
Qanortk25	0.011	0.004

\*\* part of sample holder

Local GOALS

Plagioclase\_Albite

Parameter	Value	ESD
-----------	-------	-----

Refined composition	AL4.3600 NA4 SI11.6400 O32	
A	0.813893	
B	1.279713	
C	0.715837	
ALPHA	94.2192	
BETA	116.6143	
GAMMA	87.8415	

#### CHLORITE\_Iib-2

Parameter	Value	ESD
Refined composition	AL4.6820 FE4.3736 H16 MG5.6264 SI5.2480 O36	
A	0.53659	
B	0.92777	
C	1.425446	
BETA	96.945	

#### Quartz

Parameter	Value	ESD
Refined composition	SI3 O6	
A	0.4914836	
C	0.540658	
GrainSize(1,0,1)	ERROR	

#### Calcite

Parameter	Value	ESD
Refined composition	C6 CA6 O18	
A	0.498657	
C	1.704565	
GrainSize(1,1,1)	114.6	

#### Iron\_alpha

Parameter	Value	ESD
Refined composition	FE2	
A	0.287465	

#### MUSCOVITE\_2M1

Parameter	Value	ESD
Refined composition	AL11.6800 FE0.3200 K2.4000 SI12 O48	
A	0.51946	
B	0.90571	
C	2.00674	
BETA	95.985	

#### Albite\_high\_K25

Parameter	Value	ESD
-----------	-------	-----

Refined composition	AL4 K1 NA3 SI12 O32	
A	0.827000	
B	1.29550	
C	0.713000	
ALPHA	91.6000	
BETA	116.800	
GAMMA	90.7000	

Refined Chemical Composition

Phase	Phase Quantity (wt-%)	H (wt-%)	C (wt-%)	O (wt-%)	Na (wt-%)	Mg (wt-%)	Al (wt-%)	Si (wt-%)	K (wt-%)	Ca (wt-%)	Fe (wt-%)
Albite_high_K25	1,05	0,00	0,00	48,07	6,48	0,00	10,13	31,65	3,67	0,00	0,00
CHLORITE_Ilb-2	24,59	1,29	0,00	46,20	0,00	10,97	10,13	11,82	0,00	0,00	19,59
Calcite	17,15	0,00	12,00	47,96	0,00	0,00	0,00	0,00	0,00	40,04	0,00
Iron_alpha**	2,16	0,00	0,00	0,00	0,00	0,00	0,00	0,00	0,00	0,00	100,00
MUSCOVITE_2M1	8,19	0,00	0,00	50,13	0,00	0,00	20,57	22,00	6,13	0,00	1,17
Plagioclase_Albite	19,24	0,00	0,00	48,83	8,77	0,00	11,22	31,18	0,00	0,00	0,00
Quartz	27,62	0,00	0,00	53,26	0,00	0,00	0,00	46,74	0,00	0,00	0,00
Weighted total	100,00	0,32	2,06	48,30	1,76	2,70	6,44	23,95	0,54	6,87	7,07

\*\* part of sample holder

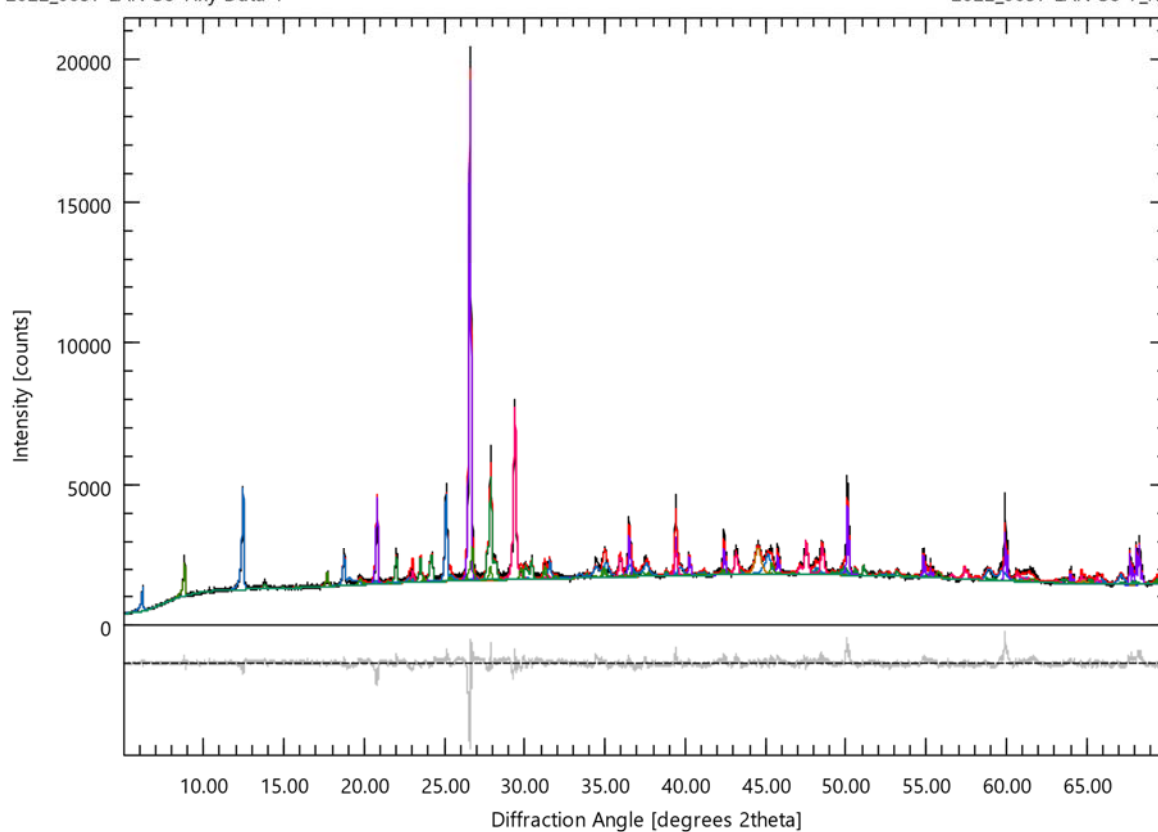
### Sample Information

S8-7				
File Name	S8-7_R02.dia			
Instrument configuration	PW1830_TU Darmstadt_adopted.geq			
Wavelength	CU (1.5406 Å)			
Directory	C:/Users/kasbo/Documents/Data_Laptop/Profex_data/BGE_Project/XRD_Profex_MUSE_Lan			
Date of Refinement	Dienstag Juli 26, 2022			
Operator	kasbo			
Statistics	$R_{wp} = 5.26$	$R_{exp} = 2.41$	$\chi^2 = 4.7636$	GoF = 2.1826

### Diffraction Pattern

2022\_0057 LAN S8-7.xy Data 1

2022\_0057 LAN S8-7\_R02.dia



### Global GOALS

Parameter	Value	ESD
Qalbite	0.191	0.003
Qchlorite2b	0.243	0.004
Qquartz	0.275	0.002
QCalcite	0.171	0.002
Qironalpha**	0.0216	0.0005
QMuscovite2M1	0.087	0.003
Qanortk25	0.011	0.004

\*\* part of sample holder

Local GOALS  
Plagioclase\_Albite

Parameter	Value	ESD
Refined composition	AL4.3600 NA4 SI11.6400 O32	
A	0.813867	
B	1.279664	
C	0.715863	
ALPHA	94.2242	
BETA	116.6145	
GAMMA	87.8331	

CHLORITE\_Iib-2

Parameter	Value	ESD
Refined composition	AL4.6820 FE4.3618 H16 MG5.6382 SI5.2480 O36	
A	0.53659	
B	0.92776	
C	1.425436	
BETA	96.945	

Quartz

Parameter	Value	ESD
Refined composition	SI3 O6	
A	0.4914818	
C	0.540661	
GrainSize(1,0,1)	ERROR	

Calcite

Parameter	Value	ESD
Refined composition	C6 CA6 O18	
A	0.498654	
C	1.704560	
GrainSize(1,1,1)	114.5	

Iron\_alpha

Parameter	Value	ESD
Refined composition	FE2	
A	0.287462	

Muscovite2M1

Parameter	Value	ESD
Refined composition	AL11.6800 FE0.3200 K2.5188 SI12 O48	
A	0.51960	
B	0.90579	

C	2.00695	
BETA	96.026	
GrainSize(1,0,0)	ERROR	

#### Albite\_high\_K25

Parameter	Value	ESD
Refined composition	AL4 K1 NA3 SI12 O32	
A	0.827000	
B	1.29550	
C	0.713000	
ALPHA	91.6000	
BETA	116.800	
GAMMA	90.7000	

#### Refined Chemical Composition

Phase	Phase Quantity (wt-%)	H (wt-%)	C (wt-%)	O (wt-%)	Na (wt-%)	Mg (wt-%)	Al (wt-%)	Si (wt-%)	K (wt-%)	Ca (wt-%)	Fe (wt-%)
Albite_high_K25	1,07	0,00	0,00	48,07	6,48	0,00	10,13	31,65	3,67	0,00	0,00
CHLORITE_Ilb-2	24,35	1,29	0,00	46,21	0,00	10,99	10,14	11,83	0,00	0,00	19,54
Calcite	17,11	0,00	12,00	47,96	0,00	0,00	0,00	0,00	0,00	40,04	0,00
Iron_alpha**	2,16	0,00	0,00	0,00	0,00	0,00	0,00	0,00	0,00	0,00	100,00
Muscovite2M1	8,70	0,00	0,00	49,98	0,00	0,00	20,51	21,93	6,41	0,00	1,16
Plagioclase_Albite	19,11	0,00	0,00	48,83	8,77	0,00	11,22	31,18	0,00	0,00	0,00
Quartz	27,49	0,00	0,00	53,26	0,00	0,00	0,00	46,74	0,00	0,00	0,00
Weighted total	99,99	0,31	2,05	48,29	1,75	2,68	6,51	23,93	0,60	6,85	7,02

\*\* part of sample holder

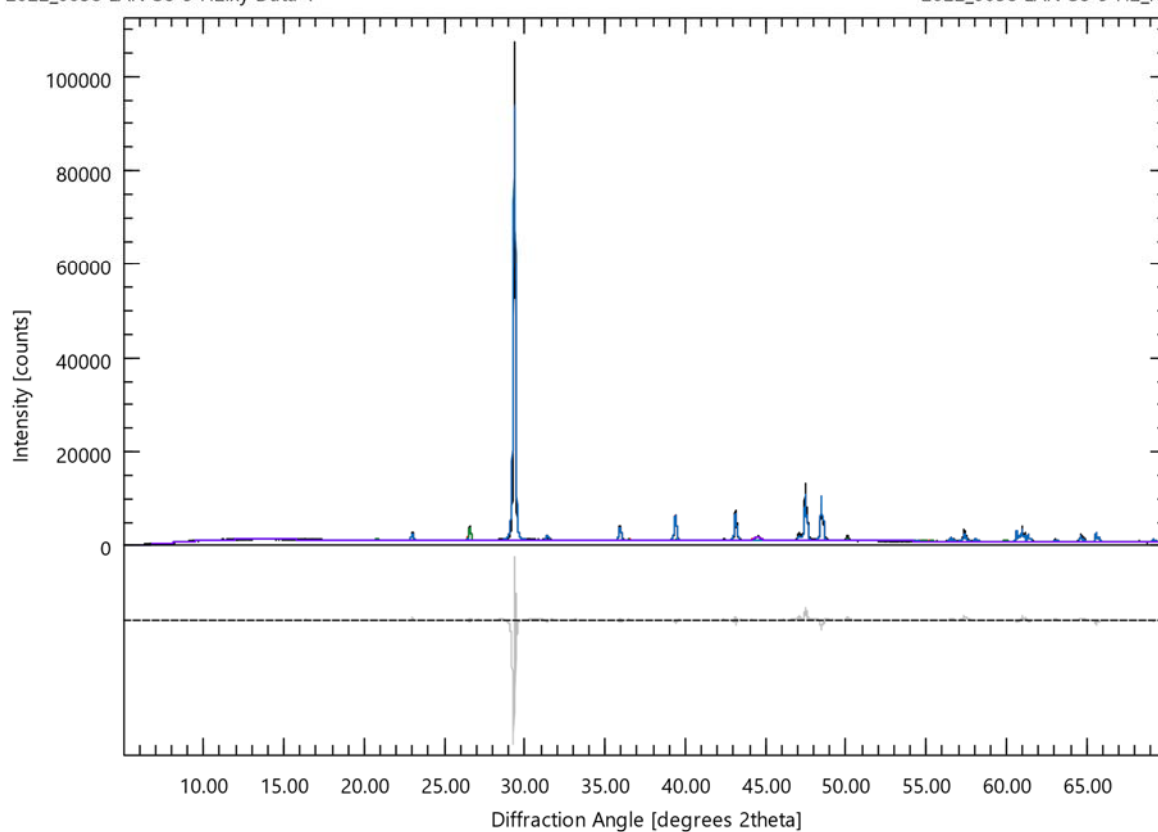
Sample Information

S8-9 H2				
File Name	S8-9 H2_R01.dia			
Instrument configuration	PW1830_TU Darmstadt_adopted.geq			
Wavelength	CU (1.5406 Å)			
Directory	C:/Users/kasbo/Documents/Data_Laptop/Profex_data/BGE_Project/XRD_Profex_MUSE_Lan			
Date of Refinement	Dienstag Juli 26, 2022			
Operator	kasbo			
Statistics	$R_{wp} = 8.04$	$R_{exp} = 3.00$	$\chi^2 = 7.1824$	GoF = 2.6800

Diffraction Pattern

2022\_0058 LAN S8-9 H2.xy Data 1

2022\_0058 LAN S8-9 H2\_R01.dia



Global GOALS

Parameter	Value	ESD
Qquartz	0.0431	0.0006
QCalcite	0.9393	0.0008
Qironalpha**	0.0176	0.0004

\*\* part of sample holder

Local GOALS

Quartz

Parameter	Value	ESD
Refined composition	Si3 O6	
A	0.491581	

C	0.540611	
GrainSize(1,0,1)	ERROR	

**Calcite**

Parameter	Value	ESD
Refined composition	C6 CA6 O18	
A	0.4989324	
C	1.705891	
GrainSize(1,1,1)	324.4	

**Iron\_alpha**

Parameter	Value	ESD
Refined composition	FE2	
A	0.287573	

Refined Chemical Composition

Phase	Phase Quantity (wt-%)	C (wt-%)	O (wt-%)	Si (wt-%)	Ca (wt-%)	Fe (wt-%)
Calcite	93,93	12,00	47,96	0,00	40,04	0,00
Iron_alpha**	1,76	0,00	0,00	0,00	0,00	100,00
Quartz	4,31	0,00	53,26	46,74	0,00	0,00
Weighted total	100,00	11,27	47,34	2,01	37,61	1,76

\*\* part of sample holder

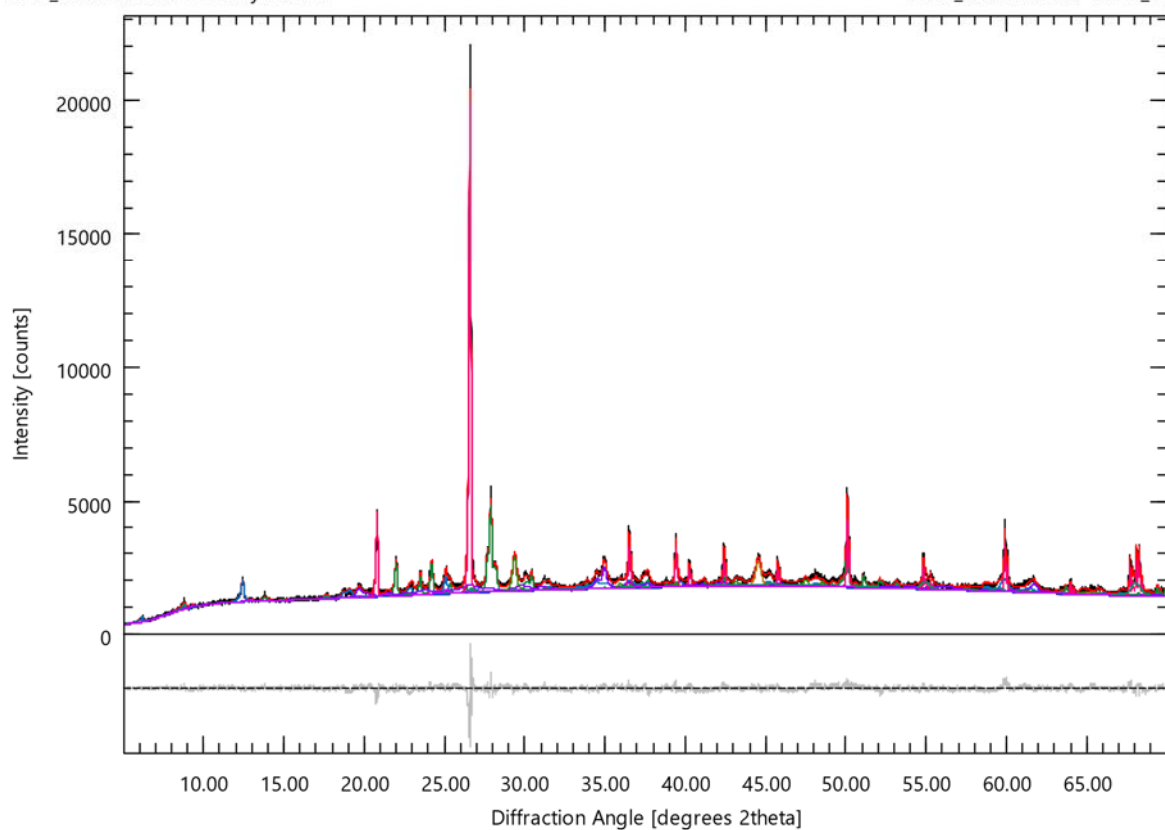
### Sample Information

S8-11 H2				
File Name	S8-11 H2_R03.dia			
Instrument configuration	PW1830_TU Darmstadt_adopted.geq			
Wavelength	CU (1.5406 Å)			
Directory	C:/Users/kasbo/Documents/Data_Laptop/Profex_data/BGE_Project/XRD_Profex_MUSE_Lan			
Date of Refinement	Mittwoch Juli 27, 2022			
Operator	kasbo			
Statistics	$R_{wp} = 3.92$	$R_{exp} = 2.37$	$\chi^2 = 2.7357$	GoF = 1.6540

### Diffraction Pattern

2022\_0059 LAN S8-11 H2.xy Data 1

2022\_0059 LAN S8-11 H2\_R03.dia



### Global GOALS

Parameter	Value	ESD
Qalbite	0.170	0.004
Qchlorite2b	0.106	0.003
Qmusc2m1	0.161	0.007
Qquartz	0.189	0.004
Qironalpha**	0.0116	0.0004
QCalcite	0.039	0.002
Qmusc1md	0.31	0.01
Qanortk25	0.000000	0.000000

Qlaumontite	0.018	0.001
-------------	-------	-------

\*\* part of sample holder

Local GOALs

**Plagioclase Albite**

Parameter	Value	ESD
Refined composition	AL4.3600 NA4 SI11.6400 O32	
A	0.814218	
B	1.280169	
C	0.715868	
ALPHA	94.240	
BETA	116.5976	
GAMMA	87.8398	

**CHLORITE\_Iib-2**

Parameter	Value	ESD
Refined composition	AL4.6820 FE6.1676 H16 MG3.8324 SI5.2480 O36	
A	0.53922	
B	0.92637	
C	1.42669	
BETA	96.850	

**MUSCOVITE\_2M1**

Parameter	Value	ESD
Refined composition	AL11.6800 FE0.3200 K3.4032 SI12 O48	
A	0.52176	
B	0.90064	
C	2.0093	
BETA	95.494	

**Quartz**

Parameter	Value	ESD
Refined composition	SI3 O6	
A	0.4915190	
C	0.540633	
GrainSize(1,0,1)	ERROR	

**Iron\_alpha**

Parameter	Value	ESD
Refined composition	FE2	
A	0.287320	

**Calcite**

Parameter	Value	ESD
Refined composition	C6 CA6 O18	
A	0.498750	

C	1.70558	
GrainSize(1,1,1)	42.4413	

#### Muscovite\_1Md

Parameter	Value	ESD
Refined composition	AL5.2000 K1 SI6.8000 O24	
A	0.515600	
B	0.89650	
C	1.02429	
BETA	102.499	

#### Albite\_high\_K25

Parameter	Value	ESD
Refined composition	AL4 K1 NA3 SI12 O32	
A	UNDEF	
B	UNDEF	
C	UNDEF	
ALPHA	UNDEF	
BETA	UNDEF	
GAMMA	UNDEF	

#### Laumontite

Parameter	Value	ESD
Refined composition	AL8 CA4 H22.2000 SI16 O61.1920	
A	1.4626	
B	1.3016	
C	0.76291	
BETA	111.89	

#### Refined Chemical Composition

Phase	Phase Quantity (wt-%)	H (wt-%)	C (wt-%)	O (wt-%)	Na (wt-%)	Mg (wt-%)	Al (wt-%)	Si (wt-%)	K (wt-%)	Ca (wt-%)	Fe (wt-%)
Albite_high_K25	0,00	0,00	0,00	48,07	6,48	0,00	10,13	31,65	3,67	0,00	0,00
CHLORITE_IIb-2	10,61	1,24	0,00	44,19	0,00	7,15	9,69	11,31	0,00	0,00	26,43
Calcite	3,87	0,00	12,00	47,96	0,00	0,00	0,00	0,00	0,00	40,04	0,00
Iron_alpha**	1,16	0,00	0,00	0,00	0,00	0,00	0,00	0,00	0,00	0,00	100,00
Laumontite	1,75	1,22	0,00	53,59	0,00	0,00	11,81	24,60	0,00	8,77	0,00
MUSCOVITE_2M1	16,11	0,00	0,00	48,88	0,00	0,00	20,06	21,45	8,47	0,00	1,14
Muscovite_1Md	30,70	0,00	0,00	50,90	0,00	0,00	18,60	25,32	5,18	0,00	0,00
Plagioclase_Albite	16,96	0,00	0,00	48,83	8,77	0,00	11,22	31,18	0,00	0,00	0,00
Quartz	18,89	0,00	0,00	53,26	0,00	0,00	0,00	46,74	0,00	0,00	0,00
Weighted total	100,05	0,15	0,46	49,33	1,49	0,76	12,08	26,98	2,95	1,70	4,15

\*\* part of sample holder

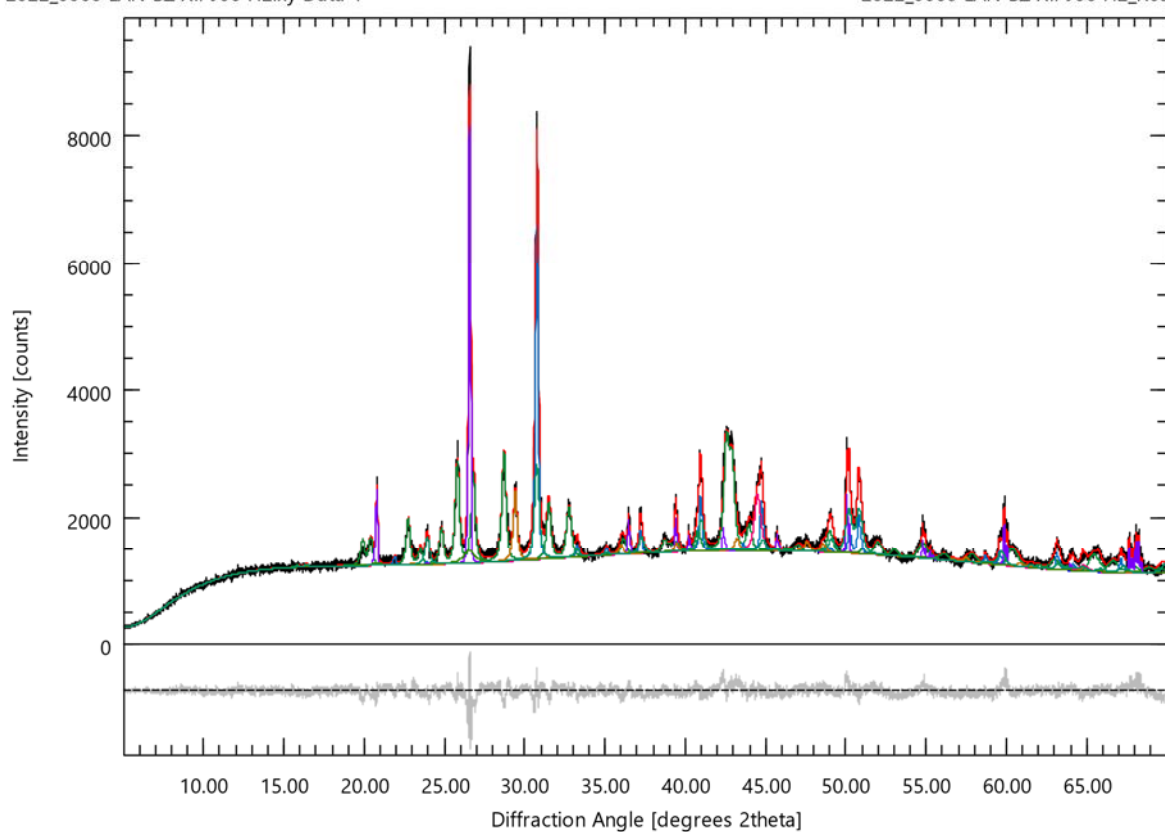
Sample Information

BZ XII-J06 H2				
File Name	BZ XII-J06 H2_R03a.dia			
Instrument configuration	PW1830_TU Darmstadt_adopted.geq			
Wavelength	CU (1.5406 Å)			
Directory	C:/Users/kasbo/Documents/Data_Laptop/Profex_data/BGE_Project/XRD_Profex_MUSE_Lan			
Date of Refinement	Sonntag Juli 31, 2022			
Operator	kasbo			
Statistics	$R_{wp} = 4.20$	$R_{exp} = 2.61$	$\chi^2 = 2.5895$	GoF = 1.6092

Diffraction Pattern

2022\_0060 LAN BZ XII-J06 H2.xy Data 1

2022\_0060 LAN BZ XII-J06 H2\_R03a.dia



Global GOALS

Parameter	Value	ESD
Qbarite	0.178	0.001
Qdolomite	0.22	0.01
QquartzCOARSE	0.175	0.003
Qironalpha**	0.033	0.001
QCalcite	0.070	0.002
QquartzFINE	0.038	0.005
Qankerit07	0.29	0.01

\*\* part of sample holder

Local GOALs

**Barite**

Parameter	Value	ESD
Refined composition	BA4 S4 O16	
A	0.888387	
B	0.545077	
C	0.715436	

**Dolomite**

Parameter	Value	ESD
Refined composition	C6 CA3 MG3 O18	
A	0.482555	
C	1.61189	
GrainSize(1,0,4)	102.5	

**QuartzCoarse**

Parameter	Value	ESD
Refined composition	SI3 O6	
A	0.491841	
C	0.540870	
GrainSize(1,0,1)	1489	407

**Iron\_alpha**

Parameter	Value	ESD
Refined composition	FE2	
A	0.287591	

**Calcite**

Parameter	Value	ESD
Refined composition	C6 CA6 O18	
A	0.498157	
C	1.70266	
GrainSize(1,1,1)	42.4413	

**QuartzFine**

Parameter	Value	ESD
Refined composition	SI3 O6	
A	0.4910	
C	0.5441	
GrainSize(1,0,1)	10.6103	

**Ankerite\_Fe0.7**

Parameter	Value	ESD
Refined composition	C6 CA2.9340 FE1.5660 MG1.5000 O18	
A	0.481832	

C	1.61400	
GrainSize(1,0,4)	42.4413	

Refined Chemical Composition

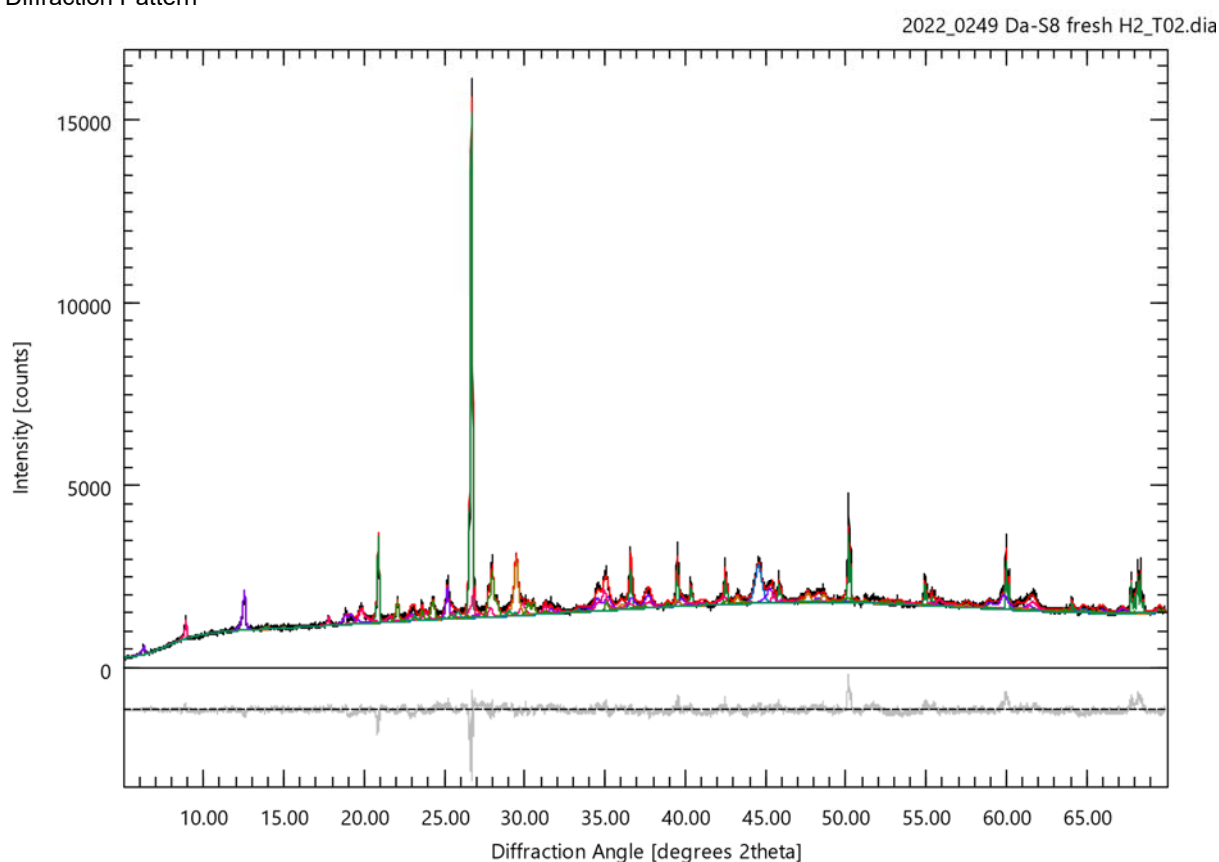
Phase	Phase Quantity (wt-%)	C (wt-%)	O (wt-%)	Mg (wt-%)	Si (wt-%)	S (wt-%)	Ca (wt-%)	Fe (wt-%)	Ba (wt-%)
Ankerite_Fe0.7	28,90	11,98	47,87	6,06	0,00	0,00	19,55	14,54	0,00
Barite	17,78	0,00	27,42	0,00	0,00	13,74	0,00	0,00	58,84
Calcite	7,00	12,00	47,96	0,00	0,00	0,00	40,04	0,00	0,00
Dolomite	21,70	13,03	52,06	13,18	0,00	0,00	21,73	0,00	0,00
Iron_alpha**	3,27	0,00	0,00	0,00	0,00	0,00	0,00	100,00	0,00
QuartzCoarse	17,51	0,00	53,26	0,00	46,74	0,00	0,00	0,00	0,00
QuartzFine	3,82	0,00	53,26	0,00	46,74	0,00	0,00	0,00	0,00
Weighted total	99,98	7,13	44,72	4,61	9,97	2,44	13,17	7,47	10,46

\*\* part of sample holder

### Sample Information

S8 fresh H2				
File Name	S8 fresh H2_T02.dia			
Instrument configuration	PW1830_TU Darmstadt_adopted.geq			
Wavelength	CU (1.5406 Å)			
Directory	C:/Users/kasbo/Documents/Data_Laptop/Profex_data/BGE_Project/XRD_Profex_MUSE_Lan			
Date of Refinement	Donnerstag Januar 05, 2023			
Operator	kasbo			
Statistics	$R_{wp} = 5.00$	$R_{exp} = 2.49$	$\chi^2 = 4.0322$	GoF = 2.0080

### Diffraction Pattern



### Global GOALS

Parameter	Value	ESD
Qquartz	0.279	0.003
Qironalpha**	0.0316	0.0006
Qchlorite2b	0.213	0.005
Qmusc2m1	0.219	0.006
QCalcite	0.080	0.003
Qalbite	0.146	0.003
QScapolite	0.033	0.003

\*\* part of sample holder

## Local GOALs

**Quartz**

Parameter	Value	ESD
Refined composition	SI3 O6	
A	0.491497	
C	0.540685	
GrainSize(1,0,1)	3806	1647

**Iron\_alpha**

Parameter	Value	ESD
Refined composition	FE2	
A	0.287773	

**CHLORITE\_Iib-2**

Parameter	Value	ESD
Refined composition	AL4.6820 FE6.2576 H16 MG3.7424 SI5.2480 O36	
A	0.53675	
B	0.92740	
C	1.42552	
BETA	96.832	

**MUSCOVITE\_2M1**

Parameter	Value	ESD
Refined composition	AL11.6800 FE0.3200 K2.9700 SI12 O48	
A	0.52089	
B	0.90377	
C	2.00704	
BETA	95.784	

**Calcite**

Parameter	Value	ESD
Refined composition	C6 CA6 O18	
A	0.49879	
C	1.70351	
GrainSize(1,1,1)	42.4413	

**Plagioclase\_Albite**

Parameter	Value	ESD
Refined composition	AL4.3600 NA4 SI11.6400 O32	
A	0.81391	
B	1.27920	
C	0.71609	
ALPHA	94.166	
BETA	116.692	
GAMMA	87.834	

### Scapolite

Parameter	Value	ESD
Refined composition	AL6.4000 C0.0530 CA0.5600 CL1.6992 K0.4800 NA6.9600 SO.0176 S117.6000 O48.2294	
A	1.21589	
C	0.75299	

### Refined Chemical Composition

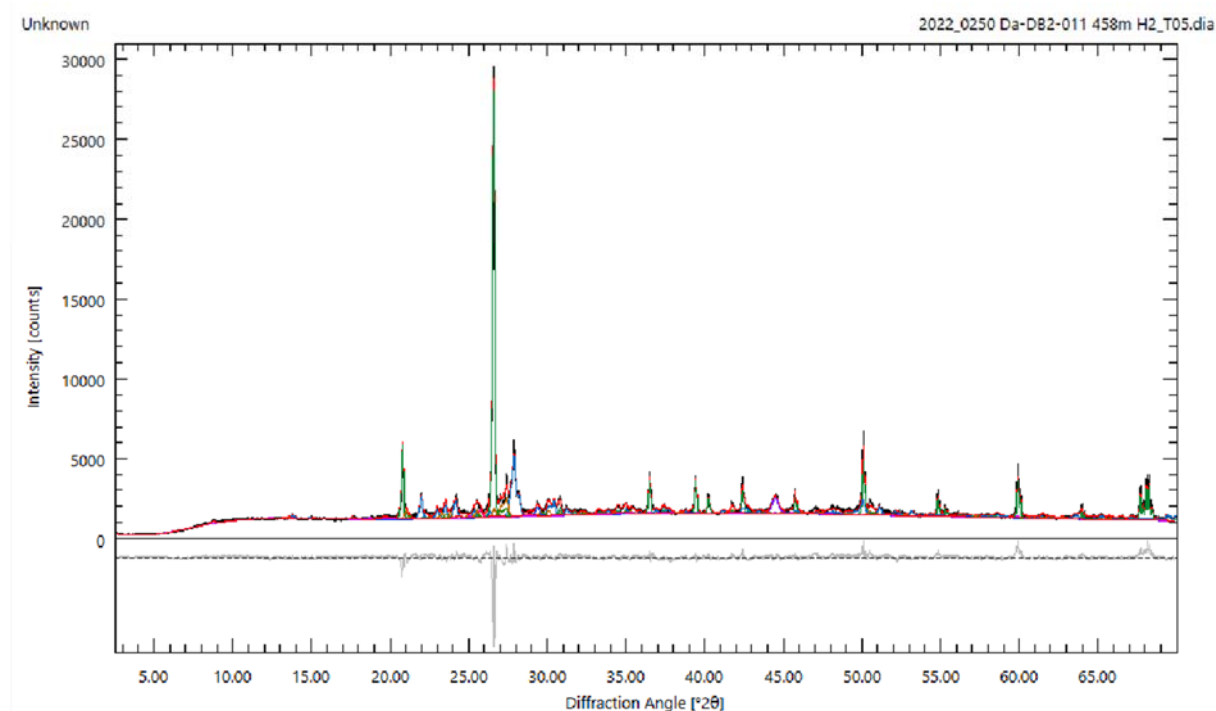
Phase	Phase Quantity (wt-%)	H (wt-%)	C (wt-%)	O (wt-%)	Na (wt-%)	Mg (wt-%)	Al (wt-%)	Si (wt-%)	S (wt-%)	Cl (wt-%)	K (wt-%)	Ca (wt-%)	Fe (wt-%)
CHLORITE_IIb-2	21,26	1,23	0,00	44,09	0,00	6,96	9,67	11,28	0,00	0,00	0,00	0,00	26,75
Calcite	7,99	0,00	12,00	47,96	0,00	0,00	0,00	0,00	0,00	0,00	0,00	40,04	0,00
Iron_alpha**	3,16	0,00	0,00	0,00	0,00	0,00	0,00	0,00	0,00	0,00	0,00	0,00	100,00
MUSCOVITE_2M1	21,86	0,00	0,00	49,41	0,00	0,00	20,28	21,69	0,00	0,00	7,47	0,00	1,15
Plagioclase_Albite	14,62	0,00	0,00	48,83	8,77	0,00	11,22	31,18	0,00	0,00	0,00	0,00	0,00
Quartz	27,87	0,00	0,00	53,26	0,00	0,00	0,00	46,74	0,00	0,00	0,00	0,00	0,00
Scapolite	3,25	0,00	0,04	45,36	9,41	0,00	10,15	29,05	0,03	3,54	1,10	1,32	0,00
Weighted total	100,01	0,26	0,96	47,46	1,59	1,48	8,46	25,67	0,00	0,12	1,67	3,24	9,09

\*\* part of sample holder

## Sample Information

Granite 458m H2				
File Name	Granite 458m H2_T05.dia			
Instrument configuration	PW1830_TU Darmstadt_adopted.geq			
Wavelength	CU (1.5406 Å)			
Directory	C:/Users/kasbo/Documents/Data_Laptop/Profex_data/BGE_Project/XRD_Profex_MUSE_Lan			
Date of Refinement	Freitag Januar 06, 2023			
Operator	kasbo			
Statistics	$R_{wp} = 6.35$	$R_{exp} = 2.58$	$\chi^2 = 6.0577$	GoF = 2.4612

## Diffraction Pattern



## Global GOALS

Parameter	Value	ESD
Qquartz	0.329	0.003
Qalbite	0.303	0.004
Qironalpha**	0.0151	0.0004
QScapolite	0.026	0.002
Qmicroint2	0.112	0.004
Qsanina16	0.051	0.004
Qepidote	0.045	0.002
QCalcite	0.0184	0.0009
Qchlorite2b	0.031	0.002
Qmuscovite1m	0.069	0.006

\*\* part of sample holder

## Local GOALS

### Quartz

Parameter	Value	ESD
-----------	-------	-----

Refined composition	SI3 O6	
A	0.4915104	
C	0.540719	
GrainSize(1,0,1)	632	39

#### Plagioclase\_Albite

Parameter	Value	ESD
Refined composition	AL4.3600 NA4 SI11.6400 O32	
A	0.814195	
B	1.28007	
C	0.716041	
ALPHA	94.224	
BETA	116.6381	
GAMMA	87.888	

#### Iron\_alpha

Parameter	Value	ESD
Refined composition	FE2	
A	0.287713	

#### Scapolite

Parameter	Value	ESD
Refined composition	AL6.4000 C0.0530 CA0.5600 CL1.6992 K0.4800 NA6.9600 S0.0176 SI17.6000 O48.2294	
A	1.21746	
C	0.75322	

#### MICROCLINE\_intermediate2

Parameter	Value	ESD
Refined composition	AL4 K4 SI12 O32	
A	0.85437	
B	1.29664	
C	0.72255	
ALPHA	89.556	
BETA	116.011	
GAMMA	91.5000	

#### Sanidine\_Na16

Parameter	Value	ESD
Refined composition	AL4 K3.3240 NA0.6760 SI12 O32	
A	0.849000	
B	1.29781	
C	0.71960	
BETA	115.500	

#### Epidote

Parameter	Value	ESD
-----------	-------	-----

Refined composition	AL4.3400 CA4 FE1.6200 SI6 O26	
A	0.88772	
B	0.56270	
C	1.01515	
BETA	115.425	

#### Calcite

Parameter	Value	ESD
Refined composition	C6 CA6 O18	
A	0.50401	
C	1.68910	
GrainSize(1,1,1)	42.4413	

#### CHLORITE\_Iib-2

Parameter	Value	ESD
Refined composition	AL4.6820 FE0.2160 H16 MG9.7840 SI5.2480 O36	
A	0.53451	
B	0.92515	
C	1.4221	
BETA	95.5000	

#### Muscovite\_1M

Parameter	Value	ESD
Refined composition	AL5.1760 H4 K1.6110 SI6.8240 O24	
A	0.526000	
B	0.8990	
C	1.01720	
BETA	101.000	

#### Refined Chemical Composition

Phase	Phase Quantity (wt-%)	H (wt-%)	C (wt-%)	O (wt-%)	Na (wt-%)	Mg (wt-%)	Al (wt-%)	Si (wt-%)	S (wt-%)	Cl (wt-%)	K (wt-%)	Ca (wt-%)	Fe (wt-%)
CHLORITE_Iib-2	3,08	1,45	0,00	51,63	0,00	21,31	11,32	13,21	0,00	0,00	0,00	0,00	1,08
Calcite	1,84	0,00	12,00	47,96	0,00	0,00	0,00	0,00	0,00	0,00	0,00	40,04	0,00
Epidote	4,53	0,00	0,00	43,68	0,00	0,00	12,30	17,69	0,00	0,00	0,00	16,83	9,50
Iron_alpha**	1,51	0,00	0,00	0,00	0,00	0,00	0,00	0,00	0,00	0,00	0,00	0,00	100,00
MICROCLINE_intermediate2	11,17	0,00	0,00	45,99	0,00	0,00	9,69	30,27	0,00	0,00	14,05	0,00	0,00
Muscovite_1M	6,94	0,52	0,00	49,08	0,00	0,00	17,85	24,50	0,00	0,00	8,05	0,00	0,00
Plagioclase_Albite	30,33	0,00	0,00	48,83	8,77	0,00	11,22	31,18	0,00	0,00	0,00	0,00	0,00
Quartz	32,93	0,00	0,00	53,26	0,00	0,00	0,00	46,74	0,00	0,00	0,00	0,00	0,00
Sanidine_Na16	5,07	0,00	0,00	46,44	1,41	0,00	9,79	30,57	0,00	0,00	11,79	0,00	0,00
Scapolite	2,60	0,00	0,04	45,36	9,41	0,00	10,15	29,05	0,03	3,54	1,10	1,32	0,00

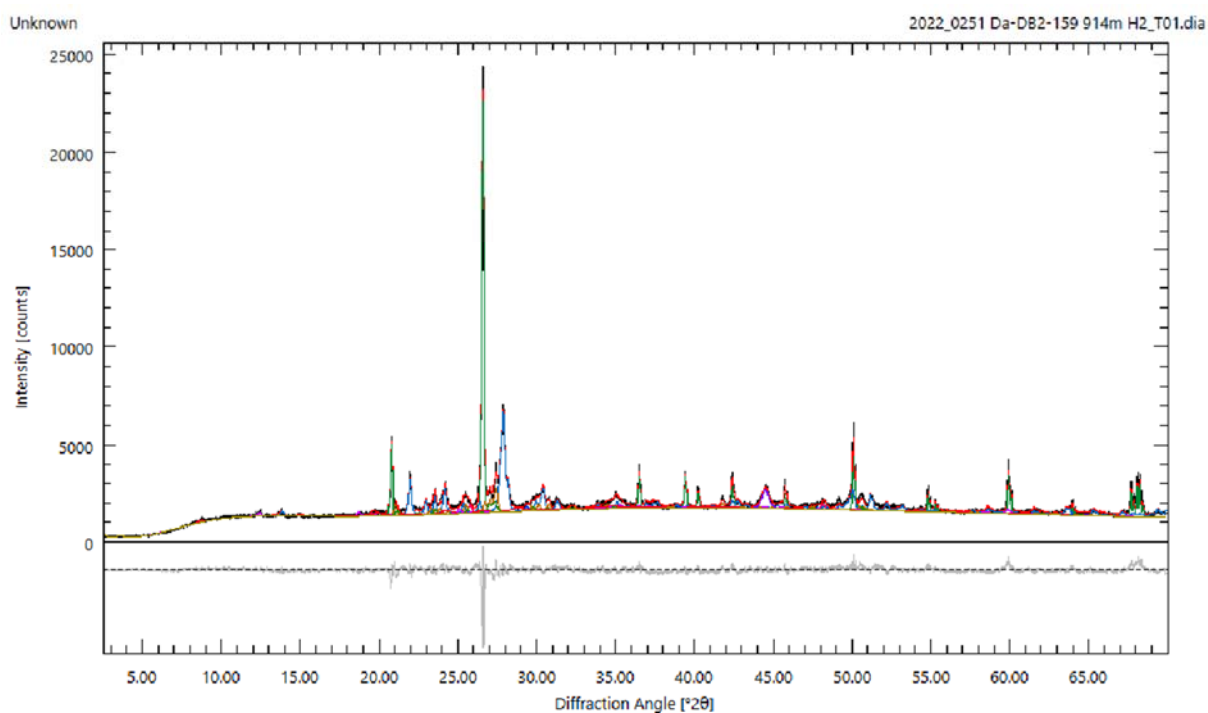
Weighted total	100,00	0,08	0,22	48,87	2,98	0,66	7,39	33,44	0,00	0,09	2,75	1,53	1,97
----------------	--------	------	------	-------	------	------	------	-------	------	------	------	------	------

*\*\* part of sample holder*

### Sample Information

Granite 914m H2				
File Name	Granite 914m H2_T01.dia			
Instrument configuration	PW1830_TU Darmstadt_adopted.geq			
Wavelength	CU (1.5406 Å)			
Directory	C:/Users/kasbo/Documents/Data_Laptop/Profex_data/BGE_Project/XRD_Profex_MUSE_Lan			
Date of Refinement	Freitag Januar 06, 2023			
Operator	kasbo			
Statistics	$R_{wp} = 5.49$	$R_{exp} = 2.45$	$\chi^2 = 5.0213$	GoF = 2.2408

### Diffraction Pattern



### Global GOALS

Parameter	Value	ESD
Qquartz	0.266	0.003
Qalbite	0.362	0.004
Qironalpha**	0.0176	0.0004
QScapolite	0.0117	0.0009
Qmicroint2	0.115	0.003
Qsanina16	0.055	0.003
Qepidote	0.000000	0.000000
QCalcite	0.0096	0.0008
Qchlorite2b	0.062	0.004
Qmuscovite1m	0.101	0.007

Qmusc2m1	0.000000	0.000000
----------	----------	----------

\*\* part of sample holder

Local GOALs

**Quartz**

Parameter	Value	ESD
Refined composition	SI3 O6	
A	0.491492	
C	0.540686	
GrainSize(1,0,1)	1031	110

**Plagioclase Albite**

Parameter	Value	ESD
Refined composition	AL4.3600 NA4 SI11.6400 O32	
A	0.814313	
B	1.280989	
C	0.715082	
ALPHA	94.2044	
BETA	116.6003	
GAMMA	88.2000	

**Iron\_alpha**

Parameter	Value	ESD
Refined composition	FE2	
A	0.287621	

**Scapolite**

Parameter	Value	ESD
Refined composition	AL6.4000 C0.0530 CA0.5600 CL1.6992 K0.4800 NA6.9600 S0.0176 SI17.6000 O48.2294	
A	1.1981	
C	0.75503	

**MICROCLINE\_intermediate2**

Parameter	Value	ESD
Refined composition	AL4 K4 SI12 O32	
A	0.85296	
B	1.29559	
C	0.72282	
ALPHA	89.492	
BETA	116.191	
GAMMA	91.5000	

**Sanidine\_Na16**

Parameter	Value	ESD
Refined composition	AL4 K3.3240 NA0.6760 SI12 O32	

A	0.849000	
B	1.29785	
C	0.72048	
BETA	115.549	

#### Epidote

Parameter	Value	ESD
Refined composition	AL4.3400 CA4 FE1.6200 SI6 O26	
A	UNDEF	
B	UNDEF	
C	UNDEF	
BETA	UNDEF	

#### Calcite

Parameter	Value	ESD
Refined composition	C6 CA6 O18	
A	0.504100	
C	1.68910	
GrainSize(1,1,1)	42.4413	

#### CHLORITE\_Iib-2

Parameter	Value	ESD
Refined composition	AL4.6820 FE0.2720 H16 MG9.7280 SI5.2480 O36	
A	0.53442	
B	0.92708	
C	1.42176	
BETA	95.5000	

#### Muscovite\_1M

Parameter	Value	ESD
Refined composition	AL5.1760 H4 K2 SI6.8240 O24	
A	0.526000	
B	0.8954	
C	1.0213	
BETA	101.000	

#### MUSCOVITE\_2M1

Parameter	Value	ESD
Refined composition	AL11.6800 FE0.3200 K2.4000 SI12 O48	
A	UNDEF	
B	UNDEF	
C	UNDEF	
BETA	UNDEF	

Refined Chemical Composition

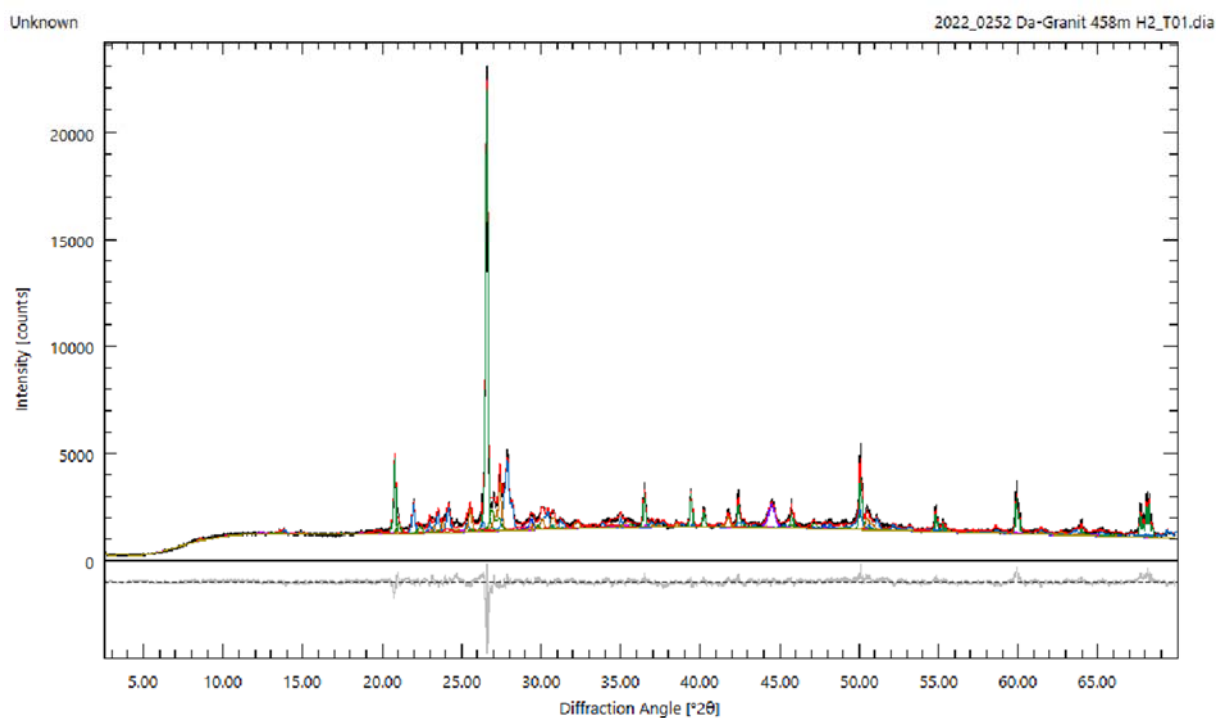
Phase	Phase Quantity (wt-%)	H (wt-%)	C (wt-%)	O (wt-%)	Na (wt-%)	Mg (wt-%)	Al (wt-%)	Si (wt-%)	S (wt-%)	Cl (wt-%)	K (wt-%)	Ca (wt-%)	Fe (wt-%)
CHLORITE_IIb-2	6,23	1,44	0,00	51,54	0,00	21,16	11,30	13,19	0,00	0,00	0,00	0,00	1,36
Calcite	0,96	0,00	12,00	47,96	0,00	0,00	0,00	0,00	0,00	0,00	0,00	40,04	0,00
Epidote	0,00	0,00	0,00	43,68	0,00	0,00	12,30	17,69	0,00	0,00	0,00	16,83	9,50
Iron_alpha**	1,76	0,00	0,00	0,00	0,00	0,00	0,00	0,00	0,00	0,00	0,00	0,00	100,00
MICROCLINE_intermediate2	11,50	0,00	0,00	45,99	0,00	0,00	9,69	30,27	0,00	0,00	14,05	0,00	0,00
MUSCOVITE_2M1	0,00	0,00	0,00	50,13	0,00	0,00	20,57	22,00	0,00	0,00	6,13	0,00	1,17
Muscovite_1M	10,14	0,51	0,00	48,15	0,00	0,00	17,51	24,03	0,00	0,00	9,80	0,00	0,00
Plagioclase_Albite	36,19	0,00	0,00	48,83	8,77	0,00	11,22	31,18	0,00	0,00	0,00	0,00	0,00
Quartz	26,56	0,00	0,00	53,26	0,00	0,00	0,00	46,74	0,00	0,00	0,00	0,00	0,00
Sanidine_Na16	5,49	0,00	0,00	46,44	1,41	0,00	9,79	30,57	0,00	0,00	11,79	0,00	0,00
Scapolite	1,17	0,00	0,04	45,36	9,41	0,00	10,15	29,05	0,03	3,54	1,10	1,32	0,00
Weighted total	100,00	0,14	0,12	48,74	3,36	1,32	8,31	32,46	0,00	0,04	3,27	0,40	1,85

\*\* part of sample holder

## Sample Information

Granit 458m H2				
File Name	Granit 458m H2_T01.dia			
Instrument configuration	PW1830_TU Darmstadt_adopted.geq			
Wavelength	CU (1.5406 Å)			
Directory	C:/Users/kasbo/Documents/Data_Laptop/Profex_data/BGE_Project/XRD_Profex_MUSE_Lan			
Date of Refinement	Freitag Januar 06, 2023			
Operator	kasbo			
Statistics	$R_{wp} = 5.59$	$R_{exp} = 2.55$	$\chi^2 = 4.8056$	GoF = 2.1922

## Diffraction Pattern



## Global GOALS

Parameter	Value	ESD
Qquartz	0.283	0.003
Qalbite	0.302	0.004
Qironalpha**	0.0181	0.0007
QScapolite	0.025	0.002
Qmicroint2	0.140	0.004
Qsanina16	0.098	0.003
Qepidote	0.013	0.002
QCalcite	0.0156	0.0007
Qchlorite2b	0.030	0.002
Qmuscovite1m	0.064	0.006
Qmusc2m1	0.011	0.002

\*\* part of sample holder

## Local GOALS

**Quartz**

Parameter	Value	ESD
Refined composition	SI3 O6	
A	0.491553	
C	0.540774	
GrainSize(1,0,1)	314	12

#### Plagioclase\_Albite

Parameter	Value	ESD
Refined composition	AL4.3600 NA4 SI11.6400 O32	
A	0.814327	
B	1.28036	
C	0.715934	
ALPHA	94.217	
BETA	116.6146	
GAMMA	87.940	

#### Iron\_alpha

Parameter	Value	ESD
Refined composition	FE2	
A	0.287626	

#### Scapolite

Parameter	Value	ESD
Refined composition	AL6.4000 C0.0530 CA0.5600 CL1.6992 K0.4800 NA6.9600 S0.0176 SI17.6000 O48.2294	
A	1.21746	
C	0.7519	

#### MICROCLINE\_intermediate2

Parameter	Value	ESD
Refined composition	AL4 K4 SI12 O32	
A	0.85572	
B	1.29661	
C	0.722284	
ALPHA	89.644	
BETA	115.916	
GAMMA	91.5000	

#### Sanidine\_Na16

Parameter	Value	ESD
Refined composition	AL4 K3.3240 NA0.6760 SI12 O32	
A	0.85429	
B	1.29420	
C	0.721500	
BETA	115.684	

**Epidote**

Parameter	Value	ESD
Refined composition	AL4.3400 CA4 FE1.6200 Si6 O26	
A	0.900300	
B	0.569600	
C	1.01801	
BETA	117.824	

**Calcite**

Parameter	Value	ESD
Refined composition	C6 CA6 O18	
A	0.50340	
C	1.68910	
GrainSize(1,1,1)	42.4413	

**CHLORITE\_Iib-2**

Parameter	Value	ESD
Refined composition	AL4.6820 FE0.5492 H16 MG9.4508 Si5.2480 O36	
A	0.53552	
B	0.92277	
C	1.4236	
BETA	95.5000	

**Muscovite\_1M**

Parameter	Value	ESD
Refined composition	AL5.1760 H4 K2 Si6.8240 O24	
A	0.526000	
B	0.908500	
C	1.0340	
BETA	101.000	

**MUSCOVITE\_2M1**

Parameter	Value	ESD
Refined composition	AL11.6800 FE0.3200 K2.4000 Si12 O48	
A	0.51745	
B	0.90859	
C	2.0589	
BETA	95.156	

**Refined Chemical Composition**

Phase	Phase Quantity (wt-%)	H (wt-%)	C (wt-%)	O (wt-%)	Na (wt-%)	Mg (wt-%)	Al (wt-%)	Si (wt-%)	S (wt-%)	Cl (wt-%)	K (wt-%)	Ca (wt-%)	Fe (wt-%)

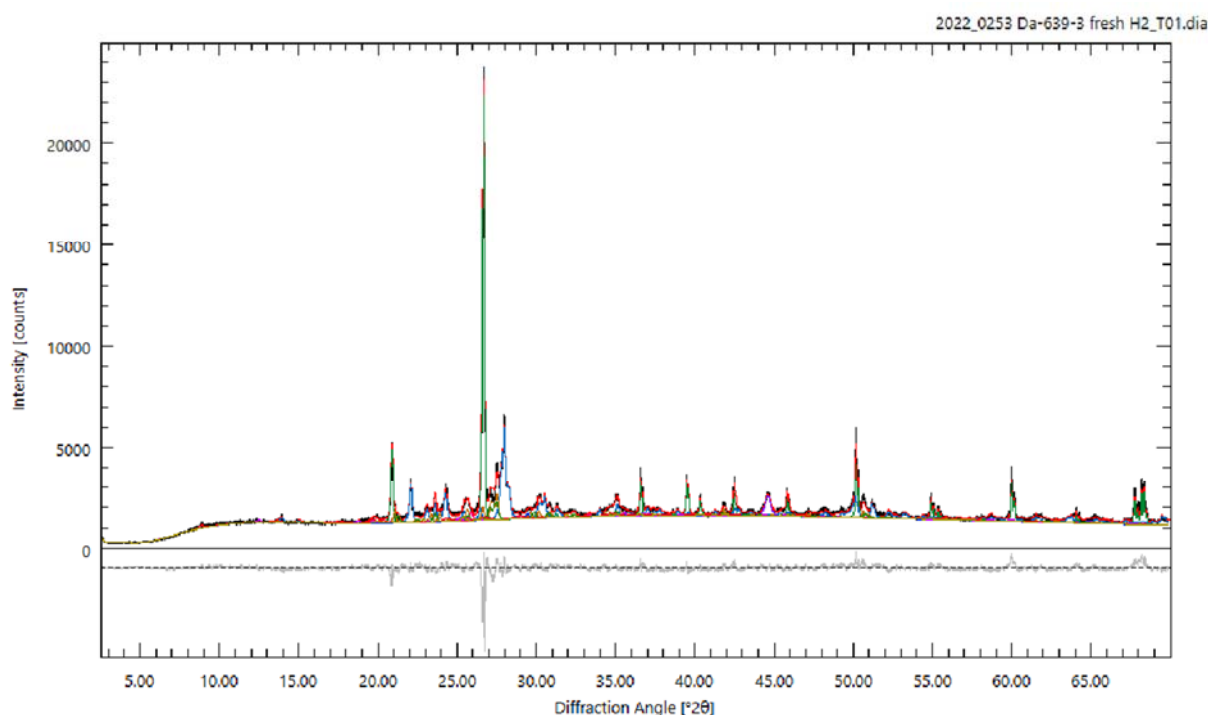
CHLORITE_Ilb-2	2,98	1,43	0,00	51,14	0,00	20,40	11,22	13,09	0,00	0,00	0,00	0,00	2,72
Calcite	1,56	0,00	12,00	47,96	0,00	0,00	0,00	0,00	0,00	0,00	0,00	40,04	0,00
Epidote	1,34	0,00	0,00	43,68	0,00	0,00	12,30	17,69	0,00	0,00	0,00	16,83	9,50
Iron_alpha**	1,80	0,00	0,00	0,00	0,00	0,00	0,00	0,00	0,00	0,00	0,00	0,00	100,00
MICROCLINE_intermediate2	14,01	0,00	0,00	45,99	0,00	0,00	9,69	30,27	0,00	0,00	14,05	0,00	0,00
MUSCOVITE_2M1	1,09	0,00	0,00	50,13	0,00	0,00	20,57	22,00	0,00	0,00	6,13	0,00	1,17
Muscovite_1M	6,43	0,51	0,00	48,15	0,00	0,00	17,51	24,03	0,00	0,00	9,80	0,00	0,00
Plagioclase_Albite	30,23	0,00	0,00	48,83	8,77	0,00	11,22	31,18	0,00	0,00	0,00	0,00	0,00
Quartz	28,27	0,00	0,00	53,26	0,00	0,00	0,00	46,74	0,00	0,00	0,00	0,00	0,00
Sanidine_Na16	9,76	0,00	0,00	46,44	1,41	0,00	9,79	30,57	0,00	0,00	11,79	0,00	0,00
Scapolite	2,53	0,00	0,04	45,36	9,41	0,00	10,15	29,05	0,03	3,54	1,10	1,32	0,00
Weighted total	100,00	0,08	0,19	48,44	3,03	0,61	7,81	33,01	0,00	0,09	3,84	0,88	2,03

\*\* part of sample holder

### Sample Information

Granitic dyke-639-3 fresh H2				
File Name	Granitic dyke-639-3 fresh H2_T01.dia			
Instrument configuration	PW1830_TU Darmstadt_adopted.geq			
Wavelength	CU (1.5406 Å)			
Directory	C:/Users/kasbo/Documents/Data_Laptop/Profex_data/BGE_Project/XRD_Profex_MUSE_Lan			
Date of Refinement	Freitag Januar 06, 2023			
Operator	kasbo			
Statistics	$R_{wp} = 5.61$	$R_{exp} = 2.50$	$\chi^2 = 5.0355$	GoF = 2.2440

### Diffraction Pattern



### Global GOALS

Parameter	Value	ESD
Qquartz	0.258	0.003
Qalbite	0.360	0.004
Qironalpha**	0.0141	0.0006
QScapolite	0.020	0.002
Qmicroint2	0.107	0.005
Qsanina16	0.081	0.004
Qepidote	0.014	0.002
QCalcite	0.0086	0.0007
Qchlorite2b	0.038	0.003
Qmuscovite1m	0.075	0.005
Qmusc2m1	0.025	0.002

\*\* part of sample holder

Local GOALS

**Quartz**

Parameter	Value	ESD
Refined composition	Si3 O6	
A	0.4915428	
C	0.540738	
GrainSize(1,0,1)	618	41

**Plagioclase\_Albite**

Parameter	Value	ESD
Refined composition	AL4.3600 NA4 Si11.6400 O32	
A	0.814254	
B	1.280070	
C	0.716024	
ALPHA	94.2491	
BETA	116.6103	
GAMMA	87.8834	

**Iron\_alpha**

Parameter	Value	ESD
Refined composition	FE2	
A	0.287523	

**Scapolite**

Parameter	Value	ESD
Refined composition	AL6.4000 C0.0530 CA0.5600 CL1.6992 K0.4800 NA6.9600 S0.0176 Si17.6000 O48.2294	
A	1.21746	
C	0.75184	

**MICROCLINE\_intermediate2**

Parameter	Value	ESD
Refined composition	AL4 K4 Si12 O32	
A	0.85731	
B	1.29679	
C	0.72182	
ALPHA	89.639	
BETA	115.917	
GAMMA	91.5000	

**Sanidine\_Na16**

Parameter	Value	ESD
Refined composition	AL4 K3.3240 NA0.6760 Si12 O32	
A	0.849000	
B	1.29941	
C	0.71960	

BETA	115.518	
------	---------	--

#### Epidote

Parameter	Value	ESD
Refined composition	AL4.3400 CA4 FE1.6200 SI6 O26	
A	0.89656	
B	0.558400	
C	1.02060	
BETA	122.621	

#### Calcite

Parameter	Value	ESD
Refined composition	C6 CA6 O18	
A	0.504100	
C	1.6896	
GrainSize(1,1,1)	42.4413	

#### CHLORITE\_Iib-2

Parameter	Value	ESD
Refined composition	AL4.6820 FE0.5844 H16 MG9.4156 SI5.2480 O36	
A	0.53646	
B	0.91734	
C	1.42461	
BETA	95.5000	

#### Muscovite\_1M

Parameter	Value	ESD
Refined composition	AL5.1760 H4 K1.3748 SI6.8240 O24	
A	0.526000	
B	0.9008	
C	1.01720	
BETA	101.000	

#### MUSCOVITE\_2M1

Parameter	Value	ESD
Refined composition	AL11.6800 FE0.3200 K2.4000 SI12 O48	
A	0.51989	
B	0.90059	
C	2.0254	
BETA	95.84	

Refined Chemical Composition

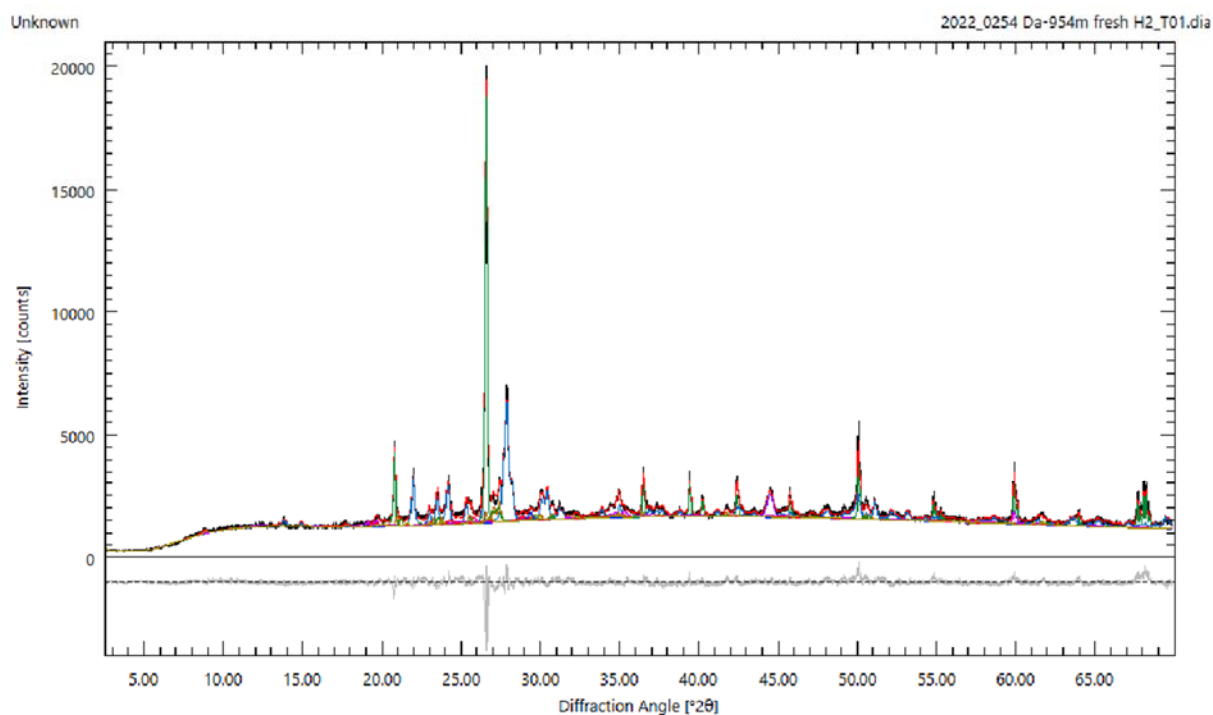
Phase	Phase Quantity (wt-%)	H (wt-%)	C (wt-%)	O (wt-%)	Na (wt-%)	Mg (wt-%)	Al (wt-%)	Si (wt-%)	S (wt-%)	Cl (wt-%)	K (wt-%)	Ca (wt-%)	Fe (wt-%)
CHLORITE_IIb-2	3,79	1,43	0,00	51,09	0,00	20,30	11,21	13,07	0,00	0,00	0,00	0,00	2,90
Calcite	0,85	0,00	12,00	47,96	0,00	0,00	0,00	0,00	0,00	0,00	0,00	40,04	0,00
Epidote	1,41	0,00	0,00	43,68	0,00	0,00	12,30	17,69	0,00	0,00	0,00	16,83	9,50
Iron_alpha**	1,41	0,00	0,00	0,00	0,00	0,00	0,00	0,00	0,00	0,00	0,00	0,00	100,00
MICROCLINE_intermediate2	10,66	0,00	0,00	45,99	0,00	0,00	9,69	30,27	0,00	0,00	14,05	0,00	0,00
MUSCOVITE_2M1	2,55	0,00	0,00	50,13	0,00	0,00	20,57	22,00	0,00	0,00	6,13	0,00	1,17
Muscovite_1M	7,46	0,52	0,00	49,67	0,00	0,00	18,06	24,79	0,00	0,00	6,95	0,00	0,00
Plagioclase_Albite	36,00	0,00	0,00	48,83	8,77	0,00	11,22	31,18	0,00	0,00	0,00	0,00	0,00
Quartz	25,77	0,00	0,00	53,26	0,00	0,00	0,00	46,74	0,00	0,00	0,00	0,00	0,00
Sanidine_Na16	8,06	0,00	0,00	46,44	1,41	0,00	9,79	30,57	0,00	0,00	11,79	0,00	0,00
Scapolite	2,03	0,00	0,04	45,36	9,41	0,00	10,15	29,05	0,03	3,54	1,10	1,32	0,00
Weighted total	99,99	0,09	0,10	48,82	3,46	0,77	8,54	32,71	0,00	0,07	3,15	0,61	1,69

\*\* part of sample holder

Sample Information

Granite 954m fresh H2				
File Name	Granite 954m fresh H2_T01.dia			
Instrument configuration	PW1830_TU Darmstadt_adopted.geq			
Wavelength	CU (1.5406 Å)			
Directory	C:/Users/kasbo/Documents/Data_Laptop/Profex_data/BGE_Project/XRD_Profex_MUSE_Lan			
Date of Refinement	Freitag Januar 06, 2023			
Operator	kasbo			
Statistics	$R_{wp} = 5.11$	$R_{exp} = 2.49$	$\chi^2 = 4.2116$	GoF = 2.0522

Diffraction Pattern



Global GOALS

Parameter	Value	ESD
Qquartz	0.219	0.002
Qalbite	0.410	0.004
Qironalpha**	0.0154	0.0007
QScapolite	0.022	0.002
Qmicroint2	0.068	0.005
Qsanina16	0.059	0.004
Qepidote	0.016	0.002
QCalcite	0.0116	0.0007
Qchlorite2b	0.086	0.004
Qmuscovite1m	0.054	0.004
Qmusc2m1	0.039	0.002

\*\* part of sample holder

## Local GOALS

**Quartz**

Parameter	Value	ESD
Refined composition	Si3 O6	
A	0.491507	
C	0.540732	
GrainSize(1,0,1)	637	49

**Plagioclase\_Albite**

Parameter	Value	ESD
Refined composition	AL4.3600 NA4 Si11.6400 O32	
A	0.814086	
B	1.279722	
C	0.716152	
ALPHA	94.2482	
BETA	116.6210	
GAMMA	87.8094	

**Iron\_alpha**

Parameter	Value	ESD
Refined composition	FE2	
A	0.287657	

**Scapolite**

Parameter	Value	ESD
Refined composition	AL6.4000 C0.0530 CA0.5600 CL1.6992 K0.4800 NA6.9600 S0.0176 Si17.6000 O48.2294	
A	1.21668	
C	0.75129	

**MICROCLINE\_intermediate2**

Parameter	Value	ESD
Refined composition	AL4 K4 Si12 O32	
A	0.85748	
B	1.29750	
C	0.72206	
ALPHA	89.512	
BETA	115.949	
GAMMA	91.5000	

**Sanidine\_Na16**

Parameter	Value	ESD
Refined composition	AL4 K3.3240 NA0.6760 Si12 O32	
A	0.849000	
B	1.29891	
C	0.72003	
BETA	115.500	

**Epidote**

Parameter	Value	ESD
Refined composition	AL4.3400 CA4 FE1.6200 SI6 O26	
A	0.89613	
B	0.56041	
C	1.01474	
BETA	114.240	

**Calcite**

Parameter	Value	ESD
Refined composition	C6 CA6 O18	
A	0.50378	
C	1.68910	
GrainSize(1,1,1)	42.4413	

**CHLORITE\_Iib-2**

Parameter	Value	ESD
Refined composition	AL4.6820 FE1.3672 H16 MG8.6328 SI5.2480 O36	
A	0.534915	
B	0.92492	
C	1.4228	
BETA	95.5000	

**Muscovite\_1M**

Parameter	Value	ESD
Refined composition	AL5.1760 H4 K1.7164 SI6.8240 O24	
A	0.526000	
B	0.8988	
C	1.0174	
BETA	101.000	

**MUSCOVITE\_2M1**

Parameter	Value	ESD
Refined composition	AL11.6800 FE0.3200 K2.4000 SI12 O48	
A	0.52171	
B	0.90121	
C	1.99103	
BETA	95.333	

Refined Chemical Composition

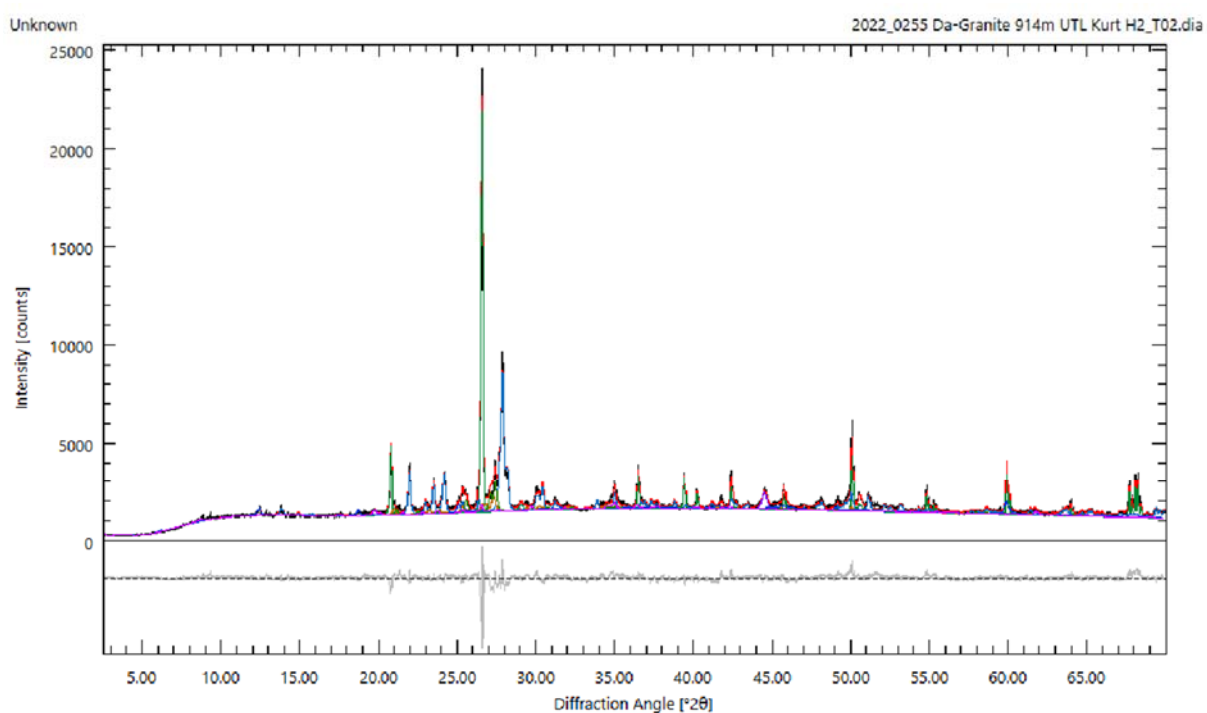
Phase	Phase Quantity (wt-%)	H (wt-%)	C (wt-%)	O (wt-%)	Na (wt-%)	Mg (wt-%)	Al (wt-%)	Si (wt-%)	S (wt-%)	Cl (wt-%)	K (wt-%)	Ca (wt-%)	Fe (wt-%)
CHLORITE_Ilb-2	8,55	1,40	0,00	50,00	0,00	18,21	10,97	12,79	0,00	0,00	0,00	0,00	6,63
Calcite	1,16	0,00	12,00	47,96	0,00	0,00	0,00	0,00	0,00	0,00	0,00	40,04	0,00
Epidote	1,58	0,00	0,00	43,68	0,00	0,00	12,30	17,69	0,00	0,00	0,00	16,83	9,50
Iron_alpha**	1,54	0,00	0,00	0,00	0,00	0,00	0,00	0,00	0,00	0,00	0,00	0,00	100,00
MICROCLINE_intermediate2	6,76	0,00	0,00	45,99	0,00	0,00	9,69	30,27	0,00	0,00	14,05	0,00	0,00
MUSCOVITE_2M1	3,87	0,00	0,00	50,13	0,00	0,00	20,57	22,00	0,00	0,00	6,13	0,00	1,17
Muscovite_1M	5,43	0,51	0,00	48,83	0,00	0,00	17,76	24,37	0,00	0,00	8,53	0,00	0,00
Plagioclase_Albite	40,99	0,00	0,00	48,83	8,77	0,00	11,22	31,18	0,00	0,00	0,00	0,00	0,00
Quartz	21,94	0,00	0,00	53,26	0,00	0,00	0,00	46,74	0,00	0,00	0,00	0,00	0,00
Sanidine_Na16	5,94	0,00	0,00	46,44	1,41	0,00	9,79	30,57	0,00	0,00	11,79	0,00	0,00
Scapolite	2,24	0,00	0,04	45,36	9,41	0,00	10,15	29,05	0,03	3,54	1,10	1,32	0,00
Weighted total	100,00	0,15	0,14	48,70	3,89	1,56	8,96	31,10	0,00	0,08	2,38	0,76	2,30

\*\* part of sample holder

### Sample Information

Granite 914m UTL Kurt H2				
File Name	Granite 914m UTL Kurt H2_T02.dia			
Instrument configuration	PW1830_TU Darmstadt_adopted.geq			
Wavelength	CU (1.5406 Å)			
Directory	C:/Users/kasbo/Documents/Data_Laptop/Profex_data/BGE_Project/XRD_Profex_MUSE_Lan			
Date of Refinement	Freitag Januar 06, 2023			
Operator	kasbo			
Statistics	$R_{wp} = 5.57$	$R_{exp} = 2.51$	$\chi^2 = 4.9245$	GoF = 2.2191

### Diffraction Pattern



### Global GOALS

Parameter	Value	ESD
Qquartz	0.239	0.002
Qalbite	0.397	0.004
Qironalpha**	0.0112	0.0003
QScapolite	0.017	0.002
Qmicroint2	0.072	0.003
Qsanina16	0.067	0.004
QCalcite	0.0122	0.0008
Qchlorite2b	0.127	0.006
Qmusc2m1	0.057	0.002

\*\* part of sample holder

## Local GOALs

**Quartz**

Parameter	Value	ESD
Refined composition	SI3 O6	
A	0.4914944	
C	0.540689	
GrainSize(1,0,1)	ERROR	

**Plagioclase Albite**

Parameter	Value	ESD
Refined composition	AL4.3600 NA4 SI11.6400 O32	
A	0.814252	
B	1.279871	
C	0.715778	
ALPHA	94.2734	
BETA	116.6084	
GAMMA	87.8480	

**Iron\_alpha**

Parameter	Value	ESD
Refined composition	FE2	
A	0.287472	

**Scapolite**

Parameter	Value	ESD
Refined composition	AL6.4000 C0.0530 CA0.5600 CL1.6992 K0.4800 NA6.9600 S0.0176 SI17.6000 O48.2294	
A	1.2172	
C	0.7527	

**MICROCLINE\_intermediate2**

Parameter	Value	ESD
Refined composition	AL4 K4 SI12 O32	
A	0.85390	
B	1.29753	
C	0.728300	
ALPHA	90.187	
BETA	116.296	
GAMMA	91.5000	

**Sanidine\_Na16**

Parameter	Value	ESD
Refined composition	AL4 K3.3240 NA0.6760 SI12 O32	
A	0.849000	
B	1.29420	
C	0.721500	

BETA	115.947	
------	---------	--

#### Calcite

Parameter	Value	ESD
Refined composition	C6 CA6 O18	
A	0.504100	
C	1.7208	
GrainSize(1,1,1)	42.4413	

#### CHLORITE\_Iib-2

Parameter	Value	ESD
Refined composition	AL4.6820 FE1.4504 H16 MG8.5496 SI5.2480 O36	
A	0.53439	
B	0.9133	
C	1.42194	
BETA	95.5000	

#### MUSCOVITE\_2M1

Parameter	Value	ESD
Refined composition	AL11.6800 FE0.3200 K2.4000 SI12 O48	
A	0.52069	
B	0.90016	
C	2.02157	
BETA	95.706	

#### Refined Chemical Composition

Phase	Phase Quantity (wt-%)	H (wt-%)	C (wt-%)	O (wt-%)	Na (wt-%)	Mg (wt-%)	Al (wt-%)	Si (wt-%)	S (wt-%)	Cl (wt-%)	K (wt-%)	Ca (wt-%)	Fe (wt-%)
CHLORITE_Iib-2	12,74	1,40	0,00	49,88	0,00	18,00	10,94	12,77	0,00	0,00	0,00	0,00	7,02
Calcite	1,22	0,00	12,00	47,96	0,00	0,00	0,00	0,00	0,00	0,00	0,00	40,04	0,00
Iron_alpha**	1,12	0,00	0,00	0,00	0,00	0,00	0,00	0,00	0,00	0,00	0,00	0,00	100,00
MICROCLINE_intermediate2	7,25	0,00	0,00	45,99	0,00	0,00	9,69	30,27	0,00	0,00	14,05	0,00	0,00
MUSCOVITE_2M1	5,74	0,00	0,00	50,13	0,00	0,00	20,57	22,00	0,00	0,00	6,13	0,00	1,17
Plagioclase_Albite	39,69	0,00	0,00	48,83	8,77	0,00	11,22	31,18	0,00	0,00	0,00	0,00	0,00
Quartz	23,90	0,00	0,00	53,26	0,00	0,00	0,00	46,74	0,00	0,00	0,00	0,00	0,00
Sanidine_Na16	6,69	0,00	0,00	46,44	1,41	0,00	9,79	30,57	0,00	0,00	11,79	0,00	0,00
Scapolite	1,65	0,00	0,04	45,36	9,41	0,00	10,15	29,05	0,03	3,54	1,10	1,32	0,00
Weighted total	100,00	0,18	0,15	49,12	3,73	2,29	8,55	31,15	0,00	0,06	2,18	0,51	2,08

\*\* part of sample holder

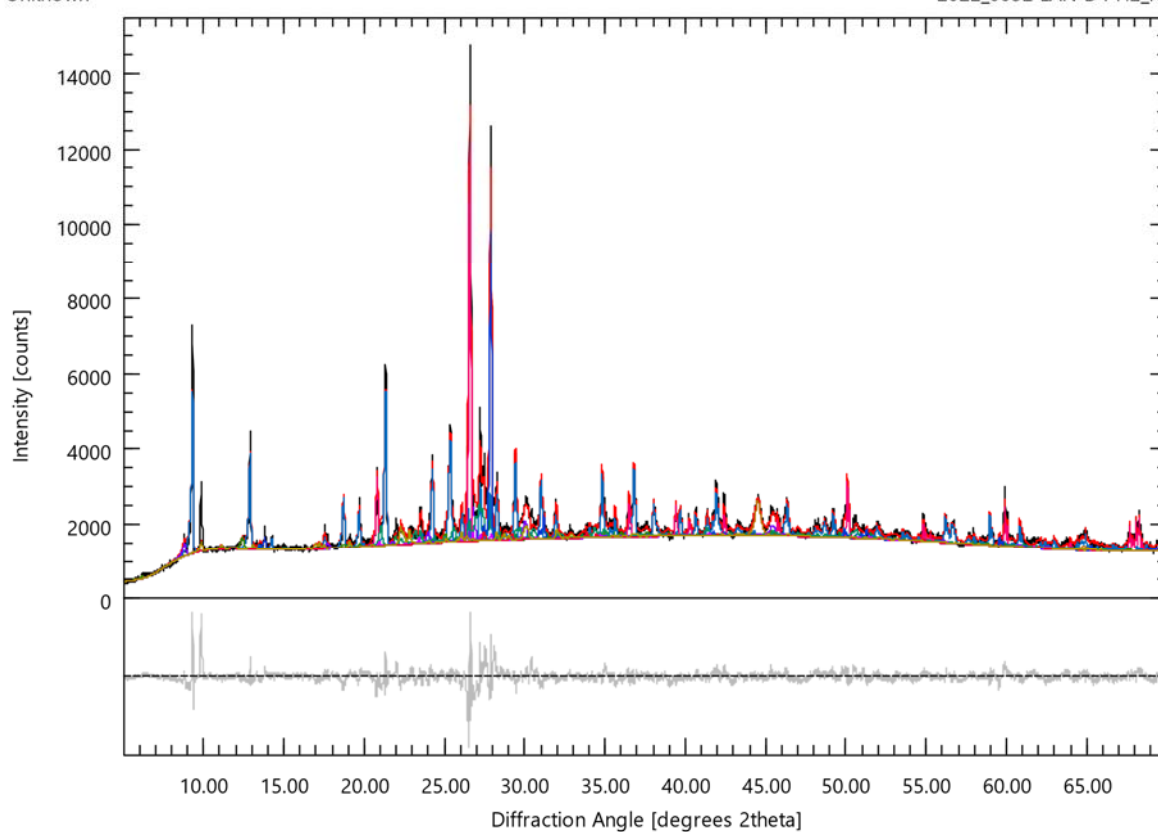
## Sample Information

D4 H2				
File Name	D4 H2_R12.dia			
Instrument configuration	PW1830_TU Darmstadt_adopted.geq			
Wavelength	CU (1.5406 Å)			
Directory	C:/Users/kasbo/Documents/Data_Laptop/Profex_data/BGE_Project/XRD_Profex_MUSE_Lan			
Date of Refinement	Dienstag Juli 26, 2022			
Operator	kasbo			
Statistics	$R_{wp} = 5.99$	$R_{exp} = 2.42$	$\chi^2 = 6.1266$	GoF = 2.4752

## Diffraction Pattern

Unknown

2022\_0052 LAN D4 H2\_R12.dia



## Global GOALS

Parameter	Value	ESD
Qanorthite	0.063	0.003
Qlaumontite	0.397	0.004
QMuscovite2M1	0.064	0.003
Qquartz	0.145	0.002
Qironalpha**	0.0171	0.0004
Qchlorite2b	0.034	0.002
Qmicroint2	0.124	0.003
Qsanina75	0.055	0.004

Qorthoclase	0.017	0.002
Qtitanite	0.013	0.002
Qheulandite	0.072	0.003

*\*\* part of sample holder*

Local GOALS

**PLAGIOCLASE\_ANORTHITE**

Parameter	Value	ESD
Refined composition	AL16 CA8 SI16 O64	
A	0.816500	
B	1.28900	
C	1.41816	
ALPHA	93.0000	
BETA	115.869	
GAMMA	90.705	

**Laumontite**

Parameter	Value	ESD
Refined composition	AL8 CA4 H22.2000 SI16 O61.1920	
A	1.475117	
B	1.306888	
C	0.755369	
BETA	112.0414	

**Muscovite2M1**

Parameter	Value	ESD
Refined composition	AL11.6800 FE0.3200 K4 SI12 O48	
A	0.525000	
B	0.890000	
C	2.00476	
BETA	96.046	
GrainSize(1,0,0)	70.7355	

**Quartz**

Parameter	Value	ESD
Refined composition	SI3 O6	
A	0.491485	
C	0.540797	
GrainSize(1,0,1)	7971	10110

**Iron\_alpha**

Parameter	Value	ESD
Refined composition	FE2	
A	0.287483	

**CHLORITE\_Lea**

Parameter	Value	ESD
-----------	-------	-----

Refined composition	AL4.6820 FE5.6000 H16 MG4.4000 SI5.2480 O36	
A	0.53252	
B	0.94070	
C	1.42240	
BETA	94.518	

#### MICROCLINE\_intermediate2

Parameter	Value	ESD
Refined composition	AL4 K4 SI12 O32	
A	0.85575	
B	1.30900	
C	0.72007	
ALPHA	89.467	
BETA	115.500	
GAMMA	91.065	

#### Sanidine\_Na75

Parameter	Value	ESD
Refined composition	AL4 K1 NA3 SI12 O32	
A	0.833900	
B	1.29552	
C	0.712900	
BETA	116.4130	

#### ORTHOCLASE

Parameter	Value	ESD
Refined composition	AL4 K4 SI12 O32	
A	0.86045	
B	1.30378	
C	0.710000	
BETA	116.053	

#### Titanite

Parameter	Value	ESD
Refined composition	CA4 SI4 TI4 O20	
A	0.74916	
B	0.880100	
C	0.70301	
BETA	125.400	

#### Heulandite

Parameter	Value	ESD
Refined composition	AL8.8992 CA3.6960 K0.1200 NA1.3000 SI27.1008 O96.7600	

A	1.75629	
B	1.78289	
C	0.73892	
BETA	115.776	

Refined Chemical Composition

Phase	Phase Quantity (wt-%)	H (wt-%)	O (wt-%)	Na (wt-%)	Mg (wt-%)	Al (wt-%)	Si (wt-%)	K (wt-%)	Ca (wt-%)	Ti (wt-%)	Fe (wt-%)
CHLORITE_Lea	3,36	1,25	44,81	0,00	8,32	9,83	11,47	0,00	0,00	0,00	24,33
Heulandite	7,16	0,00	56,66	1,09	0,00	8,79	27,86	0,17	5,42	0,00	0,00
Iron_alpha**	1,71	0,00	0,00	0,00	0,00	0,00	0,00	0,00	0,00	0,00	100,00
Laumontite	39,68	1,22	53,59	0,00	0,00	11,81	24,60	0,00	8,77	0,00	0,00
MICROCLINE_intermediate2	12,41	0,00	45,99	0,00	0,00	9,69	30,27	14,05	0,00	0,00	0,00
Muscovite2M1	6,43	0,00	48,17	0,00	0,00	19,77	21,14	9,81	0,00	0,00	1,12
ORTHOCLASE	1,66	0,00	45,99	0,00	0,00	9,69	30,27	14,05	0,00	0,00	0,00
PLAGIOCLASE_ANORTHITE	6,33	0,00	46,01	0,00	0,00	19,40	20,19	0,00	14,41	0,00	0,00
Quartz	14,47	0,00	53,26	0,00	0,00	0,00	46,74	0,00	0,00	0,00	0,00
Sanidine_Na75	5,48	0,00	48,07	6,48	0,00	10,13	31,65	3,67	0,00	0,00	0,00
Titanite	1,32	0,00	40,81	0,00	0,00	0,00	14,33	0,00	20,45	24,42	0,00
Weighted total	100,01	0,53	50,19	0,43	0,28	10,06	27,72	2,82	5,05	0,32	2,60

\*\* part of sample holder

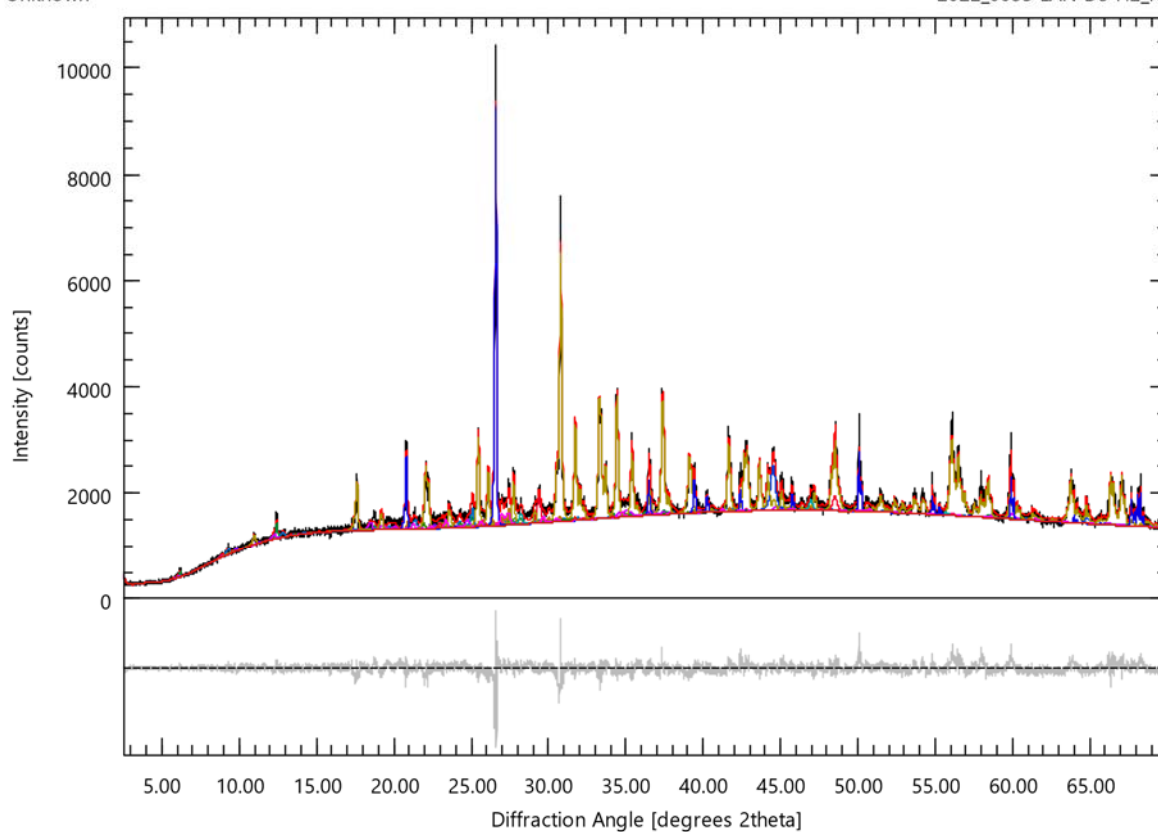
Sample Information

D5 H2				
File Name	D5 H2_R03.dia			
Instrument configuration	PW1830_TU Darmstadt_adopted.geq			
Wavelength	CU (1.5406 Å)			
Directory	C:/Users/kasbo/Documents/Data_Laptop/Profex_data/BGE_Project/XRD_Profex_MUSE_Lan			
Date of Refinement	Freitag Juli 22, 2022			
Operator	kasbo			
Statistics	$R_{wp} = 4.50$	$R_{exp} = 2.49$	$\chi^2 = 3.2661$	GoF = 1.8072

Diffraction Pattern

Unknown

2022\_0053 LAN D5 H2\_R03.dia



Global GOALS

Parameter	Value	ESD
Qchlorite2b	0.024	0.002
Qlaumontite	0.051	0.003
Qclinopt	0.013	0.002
Qmusc2m1	0.021	0.002
Qmicromax	0.025	0.002
Qalbite	0.020	0.002
QFAp	0.000000	0.000000
Qironalpha**	0.0166	0.0004
QClinochlore1A	0.048	0.002
QCalcite	0.028	0.003

Qepidote	0.574	0.004
Qankerit05	0.011	0.003
Qfluorite	0.0074	0.0008
Qquartz	0.126	0.001
Qsanid086	0.032	0.003
Qfluorapa	0.0032	0.0009

\*\* part of sample holder

Local GOALS

**CHLORITE\_Lea**

Parameter	Value	ESD
Refined composition	AL4.6820 FE6.2412 H16 MG3.7588 SI5.2480 O36	
A	0.52247	
B	0.94572	
C	1.42521	
BETA	96.119	

**Laumontite**

Parameter	Value	ESD
Refined composition	AL8 CA4 H22.2000 SI16 O61.1920	
A	1.47600	
B	1.30303	
C	0.76222	
BETA	111.666	

**Clinoptilolite**

Parameter	Value	ESD
Refined composition	AL6.8400 BA0.1500 CA0.8400 K0.3700 MG0.8000 NA2.8800 SI29.1600 O92.4800	
A	1.7551	
B	1.7876	
C	0.7466	
BETA	116.98	

**MUSCOVITE\_2M1**

Parameter	Value	ESD
Refined composition	AL11.6800 FE0.3200 K4 SI12 O48	
A	0.513000	
B	0.9022	
C	1.9896	
BETA	94.979	

**MICROCLINE\_maximum**

Parameter	Value	ESD
Refined composition	AL4 K4 SI12 O32	
A	0.86045	
B	1.29874	

C	0.72151	
ALPHA	90.914	
BETA	116.024	
GAMMA	87.829	

#### Plagioclase Albite

Parameter	Value	ESD
Refined composition	AL4.3600 NA4 SI11.6400 O32	
A	0.815000	
B	1.27000	
C	0.720000	
ALPHA	94.24	
BETA	117.000	
GAMMA	88.2000	

#### Fluorapatite

Parameter	Value	ESD
Refined composition	CA10 F2 P6 O24	
A	UNDEF	
C	UNDEF	
GrainSize(1,1,1)	UNDEF	

#### Iron\_alpha

Parameter	Value	ESD
Refined composition	FE2	
A	0.287473	

#### Clinochlore1A

Parameter	Value	ESD
Refined composition	AL3.6000 FE0.9200 H16 MG9.4800 SI6 O36	
A	0.53340	
B	0.92660	
C	1.44743	
ALPHA	90.10	
BETA	97.938	
GAMMA	89.97	
GrainSize(1,1,1)	42.4413	

#### Calcite

Parameter	Value	ESD
Refined composition	C6 CA6 O18	
A	0.50022	
C	1.6990	
GrainSize(1,1,1)	42.4413	

#### Epidote

Parameter	Value	ESD
Refined composition	AL4.3400 CA4 FE1.6200 SI6 O26	
A	0.889509	
B	0.562885	
C	1.015801	
BETA	115.4110	

#### Ankerite\_Fe0.54

Parameter	Value	ESD
Refined composition	C6 CA2.9940 FE2.1060 MG0.9000 O18	
A	0.4811	
C	1.61400	
GrainSize(1,0,4)	42.4413	

#### Fluorite

Parameter	Value	ESD
Refined composition	CA4 F8	
A	0.54652	

#### Quartz

Parameter	Value	ESD
Refined composition	SI3 O6	
A	0.491454	
C	0.540693	
GrainSize(1,0,1)	ERROR	

#### SANIDINE\_K086

Parameter	Value	ESD
Refined composition	AL4 K3.4400 NA0.5600 SI12 O32	
A	0.845800	
B	1.31141	
C	0.71835	
BETA	115.511	

#### FLUORAPATITE

Parameter	Value	ESD
Refined composition	CA9.7560 F1.8840 P5.9520 O23.9760	
A	0.94434	
C	0.68289	

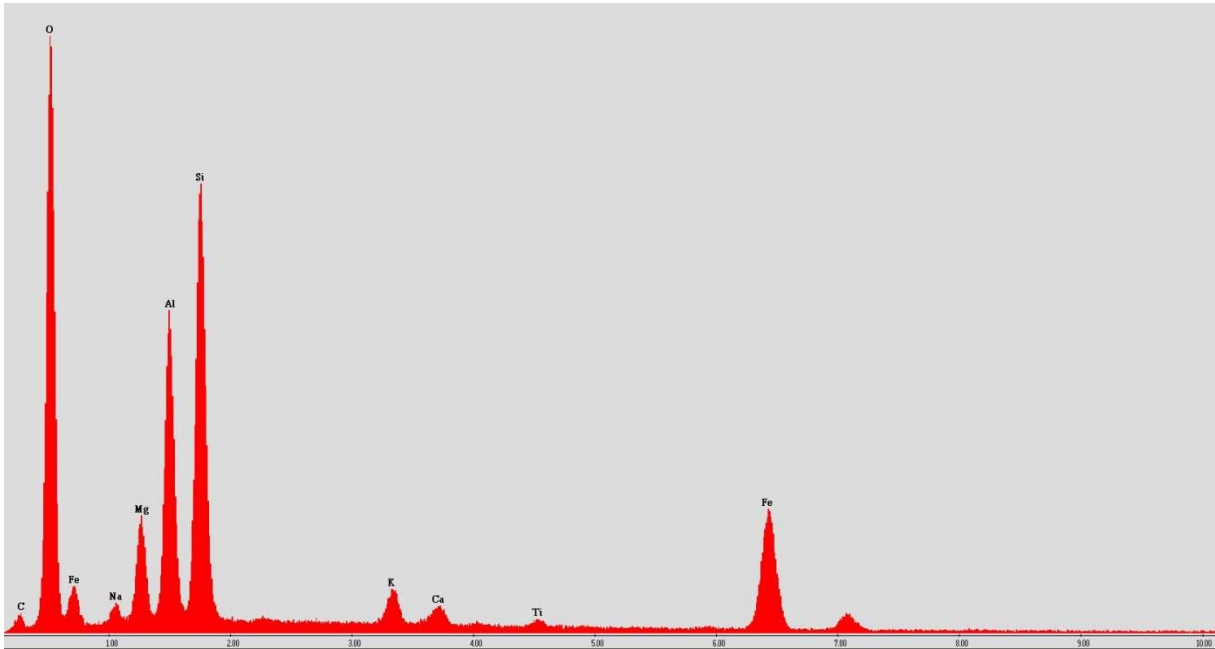
#### Refined Chemical Composition

Phase	Phase Quantity (wt-%)	H (wt-%)	C (wt-%)	O (wt-%)	F (wt-%)	Na (wt-%)	Mg (wt-%)	Al (wt-%)	Si (wt-%)	P (wt-%)	K (wt-%)	Ca (wt-%)	Fe (wt-%)	Ba (wt-%)
Ankerite_Fe0.54	1,13	0,00	11,63	46,49	0,00	0,00	3,53	0,00	0,00	0,00	0,00	19,37	18,98	0,00
CHLORITE_Lea	2,43	1,24	0,00	44,11	0,00	0,00	7,00	9,67	11,29	0,00	0,00	0,00	26,69	0,00
Calcite	2,79	0,00	12,00	47,96	0,00	0,00	0,00	0,00	0,00	0,00	0,00	40,04	0,00	0,00

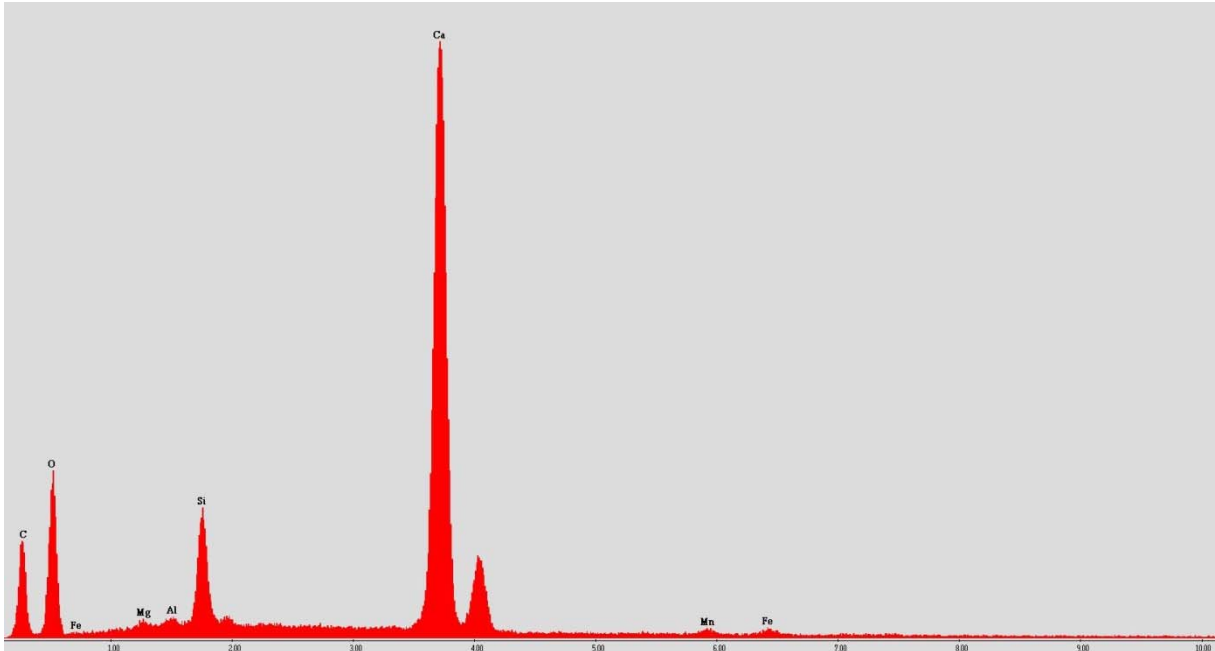
Clinochlore1A	4,82	1,42	0,00	50,54	0,00	0,00	20,22	8,52	14,79	0,00	0,00	0,00	4,51	0,00
Clinoptilolite	1,25	0,00	0,00	56,10	0,00	2,51	0,74	7,00	31,05	0,00	0,55	1,28	0,00	0,78
Epidote	57,44	0,00	0,00	43,68	0,00	0,00	0,00	12,30	17,69	0,00	0,00	16,83	9,50	0,00
FLUORAPATITE	0,32	0,00	0,00	38,56	3,60	0,00	0,00	0,00	0,00	18,53	0,00	39,31	0,00	0,00
Fluorapatite	0,00	0,00	0,00	38,07	3,77	0,00	0,00	0,00	0,00	18,43	0,00	39,74	0,00	0,00
Fluorite	0,74	0,00	0,00	0,00	48,67	0,00	0,00	0,00	0,00	0,00	0,00	51,33	0,00	0,00
Iron_alpha**	1,66	0,00	0,00	0,00	0,00	0,00	0,00	0,00	0,00	0,00	0,00	0,00	100,00	0,00
Laumontite	5,07	1,22	0,00	53,59	0,00	0,00	0,00	11,81	24,60	0,00	0,00	8,77	0,00	0,00
MICROCLINE_max	2,51	0,00	0,00	45,99	0,00	0,00	0,00	9,69	30,27	0,00	14,05	0,00	0,00	0,00
MUSCOVITE_2M1	2,11	0,00	0,00	48,17	0,00	0,00	0,00	19,77	21,14	0,00	9,81	0,00	1,12	0,00
Plagioclase_Albite	1,99	0,00	0,00	48,83	0,00	8,77	0,00	11,22	31,18	0,00	0,00	0,00	0,00	0,00
Quartz	12,57	0,00	0,00	53,26	0,00	0,00	0,00	0,00	46,74	0,00	0,00	0,00	0,00	0,00
SANIDINE_K086	3,16	0,00	0,00	46,36	0,00	1,17	0,00	9,77	30,52	0,00	12,18	0,00	0,00	0,00
Weighted total	99,99	0,16	0,47	45,30	0,37	0,24	1,19	9,59	21,45	0,06	0,95	11,97	8,22	0,01

\*\* part of sample holder

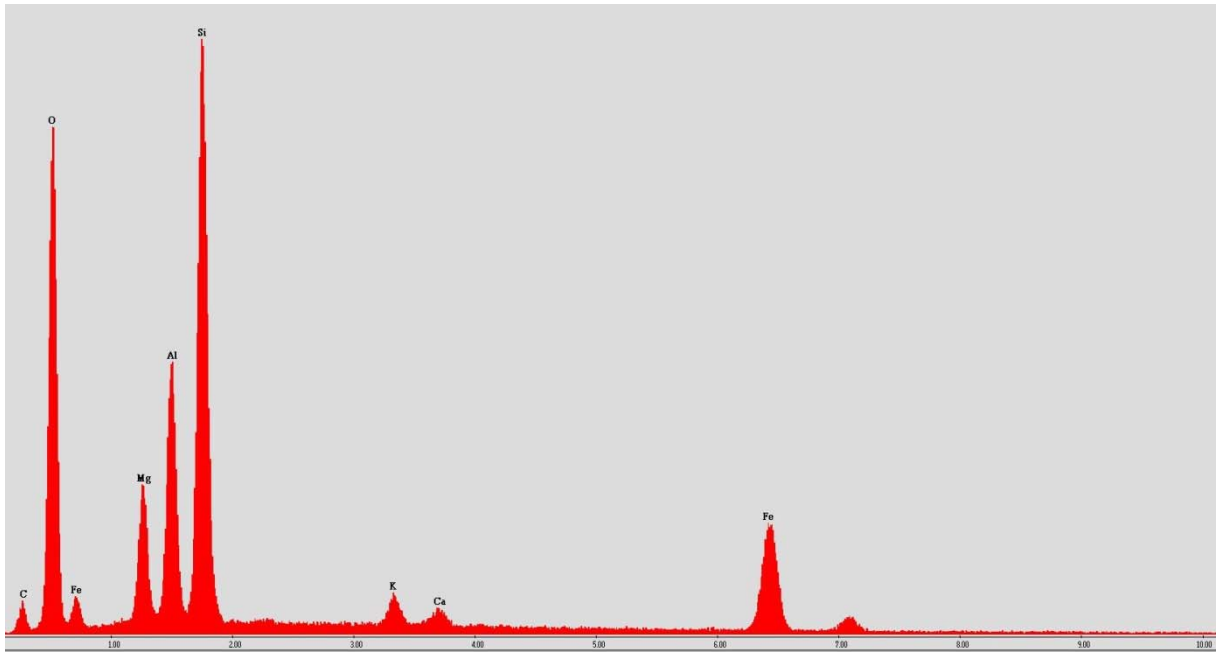
## Appendix 2. EDX-measurements



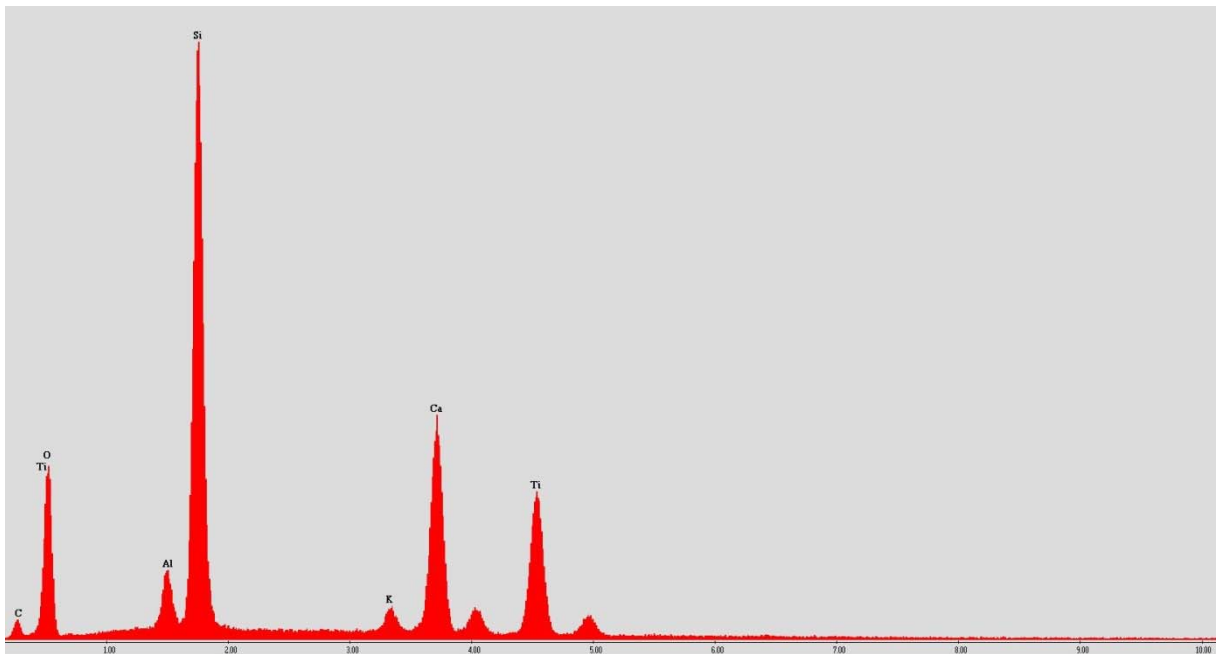
App 2.1. EDX measurement of biotite from fig 6.1B



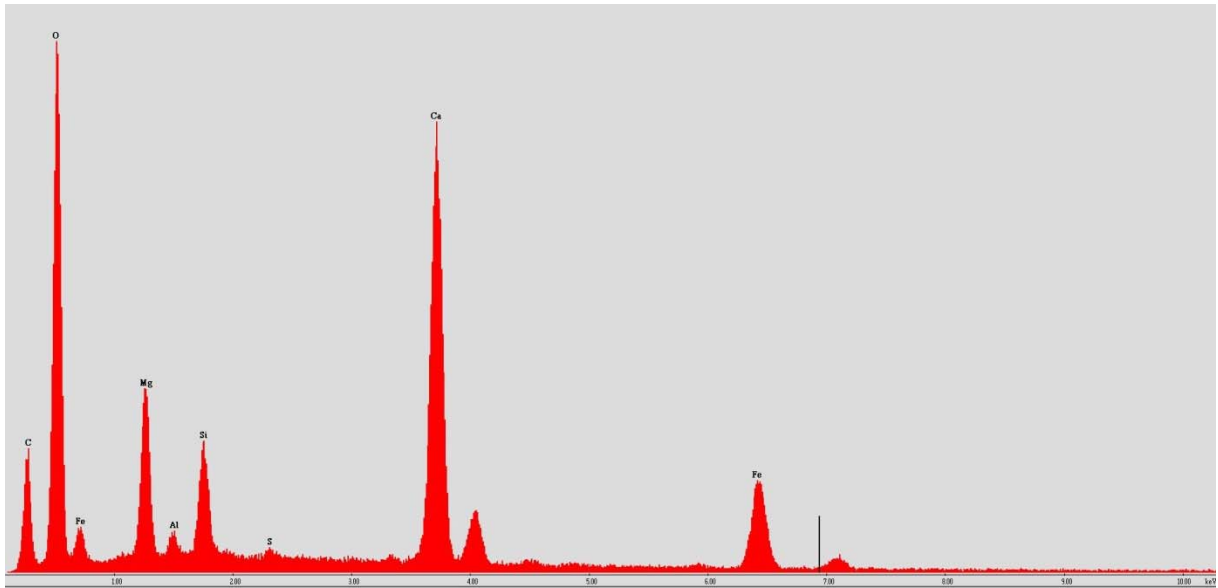
App 2.2. EDX measurement of calcite from fig 6.3A



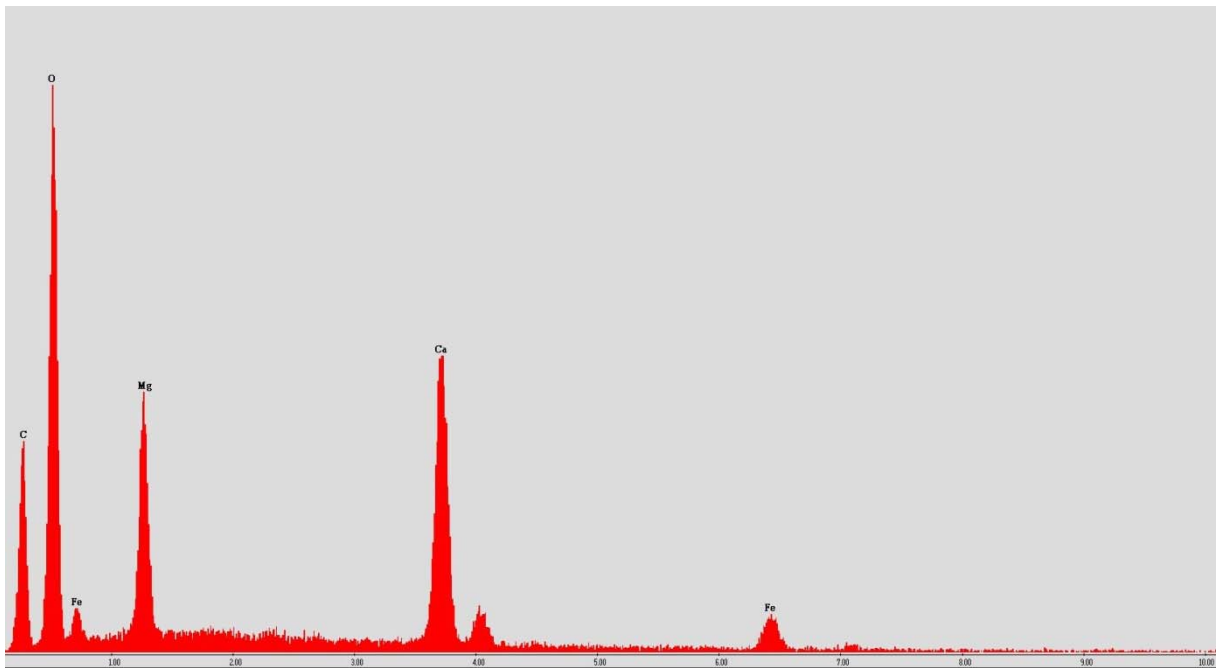
App 2.3. EDX measurement of chlorite from fig 6.3C



App 2.4. EDX measurement of titanite from fig 6.3D

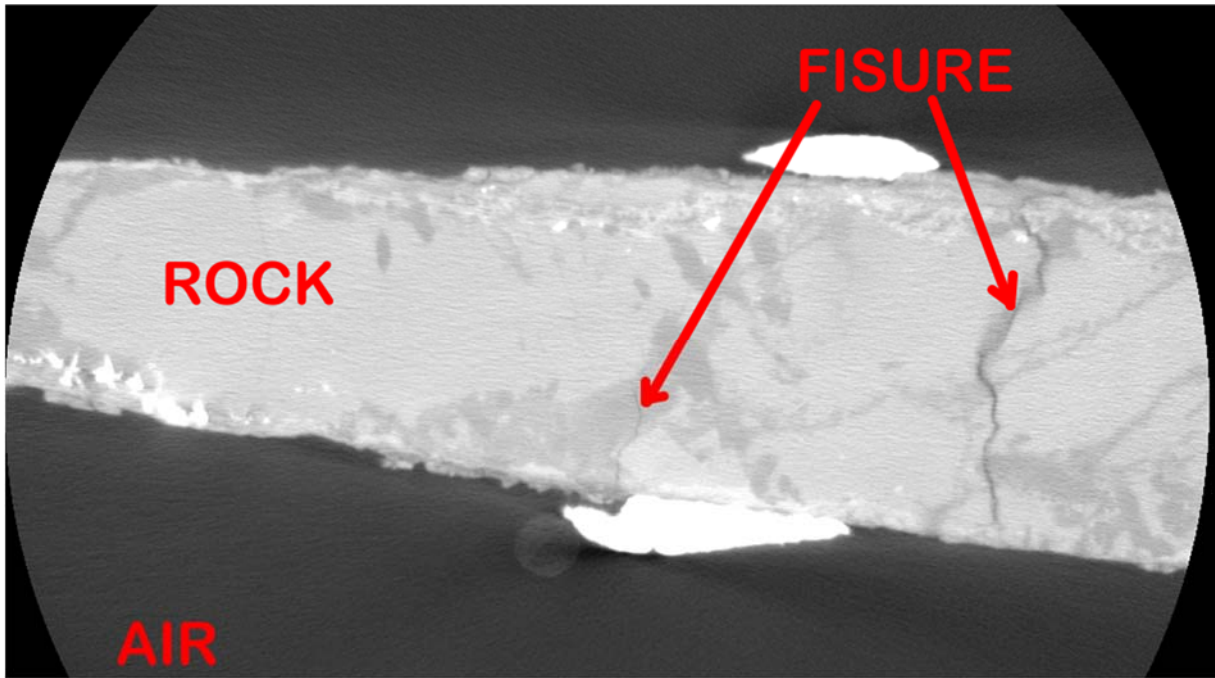


App 2.5. EDX measurement of ankerite from fig 6.4D

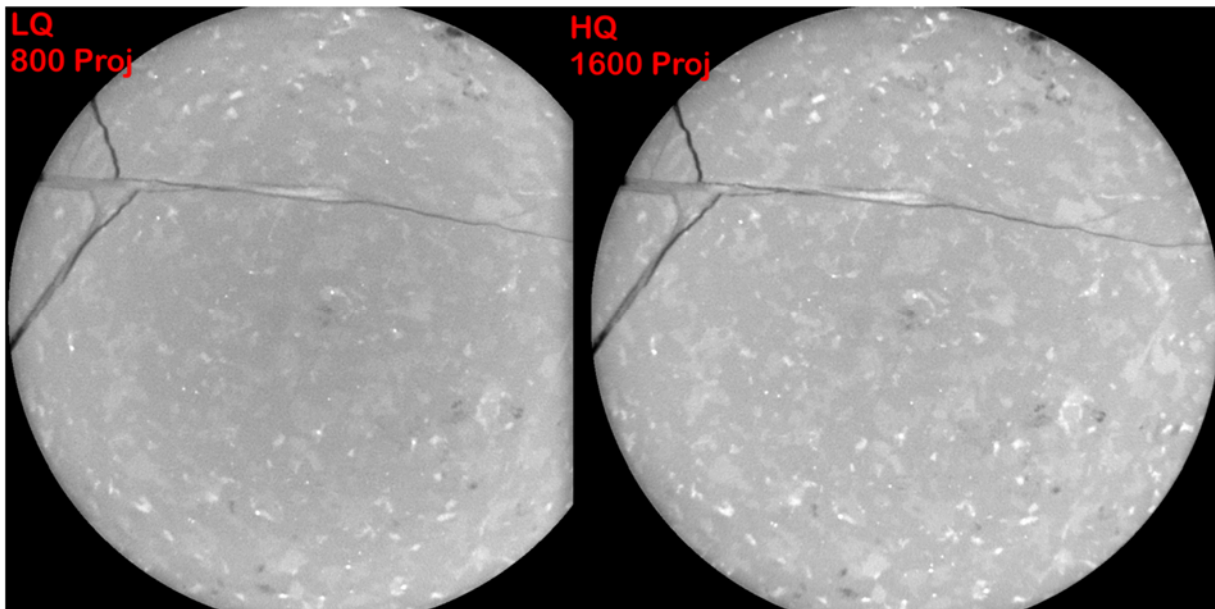


App 2.6. EDX measurement of dolomite from fig 6.4E

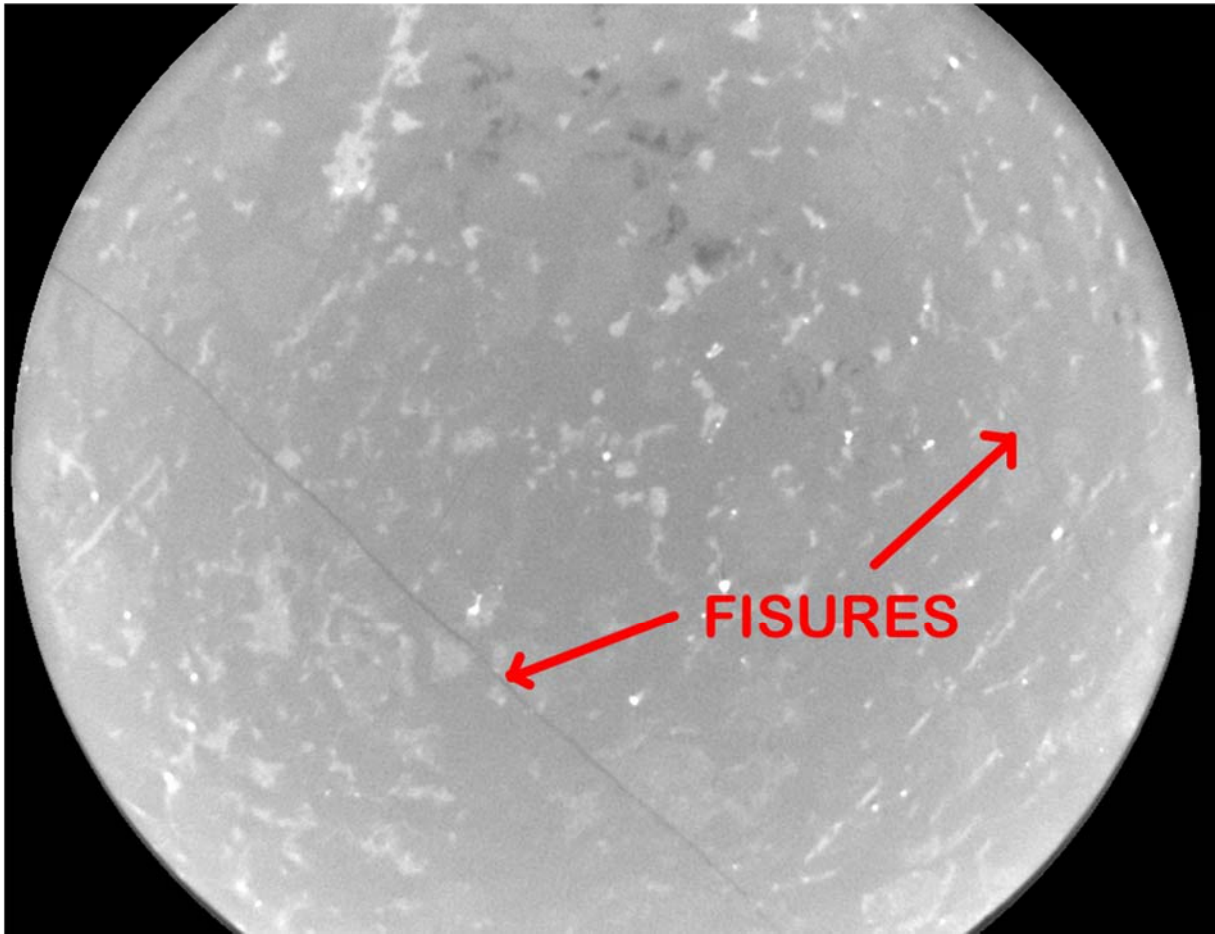
### Appendix 3. $\mu$ CT-scans of whole rocks and sub-cores



App3.1  $\mu$ CT of whole rock ZK2 (URL Bukov) shows a system of fissures inside the rock. Pixel size: 40  $\mu$ m



App 3.2  $\mu$ CT-scan of granite at depth of 639 m (URL Kurt) from 2 kinds of scans (800 Proj, left and 1600 Proj, right) with fissures and abundant of different minerals. Pixel size: 48  $\mu$ m with a field view of 49 mm (thickness) x 30 mm (height)



App 3.3  $\mu$ CT-scan of granite at depth of 954 m (URL Kurt) with fissures and abundant of different minerals.  
Pixel size: 48.8  $\mu$ m with a field view of 49 mm (thickness) x 30 mm (height)